Dissertation

EXTRACELLULAR MATRIX PROTEIN 1 AS A MEDIATOR OF INFLAMMATION-TO-FIBROSIS PROGRESSION AFTER MYOCARDIAL INFARCTION

submitted by

{title e.g., B. Biotechnology (Hons.)}

Sean HARDY

For the Academic Degree of

Doctor of Medical Science (Dr. scient. med.; Medical University of Graz) / Doctor of Philosophy in Medicine (PhD; University of Newcastle)

Jointly conducted at the

Medical University of Graz, Austria &

University of Newcastle, Australia

Research Group for Translational Cardiology / Clinical Division of Cardiology & Cardiovascular Research Group / School of Medicine and Public Health

Under the Supervision of

Assoc. Prof. Priv.-Doz. Dr. med. Dr.scient.med. Peter RAINER

&

Prof. Andrew BOYLE, MBBS. PhD. FRACP. FAHA. FACC. FSCAI

2022

This research was supported by an Australian Government Research Training Program (RTP) Scholarship

1. Statutory declaration & Statement of Originality

This thesis was formatted in accordance with the Medical University of Graz Guidelines for the Preparation of a Dissertation for Doctoral Degree Programs.

I hereby declare that this thesis is my own original work and that I have fully acknowledged by name all of those individuals and organisations that have contributed to the research for this thesis. Due acknowledgement has been made in the text to all other material used. Throughout this thesis and in all related publications I followed the "Guidelines of the Medical University of Graz on Good Scientific Practice".

I, Sean A. Hardy, hereby certify that the work embodied in the thesis is my own work, conducted under normal supervision. I confirm that the thesis contains no material which has been accepted, or is being examined, for the award of any other degree or diploma in any university or other tertiary institution, with the exception of the approved partner university associated with this Dual Award Doctoral Degree. To the best of my knowledge and belief, the thesis contains no material previously published or written by another person, except where due reference has been made. I give consent to the final version of my thesis being made available worldwide when deposited in the University of Newcastle Digital Repository and its equivalent at the partner university, subject to the provisions of the Copyright Act 1968 and any approved embargo.

2. Disclosures & Acknowledgement of Authorship

Part of this thesis has been published in *Hardy SA, Mabotuwana NS, Murtha LA et al. Novel role of extracellular matrix protein 1 (ECM1) in cardiac aging and myocardial infarction. PloS one 2019;14:e0212230.* **See supplementary PDF file of this publication**. Further, a second manuscript from this work is currently under revision with the Journal of the American College of Cardiology (JACC) Basic to Translational Science (impact factor 8.648).

I, Sean A. Hardy, hereby certify that the work embodied in this thesis contains published paper/s/scholarly work of which I am a joint author. I have included as part of the thesis a written declaration endorsed in writing by my supervisor, attesting to my contribution to the joint publication/s/scholarly work.

I, Andrew J. Boyle, confirm that Sean A. Hardy contributed [insert description / outline of contribution] to the paper/ publication entitled *Hardy SA, Mabotuwana NS, Murtha LA et al. Novel role of extracellular matrix protein 1 (ECM1) in cardiac aging and myocardial infarction. PloS one 2019;14:e0212230.*

All co-authors and respective institutional affiliations of the thesis of Sean A. Hardy are as follows: Nishani S. Mabotuwana[1,2,3], Laura Liesinger[6], Ralph Patrick[4,5], Maria Pöttler[1], Juergen Gindlhuber[6,7], Lavinia Rech[1], DiyaaEldin Ashour[8], Lucy A. Murtha[2,3], Verena Stangl[6], Mark Bigland[2,3], Brianna Coulter[2,3], Sonia Sanchez-Bezanilla[12,17,18], Mohammed S. Al-Omary[2,3,15], Tharindu Senanayake[2], Svenja Loering[3,12,17,18], Malcolm R. Starkey[10], Daniel Scherr[1], Gerald Höfler[6], Gustavo Campos Ramos[8,9], Clement Cochain[8,13], Randall J. Lee[19,20], Richard P. Harvey[4,5,14], Ruth Birner-Gruenberger[6,7], Philip M. Hansbro[11,12], Andrew J. Boyle* [2,3,15], Peter P. Rainer* [1,16]

1. Department of Internal Medicine and University Heart Center, Division of Cardiology, Medical University of Graz, Graz, Austria
2. School of Medicine and Public Health, The University of Newcastle, Callaghan, NSW, Australia
3. Hunter Medical Research Institute, New Lambton Heights, NSW, Australia
4. Victor Chang Cardiac Research Institute, Darlinghurst, Sydney, Australia
5. St. Vincent's Clinical School, Faculty of Medicine, UNSW Sydney, Sydney, Australia
6. Diagnostic and Research Institute of Pathology, Medical University of Graz, Graz, Austria
7. Faculty of Technical Chemistry, Institute of Chemical Technologies and Analytics, Technical University of Vienna, Vienna, Austria
8. Comprehensive Heart Failure Center, University Hospital Würzburg, Würzburg, Germany
9. Department of Internal Medicine I, University Hospital of Würzburg, Würzburg, Germany
10. Department of Immunology and Pathology, Central Clinical School, Monash University, Melbourne, Victoria, Australia.
11. Centre for Inflammation, Centenary Institute and University of Technology Sydney, School of Life Sciences, Faculty of Science, Sydney, NSW, Australia
12. Priority Research Centre for Healthy Lungs, Hunter Medical Research Institute, New Lambton, NSW 2305 and The University of Newcastle, Callaghan, NSW, Australia

13. Institute of Experimental Biomedicine, University Hospital Würzburg, Würzburg, Germany
14. School of Biotechnology and Biomolecular Science, UNSW Sydney, Sydney, Australia
15. Department of Cardiovascular Medicine, John Hunter Hospital, New Lambton Heights, NSW, Australia
16. BioTechMed Graz, Graz, Austria
17. School of Biomedical Sciences and Pharmacy, The University of Newcastle, Callaghan, NSW, Australia
18. Priority Research Centre GrowUpWell, School of Biomedical Sciences and Pharmacy, The University of Newcastle, Callaghan, NSW, Australia
19. Department of Medicine, Division of Cardiology, University of California San Francisco, San Francisco, CA, USA
20. Edyth and Eli Broad Center for Regenerative Medicine and Stem Cell Research, University of California San Francisco, San Francisco, CA, USA

3. Acknowledgements

The work conducted here was carried out as a dual awarded doctoral degree, to be awarded between the Medical University of Graz (Austria), and the University of Newcastle (Australia). The work of Sean Hardy was carried out under, and funding received from, the Doctoral School of Molecular Medicine and Inflammation at the Medical University of Graz, and under the School of Medicine and Public Health at the University of Newcastle. Sean Hardy was also supported by a Commonwealth funded Research Training Program (RTP) stipend, and the Emlyn and Jennie Thomas Postgraduate Medical Research Scholarship; made possible by the Hunter Medical Research Institute. Tuition fee offsets were covered by both the Medical University of Graz, and the University of Newcastle.

The work conducted at the Medical University of Graz and the University of Newcastle was supported by the Austrian Society of Cardiology, ERA-CVD and Austrian Science Fund AIR-MI

consortium [I 4168-B to P.P.R.]; the John Hunter Charitable Trust [G1800510 to A.J.B.]; the Hunter Medical Research Institute and the Emlyn and Jennie Thomas Postgraduate Medical Research Scholarship [G2100164 and G1800696 to A.J.B.]; the Austrian Society of Cardiology [to S.A.H.].

4. Table of contents

Contents

5. Abbreviations and Definitions

DCM – dilated cardiomyopathy

DEG – differentially expressed genes

EC – endothelial cell

ECM – extracellular matrix

ECM1 – extracellular matrix protein 1

GOBP – gene ontology biological process

GOCC – gene ontology cellular compartment

HF – heart failure

HuCFb – human cardiac fibroblast

ICM – ischemic cardiomyopathy

IHC – immunohistochemistry

LV – left ventricle

MI – myocardial infarction

Mo – monocyte

MΦ – macrophage

MS – mass spectrometry

NF – non-failing

sc/snRNAseq – single cell / single nuclei RNA sequencing

TNF – tumour necrosis factor

6. Abstract in German

Hintergrund: Der Umbau der extrazellulären Matrix mit Vermehrung von interstitiellem Gewebe und Narbenbildung (Fibrose) ist gemeinsame Endstrecke fast aller Herzerkrankungen und oft irreversibel. In der Vergangenheit konnten wir eine Schlüsselrolle für das Molekül ECM1 in der Vernarbung nach Myokardinfarkt identifizieren. Ziel der vorliegenden Doktorarbeit war es, die zelluläre Quelle und Dynamik von ECM1 nach Myokardinfarkt zu beschreiben und Einblicke in die zugrundeliegende Signaltransduktion und den fibrotischen Gewebeumbau zu gewinnen.

Methoden: Immunoblotting, Immunhistochemie und mRNA in-situ Hybridisierung zeigten die Expression von ECM1 in humanen und murinen Herzgeweben. In Mausgeweben wurde zusätzlich Durchflusszytometrie verwendet (Herz, Knochenmark). Einzel-Zell/Zellkern RNA Sequenzierung ermöglichte die Expressionsanalyse in unterschiedlichen Zelltypen. Humane Fibroblasten wurden in Zellkultur mit ECM1 behandelt und mittels Massenspektroskopie (Phospho-MS, Identifikation von ECM1 Liganden) untersucht. In der Zellkultur wurden Zellmigrationsassays, MTT assays, qPCR und Immunoblotting eingesetzt.

Ergebnisse: ECM1 ist in ischämischen und nicht-ischämischen insuffizienten Herzen hochreguliert, v.a. in interstitiellen, peri-vaskulären und fibrotischen Zonen. Die Einzelzell/Zellkern Sequenzierung ermöglichte die Darstellung der dynamischen Expression post-MI in Fibroblasten und Makrophagen Subpopulationen. In der MS Analyse zeigte sich ECM1 mit Signalwegen für Fibrose, Zell-Zell Kommunikation, Zelladhäsion, Zellmigration und Inflammation assoziiert. In der Zellkultur verminderte ECM1 die Migration von humanen Fibroblasten und reduzierte die CCL2 Expression. Profibrotische/inflammatorische Marker (IL-6, IL-1β, TGFβ1, Col1a2) und Wnt5a waren hochreguliert. Die Analyse der MS Daten zeigte CTNND1 als möglichen ECM1 Bindungspartner. Homozygote ECM1 knockout Tiere haben einen schweren generalisierten Phänotyp mit deutlich verkürztem Überleben und Untergewicht.

Konklusion: ECM1 ist eine neues Adaptormolekül, welches inflammatorische und fibrotische Signaltransduktionswege koppelt und eine wesentliche Rolle im Gewebeumbau nach Myokardinfarkt spielt.

5. Abstract in English

Background: Fibrosis is a hallmark of heart disease, particularly following myocardial infarction (MI) and in heart failure. We previously identified a key role for ECM1 in wound healing post-MI but the precise cellular origin and mechanism of ECM1 remained elusive. Here, we aimed to investigate the spatiotemporal cellular origin of ECM1 in healthy and

diseased human and mouse hearts, and ECM1 dependent human cardiac fibroblast (HuCFb) signalling mechanisms.

Methods: Immunoblotting, immunohistochemistry and mRNA in-situ hybridisation were conducted on non-failing, ischemic (ICM) and dilated (DCM) failing human heart tissue. In-situ hybridisation, flow cytometry and immunoblotting were conducted on mouse heart and bone marrow samples. ECM1 specific analysis of existing single-cell/-nuclei RNA sequencing (sc/snRNAseq) data was conducted. HuCFbs were treated with recombinant ECM1 and phosphoproteomics mass spectrometry (MS), MS of ECM1-HuCFb cell binding partners, wound healing assay, MTT assay, qPCR, and immunoblotting was conducted.

Results: ECM1 expression was upregulated in human ICM and DCM, localised interstitially to fibrotic, inflammatory, and peri-vascular areas. ECM1 originates from fibroblasts, macrophages, and pericytes/vascular cells in uninjured human and mouse hearts. In mouse hearts post-MI, ECM1 predominantly originates from M1 macrophages/monocytes (MΦ/Mo) at day-3, and myofibroblasts and M2MΦ's at day-7. Further, ECM1 expression was correlated with cell-cell communication, collagen organisation, inflammation, cell adhesion and migration. In vitro, ECM1 inhibited HuCFb migration and CCL2 mRNA expression, and stimulated mRNA expression of inflammatory (IL-6, IL-1β), fibrotic (TGF-β1, Col1a2), and non-canonical Wnt gene Wnt5a. MS experiments showed ECM1 stimulates HuCFb Rho protein, cell-cell adhesion, and chemotactic signalling pathways, potentially initiated by ECM1-CTNND1 protein binding. Finally, we created an ECM1 genetic knockout animal (ECM1Δ2). Homozygous ECM1Δ2 knockout resulted in lower body weight, smaller body size, and a significantly lower rate of survival over the first 16 weeks of life, relative to WT.

Conclusions: ECM1 represents a novel mechanism in facilitating inflammation-fibrosis crosstalk post-MI and thus a potential therapeutic target.

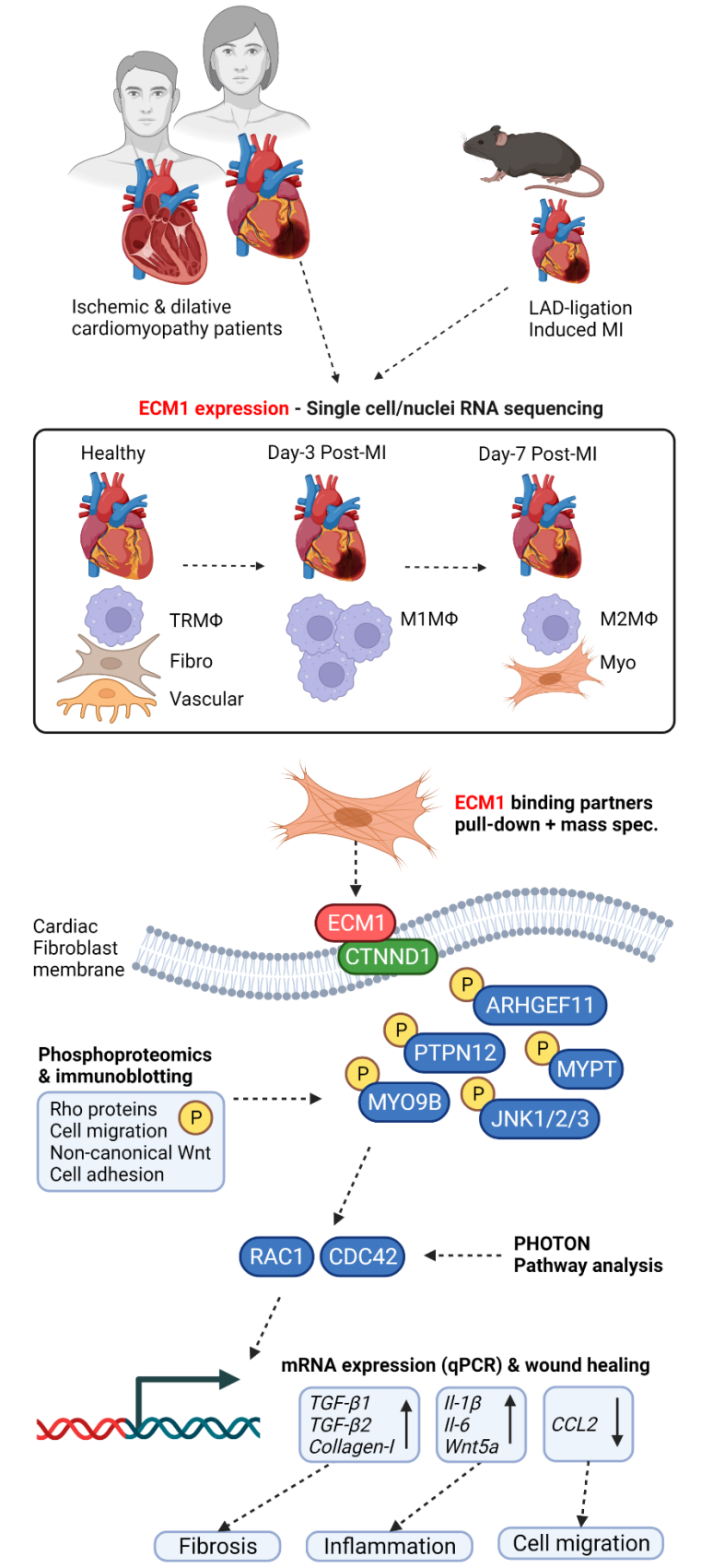

Graphical abstract: we previously showed that ECM1 is upregulated in the infarct zone post-MI in mice (1). Here, we confirm ECM1 upregulation in both ischemic and dilated human

heart failure patients, localised to fibrotic, inflamed, and peri-vascular areas. Single cell/nuclei RNA sequencing analysis revealed ECM1 originates predominantly from tissue resident macrophages (TRMΦ), fibroblasts (Fibro) and vascular cells in uninjured human and mouse hearts, M1 macrophages (M1MΦ) at day-3 post-MI, and M2 macrophages (M2MΦ) and myofibroblasts (Myo) at day-7 post-MI. ECM1 dependent pull-down with purified human cardiac fibroblast (HuCFb) membrane proteins and mass spectrometry of binding partners suggested ECM1 binds catenin delta-1 (CTNND1). Phosphoproteomics and western blotting showed ECM1 stimulates phosphorylation of proteins involved in Rho protein, cell migration, cell adhesion, and non-canonical Wnt signalling. PHOTON pathway analysis of our phosphoproteomics data showed signalling through Rho GTPase mediators RAC1 and CDC42. qPCR analysis and wound healing assays of ECM1 treated HuCFbs showed ECM1 stimulates inflammatory, pro-fibrotic, and non-canonical Wnt pathways, inhibits *CCL2* expression, and reduces HuCFb cell migration. Created with BioRender.com.

12. Introduction

12.1 Overview

Cardiovascular disease is the leading cause of death worldwide, and myocardial infarction (MI) is one of the most common (2, 3). MI causes mass cardiomyocyte death (necrosis and/or apoptosis), lead to extensive tissue and cellular damage and triggers acute inflammatory responses (4, 5). As the adult mammalian heart has limited regenerative capacity (6, 7), cell death, tissue damage and inflammation are followed by pro-fibrotic ECM remodelling and scar formation, called cardiac fibrosis. Cardiac fibrosis is defined as the net accumulation of extracellular matrix (ECM) proteins in tissue and has long been regarded as a ‘hallmark’ of cardiac disease, as it is evident in all forms of cardiac disease. Fibrosis produces scar tissue in an attempt to maintain the integrity of the heart and prevent cardiac rupture, but this also impairs cardiac structure, function, and promotes the progression of heart failure (5, 8). Inflammation followed by fibrosis is a well-established tenet of cardiac wound healing, though surprisingly little is known of the molecular signals that mediate these sequential phases of recovery from injury. Since the 1960’s many treatments have

tried and failed to modulate inflammation to produce better clinical outcomes (9), while others have targeted fibrosis but few have successfully become the cornerstones of heart failure therapy. A such, the morbidity and mortality from cardiac disease remains high and novel therapies are desperately needed to further reduce the burden heart disease places on health care systems worldwide.

Recently, there has been new appreciation of the critical importance of inflammation-fibrosis crosstalk in wound healing post-MI, as opposed to approaching inflammation and fibrosis as two mutually exclusive events. This novel axis of inflammation-fibrosis crosstalk may be why past 'unidirectional' therapies which target inflammation or fibrosis alone have failed to significantly reduce the mortality associated with fibrotic cardiac diseases (10). As such, inflammation-fibrosis crosstalk should be considered a key factor in the investigation of novel therapeutic strategies to battle the mortality of fibrotic cardiac disease. A better understanding of the molecular events which underpin the inflammation, fibrosis, and the interplay between the two is an essential first step towards the development of affective therapeutic strategies.

Novel proteins and factors involved in wound healing with cardiac disease are constantly emerging and reshaping our knowledge base. One such novel protein is extracellular matrix protein 1 (ECM1). ECM1 is implicated in numerous diseases throughout the body, but importantly, ECM1 interacts with several ECM proteins (11), acts as a structural basement membrane protein, and even regulates inflammatory cell function (12-14). To date, only one study has been previously conducted on ECM1 in the heart (15). In this study they identified an association between ECM1 mRNA expression and left ventricular inflammation in chronic sustained hypoxia. In keeping with this literature, our preliminary results suggest that ECM1 plays a role in cardiac ECM remodelling and fibrosis associated with MI. Therefore, ECM1 could play a key role in both the inflammatory response and the development of fibrosis, or in facilitating inflammatory-fibrosis crosstalk in cardiac wound healing. In this way, ECM1 is a prime candidate worthy of investigation as a novel therapeutic target in wound healing with fibrotic cardiac disease.

The following review outlines our current understanding of the effects of disease on the myocardium, with particular focus on MI, inflammation, ECM remodelling, fibrosis, and the new appreciation of the intricate interplay between inflammation and fibrosis in cardiac

disease. This review also includes an in-depth review of the current literature available on the structure and function of ECM1.

12.2 Cardiomyocytes and cardiac fibroblasts

Two of the most populous cell types throughout the heart are the cardiomyocytes, and the cardiac fibroblasts (CFs). Cardiomyocytes are the muscle cells/beating cells of the heart. They are non-structural components of cardiac tissue that are surrounded by the cardiac ECM and confer the contractile force to the heart and control cardiac rhythm. Cardiomyocytes form a major part of the cardiac conduction system via transmission of electrical signals from the *sino*-atrial pacemaker node, located in the right atrium (16, 17). On the other hand, CFs play a very different role. CFs surround cardiomyocytes, fill the gaps, bridge layers of the myocardial tissue, and are one of the most populous major cell types in the heart (18, 19). CFs are the major source/secretors of ECM proteins and are responsible for maintaining the structure of myocardial cells and tissue. They also contribute to the mechanical, electrical, biochemical and structural properties of the myocardium by bridging electrochemical interactions between cardiomyocytes and act as cellular conductors (20). Importantly, CFs are the major cell type which lay down fibrotic tissue during wound healing with cardiac disease, as I will discuss later. One major job of CFs is to manage ECM homeostasis, which involves maintaining the balance between synthesis and degradation of components of the ECM/connective tissue depending on cardiovascular requirements. This is done via the expression of the major ECM degrading enzymes matrix metalloproteinases (MMPs), and their inhibitory counterparts tissue inhibitors of metalloproteinases (TIMPs), (21); described in more detail below.

In response to cellular signalling in conditions such as disease and injury, the ‘at rest’ fibroblast will differentiate into a myofibroblast; myofibroblasts are generally only present in response to these stressors. Myofibroblasts are often referred to as ‘activated fibroblasts’, and are a highly active cell which are responsible for the majority of ECM remodelling, collagen turnover, fibrotic tissue production, tissue repair and have significantly higher capacity for carrying out these processes than the at-rest fibroblast (18, 19, 22-26). Specifically, myofibroblasts have a phenotype which closely resembles smooth muscle cells (SMCs), and secrete large amounts of ECM proteins (e.g., collagen I & III), as

well as α-smooth muscle actin, growth factors, cytokines, chemokines, MMPs, TIMPs, and exhibit higher motility than at-rest fibroblasts. These features allow myofibroblasts to stabilise scar tissue, promote wound contracture at the site of an infarct, and efficiently carry out ECM remodelling (27-31). Once myofibroblasts have presented in response to cardiac disease or injury such as MI, they can persist in the myocardium for prolonged periods of time in order to promote reparative fibrosis and wound healing, which occurs widely in the infarct zone, border zone and to a lesser extent the remote zones from the initial site of injury post-MI (18, 19, 25, 26, 32, 33).

12.3 The cardiac extracellular matrix (ECM) and ECM remodelling

The ECM is a network of both structural and non-structural components including glycoproteins, proteoglycans and glycosaminoglycans (GAGs), as well as several receptors and enzymes that form three-dimensional (3D) scaffold networks (34, 35). The cardiac ECM is maintained by CFs, and provides structural support and alignment for cardiomyocytes, blood vessels, lymphatic vessels, and myocardial tissue, as well as providing biophysical and biochemical tissue-specific properties. The ECM also promotes spatial coordination of signalling processes for cells in the myocardium, by binding growth factors, cytokines, ECM transmembrane receptors and soluble ligands (35-38).

Collagens are the most abundant ECM protein throughout the body, with more than 28 different variants of collagen present throughout the cardiac ECM. The most abundant forms of collagen are type I, which makes up approximately 80% of total cardiac collagen content, and collagen type III, which makes up approximately 11% of total cardiac collagen (35, 39). Collagens form 3D collagen scaffold networks, which are involved in adult heart development and maintenance of cardiac elasticity and structural integrity (40). Collagen-I also plays a huge role in maintaining structural integrity in cardiac disease (as well as the normal/healthy heart), and is the most predominant form of collagen in fibrosis with cardiac disease such as MI, pressure overload (24, 41-44).

The ECM of the diseased heart is subject to extensive remodelling, which often results in, or is the result of, cardiomyocyte death and/or displacement. ECM remodelling also leads to a decrease in the thickness of muscle layers in the ventricular wall and dilation of the left

ventricle, leading to accumulation of fibrotic collagen-based scar tissue (24, 45). ECM remodelling involves coordinated degradation of ECM structural components and the synthesis of new ECM proteins. In some instances, ECM remodelling confers a change in the overall shape of the myocardium. ECM remodelling is facilitated by a family of key proteases, called MMPs; briefly mentioned above. MMPs are a large zinc-dependent family of endopeptidases, most of which are secreted by fibroblasts, cardiomyocytes, macrophages and neutrophils (43). MMPs carry out physiological and pathophysiological ECM remodelling by cleaving structural elements of the ECM (40). Currently there are 25 vertebrate MMP family members known (22 in humans), which collectively play a role in regulating cell motility, cell growth, tissue morphogenesis and tissue remodelling in response to injury (46-48). Dysregulation in MMP activity can lead to several conditions such as excessive inflammation, left ventricular hypertrophy, and cardiomyopathy. Therefore, correct regulation of MMP activity is important in maintaining a healthy myocardium. The proteolytic activity of MMPs is regulated by a family of inhibitors, TIMPs (48-50). TIMPs are a small family of four broad-spectrum endogenous proteinase, collagenase, gelatinase, and proteoglycanase inhibitors (TIMP-1 to -4). TIMPs are secreted by CFs and myofibroblasts, and their role is to manage the level of MMP ECM degradation (51). Each TIMP differs in its expression pattern, specificity and affinity for various MMPs, and acts as a 'wedge', entering and binding to the active-site of MMPs via TIMP N-terminal domain folds, reversibly blocking the proteolytic activity of MMPs in a 1:1 ratio (52).

12.4 Cardiac Fibrosis

Cardiac fibrosis is defined as the net accumulation of ECM proteins leading to stiff and distorted myocardial architecture, function, and cardiomyocyte coupling (32, 53). Fibrosis is present throughout the heart with ageing and disease and has been implicated in almost all forms of cardiac disease and heart failure (32, 54). In the normal heart, ECM proteins such as collagens, fibronectin and laminins form complex, tightly structured networks that confer tensile strength to the cardiac tissue and allow correct regulation of myocardial contraction to occur. However, in the diseased or injured heart, the cardiac tissue accumulates excess collagen, and the ECM network is subject to remodelling to preserve cardiac tissue integrity. This results in the production of stiff, fibrotic scar tissue and disruption of cardiomyocyte

excitation-contraction coupling, leading to a decrease in the contractility of the heart (24, 45, 55). There are two major kinds of fibrosis: replacement fibrosis (reparative fibrosis) and interstitial (reactive) fibrosis (56). Replacement fibrosis is closely linked to the inflammatory response and occurs mainly in response to diseased conditions such as MI. It is associated with the loss of cardiomyocytes throughout the myocardium, which causes an intense inflammatory reaction, resulting in mass deposition of fibrotic scar tissue (24, 53, 57). Whereas interstitial fibrosis is usually observed in non-ischaemic cardiomyopathies (e.g., pressure overload), and is an adaptive expansion of fibrotic tissue in the interstitial space without loss of cardiomyocytes (24, 53, 57). This occurs in an attempt to preserve the ability of the heart to generate pressure.

12.5 Overview of inflammation and ECM remodelling in myocardial infarction

MI is defined as myocardial cell death due to prolonged ischemia, as the result of partial or complete occlusion/blockage of an artery (58). This is usually the caused by atherosclerosis/atherosclerotic plaque formation and/or rupture in the coronary arteries, also referred to as coronary artery disease (CAD); atherosclerosis is characterised by the accumulation of lipids, leukocytes and fibrous elements in the arterial wall that gives rise to these obstructive atherosclerotic plaques (59-61). The ECM of the heart during wound healing with MI is subject to extensive remodelling. This involves coordinated degradation of structural ECM components by MMP enzymes, and the synthesis of new ECM proteins by CFs and their differentiated counterparts, myofibroblasts. As the heart is unable to regenerate lost cardiomyocytes to a level which is sufficient to functionally replace damaged tissue (6, 7), ECM remodelling post-MI instead gives way to the accumulation of fibrotic collagen-based scar tissue. This results in stiff, distorted myocardial architecture, ventricular wall thinning, impaired cardiomyocyte coupling and a substantial loss of cardiac function (24, 32, 45, 53). With MI especially, inflammation is innately linked to and precedes ECM remodelling and cardiac fibrosis. The process of wound healing post-MI has long been described as an overlapping three phase process: the “inflammatory phase” consisting of acute leukocyte infiltration and activity (~0–3 days), the “proliferative phase” of angiogenesis and fibrotic tissue deposition (~2–7 days), and the “maturation phase” (~7+ days) consisting of vascular maturation and ECM crosslinking (4, 5). For decades, the

inflammatory phase has been an exciting study area for pre-clinical research, and a promising target for therapeutic intervention (although very poorly understood in the past), as it sets the stage for wound healing, and precedes the development of cardiac fibrosis.

To briefly outline our current understanding of the inflammatory event that occurs with MI: following the initial occlusion of a coronary artery, cardiomyocytes in the affected area become necrotic or apoptotic, and release damage associated molecular patterns (DAMPs), reactive oxygen species (ROS), and a range of pro-inflammatory cytokines and chemokines. This gives rise to an acute sterile inflammatory event, which effectively marks the beginning of this 'inflammatory phase' post-MI. Specifically, tissue resident leukocytes, particularly tissue resident macrophages are also crucial in kickstarting this process. Directly following infarction, tissue resident macrophages, as well as cardiomyocytes as mentioned above, also begin to die (generally all lost by 24 h post-MI) and produce pro-inflammatory cytokines such as: CC-chemokine ligand 2 (CCL2 aka macrophage chemoattractant protein-1 (MCP1), pro-inflammatory interleukin (IL) subtypes IL-1 and IL-6, and tumour necrosis factor-α (TNF-α). At this time, fibroblasts begin to release growth factors, and endothelial cells become activated (60, 61). This induces mass recruitment of neutrophils (considered inflammation first responders) and monocytes to the infarct site from the spleen and bone marrow (62, 63). Upon arrival in the heart, monocytes will differentiate into mainly pro-inflammatory M1 macrophages (M1MΦ) (64). These neutrophils and monocytes/M1MΦ's sense and respond to cardiomyocyte and tissue resident macrophage derived factors, being to clear cellular debris and dead materials, and subsequently secrete an array of chemokines and pro-inflammatory cytokines of their own, (CCL2, IL-1, IL-6, TNF-α). This cytokine production recruits more leukocytes to the infarcted myocardium including lymphocytes from lymph nodes, spleen, bone marrow, and perpetuate the inflammatory response (5, 8, 60, 61, 65). As the infarcted myocardium is cleared of debris, and the inflammatory phase progresses, recruited neutrophils become apoptotic and are engulfed by macrophages. This triggers both a shift in macrophage phenotype towards pro-reparative M2MΦ's, and production of anti-inflammatory factors, such as and IL-10, and TGF-β1 (5, 8, 10, 61, 64, 66, 67). This effectively marks a point of resolution of this inflammatory phase, promotes the recruitment of fibroblasts and stimulates fibrotic tissue deposition; marking the beginning of the 'proliferative' (~day 3-7+ post-MI), fibrogenic phase.

12.6 The importance of macrophages in post-MI wound healing

Outlining the role of all leukocytes in post-MI wound healing is beyond the scope of this study and has been extensively reviewed in the past (10, 68). However, a particularly important leukocyte to this study are macrophages. Macrophages more-so than other leukocytes, have a close relationship with fibroblasts in wound healing post-MI. They are versatile and critically important cells post-MI which bridge the innate and adaptive immunity through their antigen presentation role, and play both a pro-inflammatory, anti-inflammatory, and direct ECM remodelling role via their secretion of an array of proteins and factors (e.g., TGF-β1, TNF-α, IL-6/-1/10, VEGF) (61, 69). Importantly, macrophages have even been shown to directly contribute to fibrotic tissue deposition in cardiac fibrosis, as I will discuss later in greater depth. Another key function for macrophages (as mentioned briefly above) is in clearing dead cardiomyocytes, cellular debris, and apoptotic neutrophils from the infarct site post-MI via phagocytosis (70, 71); they also eliminate pathogens (61). In the most basic view, macrophages have long been described by a paradigm of either M1 pro-inflammatory/classically activated, or M2 alternatively activated reparative/pro-healing macrophages (61, 72). M1 macrophages produce high levels of pro-inflammatory cytokines, such as IL-1 and IL-6 and in doing so perpetuate the inflammatory response (61). Whereas M2 macrophages are anti-inflammatory and pro-healing/pro-regenerative, and express high levels of anti-inflammatory IL-10, TGF-β1, VEGF and MMPs (61, 72). Although the traditional M1/M2 paradigm of macrophages is useful for describing phenotype and transition over time during wound healing post-MI, it is important to note that macrophage phenotype is a much more nuanced continuum of phenotypic states; the M1/M2 paradigm also does not account for the context of the tissue environment or source of the stimuli. Techniques like single cell RNA sequencing are demonstrating this by delineating immune cell sub-populations in far greater detail than we had the tools to investigate in the past (73).

The close relationship between fibroblasts and macrophages has recently gained a significant amount of attention as a critical factor in maintaining cardiac homeostasis, as well as carrying out crosstalk between immune and fibrotic responses in cardiac wound healing (8). This novel mechanism, which has particular relevance to post-MI wound healing, is often referred to as inflammation-fibrosis crosstalk; discussed below.

12.7 Inflammation-fibrosis crosstalk in wound healing post-MI: a promising therapeutic target

Inflammatory-fibrosis crosstalk is a term encapsulating the new appreciation that inflammation and fibrosis are closely interweaved and are reliant on each other throughout the course of wound healing, especially post-MI. Inflammatory-fibrosis crosstalk is clearly reported to occur in at least two main ways:

1. Paracrine leukocyte to fibroblasts signalling, and reciprocal fibroblast to leukocyte signalling (e.g., via secretion of cytokines, chemokines, and various other factors).
2. Leukocytes directly conduct ECM remodelling, ECM production and contribute to fibrotic scar formation themselves.

12.7.1 Fibroblast-leukocyte, and leukocyte-fibroblast cell signalling

The most well documented form of fibrosis-inflammation crosstalk today is in the form of paracrine fibroblast-leukocyte and leukocyte-fibroblast cell signalling via secretion of cytokines (e.g., IL-1β/-6/-10), chemokines (e.g., CCL2/MCP-1), and other factors like TGF-β, TNF-α, MMPs, and TIMPs which can stimulate cell recruitment, survival and vast array of cellular behaviours (10, 68, 74). In this space, some cell types more than others, like macrophages, have a close relationship with fibroblasts in wound healing post-MI, and are a prime example of this form of paracrine inflammatory-fibrosis crosstalk. For instance, macrophages signal to fibroblasts via secretion of TGF-β, FGF, PDGF and IL-1β, all of which act on fibroblasts to stimulate fibroblast-myofibroblast differentiation and/or increased production of MMPs (68), and macrophage IL-10 secretion stimulates fibroblast migration and proliferation (75). Reciprocally, fibroblasts signal to and influence leukocytes via secretion of chemokines like MCP1 (CCL2), IL-10, RANTES, and MIP-1, which can promote the recruitment, homing and retention/survival of leukocytes to sites of tissue injury (10), and enhance monocyte-fibroblast cellular adhesion and production of chemokines (76). Once they have been recruited to the myocardium fibroblasts can influence survival of leukocytes. Ultimately, fibroblasts can both stimulate or supress the inflammatory response via paracrine signalling to leukocytes during post-MI wound healing.

12.7.2 Leukocytes carry out ECM remodelling and contribute to collagen deposition in fibrosis

Another mode of fibrosis-inflammation crosstalk is by leukocytes directly promoting and carrying out ECM remodelling and fibrotic tissue deposition themselves. Macrophages, like fibroblasts, are a major source of TGF-β1, MMPs, TIMPs and other factors which play a direct, critical role in ECM remodelling (76, 77). Recently macrophages have been shown to directly contribute to fibrotic scar formation in MI via secretion of collagens (78, 79). Studies demonstrated the presence of monocyte/macrophage derived collagen-I in the fibrotic scar post-MI (78), and that recruited macrophages (CCR2+ macrophages) at day-7 post-MI directly secrete ECM proteins collagen-I, collagen-III and periostin (79). And strikingly, macrophages have even been shown to transform and adopt a "fibroblast-like" phenotype in wound healing post-MI (80). Although other leukocytes like neutrophils, eosinophils, and T- & B-cells are understood to contribute to ECM remodelling (e.g., neutrophils through MMP expression), a direct role in collagen deposition is less clear (68, 81, 82).

Inflammation-fibrosis crosstalk is an emerging paradigm with critical control over the progression of wound healing post-MI and is therefore an excellent therapeutic target worthy of basic, translational, and clinical investigation.

12.8 Extracellular Matrix Protein 1 (ECM1)

Clearly, the investigation of novel proteins with potentially crucial roles in cardiac fibrosis, inflammation, and the crosstalk between the two is essential. One such novel protein with this potential is ECM1. To date, studies have shown that ECM1 interacts with many ECM proteins and acts as a structural basement membrane protein which regulates ECM integrity, as well as regulating inflammatory cell function (11-14). ECM1 has also been shown to play a crucial role in cell architecture, cell adhesion, cell migration, and in several diseases such as cancer as will be discussed below. As such, ECM1 has great potential to play a pivotal role in fibrotic cardiac disease as well.

ECM1 is a widely expressed membrane bound and secreted 85-kDa glycoprotein protein encoded by the *ECM1* gene located at chromosome 1q21. ECM1 expression was first

described by Bhalerao, Tylzanowski (83) who showed that ECM1 is secreted by cells of the stromal osteogenic cell line MN7. To date, ECM1 is known to be widely expressed in many tissues throughout the body, but the cellular origins of ECM1 in the heart remain unknown (prior to the present work); although some studies have identified that ECM1 is expressed by leukocytes, such as T_h2 lymphocytes and macrophages (12, 14, 84, 85). The *ECM1* gene encodes a 1.85kb *ECM1* full length DNA sequence (1.8kb *ECM1a* full length human DNA sequence) and encodes for four alternatively spliced *ECM1* isoforms: *ECM1a*, *ECM1b*, *ECM1c* and *ECM1d*. *ECM1a* is the full length human *ECM1* gene (1.8kb) encoding a 540aa protein. *ECM1b* is a shorter 415aa protein expressed in both mice and humans. Human *ECM1c* is homologous to the full-length murine *ECM1* gene (1.85kb) and encodes a 559aa protein. The fourth *ECM1* splice variant is *ECM1d*, which is a newly discovered truncated 72bp transcript encoding a 57aa protein, of currently un-characterised expression and function (83, 86-92).

The protein structure of ECM1 is closely conserved between mice and humans (79% homology), as well as between ECM1a/ECM1c and ECM1b splice variants (83, 93). Studies show that ECM1a consists of a 19-amino acid signal sequence, and four distinct domains including a cysteine-free terminal NH_2 domain which forms α-helices, a C-terminal domain, and two tandem repeat domains. The C-terminal domain and the two tandem repeats contain a cysteine arrangement, typical of a double helix loop structure, which contributes to the ability of ECM1 to carry out protein-protein interactions (83, 84, 93, 94). More recent studies have characterised the 3D structure of ECM1a as four protein segments (aside from the C-terminal domain): the N-terminal domain with the potential to form α-helices, and three serum albumin-like domains SASDL2, SASDL3 and SASDL4 (89, 91-93, 95, 96). The three SASDL domains form numerous C-CC-C motifs via disulphide bonds and share putative double loop structures. It is suggested that these motifs form finger-like structures, providing the SASDL domains the potential for fatty acid binding via formation of fatty acid binding clefts. It is also suggested that ECM1 utilises different binding sites for each respective protein binding partner, and that in this way, ECM1 acts as a core binding protein, and functions as a scaffold for a large variety of interactions with site specific binding partners. These studies lead to the description of ECM1 as a ‘multifunctional core binding, scaffolding, basement membrane protein’, which has been identified to bind with

the majority of ECM proteins identified to date, including: collagens, perlecan, fibulin-1, MMP-9, heparin, hyaluronan, laminin 332, fibronectin and chondroitin sulfate-A (91, 92, 97).

12.9 ECM1 in cardiac hypoxia and liver fibrosis

12.9.1 ECM1 is upregulated in rat left ventricle tissue in response to chronic sustained hypoxia

Only one study has investigated the expression of ECM1 in the heart (15). This study did gene expression analysis on an array of genes expressed in left ventricular tissue (including *ECM1*) in response to chronic intermittent hypoxia (CIH) and chronic sustained hypoxia (CSH) at 7 days post-CSH/CIH. In response to CSH, they showed increased left ventricle (LV) inflammation and a corresponding increase in *ECM1* expression (1.3-fold). Inversely, in response to CIH, they saw decreased LV inflammation, decreased fibroblast activity, and downregulated *ECM1* expression (2.6-fold). As such, they suggested that ECM1 expression levels were dependent on fibroblast numbers and/or activity level and inflammation in the LV. Therefore, it is possible that ECM1 in the heart may originate from fibroblasts and leukocytes and may be involved in the inflammatory and fibrotic response.

12.9.2 ECM1 in liver fibrosis

ECM1 has recently been implicated to be an inhibitory factor in liver fibrosis (98). In this study they demonstrated that whole body ECM1 knockout in mice led to death by 8 weeks of age due to significant liver fibrosis. They show ECM1 expression decreases as liver fibrosis worsens (METAVIR score) in human liver disease patients. ECM1 was highly expressed by hepatocytes in the liver, and inhibited fibrosis via blocking TGF-β activation and sequestering TGF- β in its latent form in the ECM. This was achieved via a co-operative binding interaction between ECM1, αv integrin and Latent TGFβ. Thus, ECM1 may have anti-fibrotic properties in the liver.

12.10 ECM1 binds various ECM proteins and maintains ECM integrity

12.10.1 ECM1 in lipoid proteinosis and skin

ECM1 is shown to be localised in several areas in human skin, including the basal epidermal cell layers, basement membranes and the extracellular matrix in a dermal-fibroblast dependent pattern (90-92, 94). These studies identified ECM1 to interact with collagen IV (Col-IV), and laminin 332, perlecan, fibulin-1, MMP-9, heparin, hyaluronan, fibronectin and chondroitin sulfate-A to form part of several structural networks. ECM1 was also shown to enhance Col-IV to laminin 332 binding. As such, ECM1 is thought to be of great structural importance in the interstitial dermis and dermal-epidermal junction, and in maintaining the overall integrity of the skin. Mutations in the *ECM1* gene lead to the pathological skin condition lipoid proteinosis (LP) (89, 93, 99). Several LP studies identified interactions between ECM1, fibulin-1, fibulin-3, and laminin 322 to be involved in maintaining correct structural integrity of ECM basal lamina (89, 93). Importantly, the interaction between ECM1 and MMP-9 via the second tandem repeat region of the ECM1 c-terminal domain inhibits MMP-9 proteolytic activity in connective tissue remodelling (11, 99). Thus, ECM1 mutation reduces the level of MMP-9 inhibition, leading to excessive MMP-9 activity, and the pathophysiology of LP.

12.10.2 ECM1 in the skin disorder lichen sclerosus

Circulating autoantibodies specific to ECM1 have been implicated in the acquired chronic inflammatory disorder of skin and mucous membranes, lichen sclerosus (LS) (100-102). LS is associated with chronic skin and mucous membrane inflammation, dermal fibrosis, hyperkeratosis, atrophy, and pale indurated papule and plaque formation. Importantly, LS has several clinicophathological similarities to LP including skin inflammation and similar hyaline alterations in the dermis. Thus, the acquired auto-immune disease with antibodies to ECM1 (LS) recapitulates the phenotype of the genetic loss of ECM1 (LS), confirming the central role of ECM1 deficiency in these diseases. Via epitope-mapping, Oyama, Chan (101) identified that sera from LS patients recognised ECM1 with specificity to the carboxyl-terminus and the second tandem repeat domain. The authors suggested that autoantibodies specific to ECM1 are present in high amounts in LS and have a direct implication to the disease pathology. As such, ECM1 is a target antigen for acquired

autoimmune skin disorders, as well as inherited skin disorders (102). These studies in both LP and LS clearly highlight the importance of ECM1 in maintaining homeostasis of the ECM.

12.10.3 ECM1 in epidermal barrier acquisition

One study conducted on the effect of corticosteroids, and the transcription factor Klf4, on *in utero* epidermal barrier acquisition, identified significant changes in ECM1 expression in murine skin in response to treatment with such drugs (88). Klf4 and corticosteroid treatment both accelerate lung epithelium and skin barrier acquisition; corticosteroids are administered to humans in the case of premature birth. Upregulation of *ECM1* mRNA was identified in response to both corticosteroid treatment (5.0-fold) and enhanced Klf4 expression (5.5-fold). Furthermore, significant downregulation of *ECM1* was identified in Klf4 knockout mice (3.0-fold). This study suggests ECM1 plays a role in epidermal barrier acquisition, and development and maintenance of dermal/epidermal ECM.

12.10.4 ECM1 in Endochondral Bone Formation

ECM1 has also been implicated in the regulation of endochondral bone formation in the perichondrium (connective tissue surrounding cartilage of the developing bones) (86, 87, 103-105). These studies show that ECM1 inhibits alkaline phosphatase activity in matrix mineralisation, as well as chondrocyte hypertrophy and proliferation. The activity of ECM1 was neutralised when a non-collagenous ECM component, cartilage oligomeric matrix protein (COMP), was bound to the EGF-like domain of ECM1. COMP is a protein essential for organisation and assembly of limb development and chondrogenesis regulation (cartilage development). Subsequently, the inhibitory interaction between COMP and ECM1 is suggested to regulate the level of endochondral bone formation.

12.11 ECM1 is expressed by leukocytes and regulates leukocyte cell function

12.11.1 ECM1 regulates Th2 cell migration

ECM1 has been implicated to carry out many roles in the immune response. In the first study by Li, Zhang (12), ECM1 was highly expressed in T_h2 cells in allergic airway

inflammation, and was 'crucial for the egress' of newly primed T_h2 cells from the lymph node to the site of inflammation. T_h2 cell migration requires the interaction of sphingosine-1-phosphate (S1P) with its receptor S1P1. The authors show a feedback loop, in which ECM1 directly binds the IL-2 receptor, activates the expression of the S1P transcription factor KLF2, and therefore stimulates further S1P receptor ($S1P_1$) expression. Subsequently, mutation or deficiency of ECM1 expression resulted in impaired T_h2 cell migration, and significantly reduced allergic airway inflammation. The authors concluded that ECM1 controls T_h2 cell lymph node migration to the site of inflammation, via this KLF2 and $S1P_1$ feedback loop dependent mechanism.

12.11.2 ECM1 suppresses T_h17 cell development

A study by Su, Chen (106) showed that ECM1 significantly affects T_h17 cell development in the murine multiple sclerosis model disease – experimental autoimmune encephalomyelitis (EAE). T_h17 cells are shown to be critical in the development of EAE. T_h17 cell generation requires active TGF-β, and αv integrins are critical regulators of TGFβ activation from its latent form. This study showed that ECM1 administration between day 1-7 of EAE induction, could suppress T_h17 cell responses as well as the development of EAE itself. The mechanism behind this T_h17/EAE suppression was ECM1 interaction with αv integrin, leading to blockage of αv integrin-mediated activation of latent TGF-β. Indeed, overexpression of ECM1 *in vivo* also dampened T_h17 responses and the development of EAE. This study shows that ECM1 is an important binding protein involved in TGF-β signalling and inflammatory cell responses.

12.11.3 ECM1 promotes follicular helper T cell differentiation and antibody production

A study by He, Gu (13) suggests that ECM1 could be a positive regulator of humoral responses. This study suggests ECM1 is a positive regulator of T-follicular helper cell (T_{fh}) differentiation, via repression of the IL-2-STAT5-Bcl6 signalling pathway. ECM1 knockout impaired T_{fh} cell differentiation and antibody responses, whereas exogenous ECM1 treatment promoted T_{fh} differentiation. In this manner, ECM1 enhanced T_{fh} germinal centre

responses and neutralizing antibody production in response to both influenza infection and immunized conditions; highlighting the critical role of ECM1 in inflammatory diseases.

12.11.4 ECM1 is expressed by macrophages and is essential for macrophage polarisation

ECM1 has been shown to be highly expressed by, and control M1MΦ polarisation in inflammatory bowel disease (IBD) (14). In this study they showed that ECM1 is strongly correlated with the pathogenesis of IBD, and that ECM1 is highly expressed in both mouse and human MΦ's in the colon with IBD. Further, MΦ's from ECM knockout animals were protected from IBD (DSS-induced), showed impaired pro-inflammatory functions, and resulted in the colon tissue being enriched/preferential for M2MΦ's; opposed to the inflammatory M1MΦ phenotype. This demonstrates that ECM1 is expressed by colonic MΦ's and plays a role in inflammatory diseases via MΦ-dependent mechanisms.

12.12 ECM1 regulates cellular architecture, ECM organisation, cell adhesion and migration

12.12.1 ECM1 maintains cell architecture, ECM organisation, cell adhesion and migration

A recent study by Utsunomiya, Utsunomiya (107) showed upregulation of a large number of genes associated with cell adhesion, ECM organisation, proliferation and cell migration in ECM1 siRNA silenced dermal fibroblasts. These ECM1 silenced cells exhibited delayed cell migration and contraction and had altered expression of fibrogenic and carcinogenic genes including laminin-331 and collagen-IV. Further, ECM1 was shown to bind and co-localise collagen-VII in immunoassays. They concluded that ECM1 knockdown leads to structural ECM dysregulation/disassembly and may result in microstructural abnormalities similar to the medical condition of LS.

12.12.2 ECM1 regulates actin cytoskeletal architecture via S100A4 and Rho-family GTPases

A study by Gómez-Contreras, Ramiro-Díaz (108) showed that ECM1 is essential in the regulation of cell architecture and microtubule organisation in triple-negative breast cancer cells. In their study, ECM1 siRNA silencing significantly distorted cellular architecture and diminished cell migration and adhesion. They attributed these features, at least in part, to

alterations in the Rho GTPase regulator protein Rho A, and S100A4 which is a calcium-binding protein that plays a role in various processes including cell morphology and motility. A similar recent study by Yin, Wang (109) suggested influence of ECM1 over the cytoskeleton in cancer cells via AKT/FAK/Rho signalling. They showed that the ECM1a isoform induces cancer cell tumorigenesis via a Gly-Pro-Arg motif of ECM1 interacting with integrin αXβ2. This in turn facilitated phosphorylation of AKT/FAK/Rho/cytoskeletal molecules, and conferred cisplatin resistance in cancer cells through up-regulation of CD326-mediated cellular stemness. Further, the ECM1b isoform (which they suggest is non-secretory) bound to myosin and blocked its phosphorylation, which impaired cytoskeleton mediated signalling evens in tumorigenesis. Together, these studies implicate significant influence of ECM1 over Rho signalling pathways, cellular architecture, cell adhesion and migration.

12.13 ECM1 in cancer: angiogenesis, cell migration and proliferation

12.13.1 ECM1 in Angiogenesis and Tumour Progression

ECM1 has been widely studied in the field of cancer, angiogenesis, and tumour progression as a pro-angiogenic factor. ECM1 is overexpressed in a variety of human carcinomas including thyroid, epithelial, cervical, gastric, lung, colon, prostate, and breast cancers (particularly ductal breast carcinomas) (85, 92, 97, 110-120). ECM1 is also overexpressed in response to the malignant transformation of cells, such as non-squamous epithelium, breast lobular/ductal epithelium, adenoepithelioma of the lung, colon and stomach, and thymus follicular adenomas (92, 110-115). Studies also focus on the use of ECM1 as a biomarker for prediction of both carcinogenesis, poor cancer prognosis, as well as a potential target for micro-RNA silencing as a strategy to battle cancer progression (112-115).

Some studies suggest interactions of ECM1 with several ECM proteins are responsible for regulation of tumour progression and angiogenesis. ECM1/domain-V of perlecan binding is shown to inhibit the anti-angiogenic properties of perlecan, thus stimulating angiogenesis and tumour progression (97, 116). ECM1/fibulin-1 binding via ECM1 second tandem repeat is suggested to reduce tumour invasion and transformation of fibrosarcoma cells via inhibition of fibulin-1 activity (92). ECM1/MMP-9 binding is suggested to regulate metastatic

potential of breast cancer cells and stimulate trastuzumab resistance (92, 97). The interaction between ECM1 and MMP-9 is implicated to regulate cell proliferation via activation of epidermal growth factor receptor (EGFR) and extracellular signal-regulated kinase (ERK) pathways (97, 117). ECM1 has more recently been suggested to promote the 'Warburg effect' via ECM1 regulated EGF-dependent ERK activity induced PKM2 phosphorylation (118). The Warburg effect is an 'oncogenic metabolic switch' which facilitates increased glucose uptake of cancer cells (favouring anaerobic glycolysis). Another study implicated the Warburg effect to be, at least in part, responsible for ECM1's association with tumour growth, migration and apoptosis (119). Finally, Steinhaeuser, Morera (120) showed that secreted ECM1 protein is a key angiogenic inducer, critical for endothelial network formation and endothelial feedback (epithelial-endothelial cell crosstalk) in angiogenesis. The authors implicated NOTCH proteins to be the target/responsible protein for ECM1 induced effects on endothelial network formation.

12.13.2 ECM1 is expressed in extracellular exosomes, and influences cytokine expression

Philley, Kannan (85) studied ECM1 positive exosomes isolated from sera of ECM1 positive breast cancer patients who had nontuberculous mycobacterium infections. ECM1 significantly influenced human T cell cytokine expression when co-cultured with $ECM1^{+}$ exosomes. They suggested that the presence of these $ECM1^{+}$ exosomes may induce production of immunosuppressive cytokines and facilitate immunosuppression and cellular transformation (e.g., EMT) of mycobacterium. As such, the authors suggest ECM1 is expressed as circulating exosomes, which allows ECM1 to conduct immunosurveillance and alter immune responses and cellular transformation.

12.14 Summary of the role of ECM1

ECM1 is an important protein which is expressed by leukocytes and stromal cells throughout the body and plays many important roles in both ECM structural integrity, cellular behaviour/architecture, and inflammatory/immune responses. Therefore, ECM1 has great potential to regulate both inflammatory and fibrotic molecular events throughout the course of wound healing with cardiac disease too. As such, ECM1 may represent a prime

novel therapeutic target to battle irreversible cardiac fibrosis. Investigation into the role of ECM1 in cardiac disease is warranted.

12.15 Preliminary data: ECM1 is upregulated in the ageing and diseased mouse heart

Prior to commencement of my PhD candidature (during my B. Biotechnology Honours year), we conducted preliminary experiments to assess whether ECM1 played a role in fibrotic cardiac disease. These experiments aimed to assess the expression levels of ECM1 in ageing and MI associated fibrotic and inflammatory disease in mice. As published (1), ECM1 mRNA ($p=0.0002$) and protein ($p=0.0006$) expression were significantly upregulated in the left ventricle (LV) of aging mice compared to young LV tissue (**Fig 1**). Following-MI, a significant upregulation of ECM1 mRNA ($p=0.004$) and protein ($p=0.005$) occurred early at day-3 in the 'infarct zone', relative to healthy non-infarcted LV (1). The 'border zone' showed upregulation in ECM1 mRNA but not protein (mRNA, $p=0.02$; protein, $p=0.89$) and no significant difference was seen in ECM1 expression in the 'remote zone'. Later, at day-28, these changes are beginning to resolve. There remained a slight numerical increase in ECM1 protein expression in the 'infarct zone', but this was no longer significant. To test if ECM1 is expressed by cardiac fibroblasts, we then cultured primary mouse cardiac CFbs; data not included in Hardy, Mabotuwana (1) publication. No ECM1 protein expression was detected under standard culture conditions, nor when stimulated with recombinant TGF-β1 (10ng/ml) or ANG-II (100 nM) (**Fig 2**). However, when recombinant ECM1 was added to primary mouse CFbs in culture (for 48 hours), it was sufficient to increase collagen production at both a low (20ng/ml) and high dose (200ng/ml) (**Fig 2**); to an extent comparable to TGF-β1 and ANG-II.

These preliminary experiments suggest that ECM1 plays a role in ageing associated fibrosis, as well as wound healing post-MI at an early inflammatory time-point. Further, ECM1 may act to stimulate fibroblast collagen-I production in fibrosis associated with ageing and MI, and that ECM1 may be derived from non-fibroblast cell types. As such, it is possible that ECM1 may be secreted by infiltrating leukocytes or non-fibroblast resident cardiac cells to act on fibroblasts as a pro-fibrotic stimulus. Such findings formed the basis of my thesis, and posed several questions centred on the role and cellular origins of ECM1 throughout the heart:

1. What cell(s) are responsible for ECM1 production in the healthy and diseased heart?
2. Where is ECM1 expression localised in the healthy and diseased heart?
3. Are our murine results reproducible in humans?
4. What are the cell signalling mechanisms underpinning the effect of ECM1 on cardiac fibroblasts/fibrosis?

It is evident that ECM1 warrants further investigation as a potential drug target for the development of new treatments for cardiac fibrosis. Ongoing research into the role ECM1 may be critical to understanding the mechanisms of fibrosis in a variety of different cardiac diseased states.

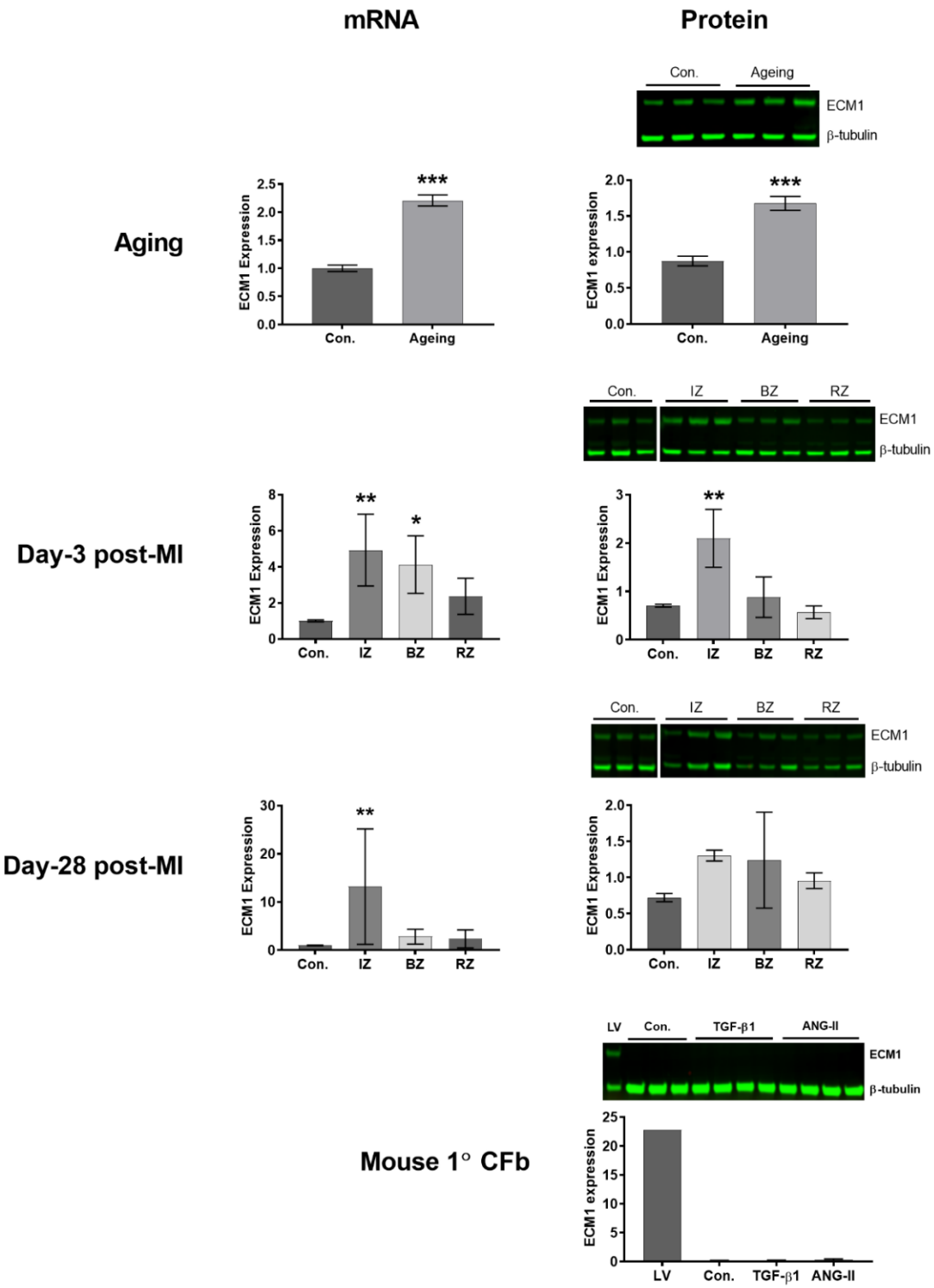

Figure 1: Reproduced from Hardy, Mabotuwana (1) with permission of the publisher (PLOS ONE). ECM1 mRNA and protein levels are upregulated in aging LV tissue and in the infarct zone day-3 post-MI, but ECM1 is not expressed by cardiac fibroblasts. ECM1 mRNA and protein (~75kDa) is upregulated in aging and specifically in the infarct zone of day-3 post-MI LV tissue; analysed by Student's T-test for Aging data, and ordinary one-way ANOVA with Dunnett's multiple comparisons post-hoc test for day-3 and day-28 post-MI

data. However, mouse primary cultured CFbs show no ECM1 expression under control conditions (Con.), nor in response to 48 h of treatment with recombinant TGF-β1 (10 ng/ml), or ANG-II (100 nM) (left); positive control shows ECM1 expression in mouse LV (LV - left lane). Data is expressed as mean ± SD. Control: n=3 mice for mRNA, post-MI: n≥6 mice/group for mRNA. Blot images of Day-3 post-MI, Day-28 post-MI and Mouse 1° CFb were cropped only to re-arrange the order of control lanes of the same blot. β-tubulin (~55kDa) is included as the loading control. All protein n=3 mice/group for each pathological state, and n=3 technical replicates/group for control Mouse 1° CFb, and n=4 for TGF-β1 and ANG-II Mouse 1° CFb. *p<0.05; **p<0.01; ***p<0.001 relative to control.

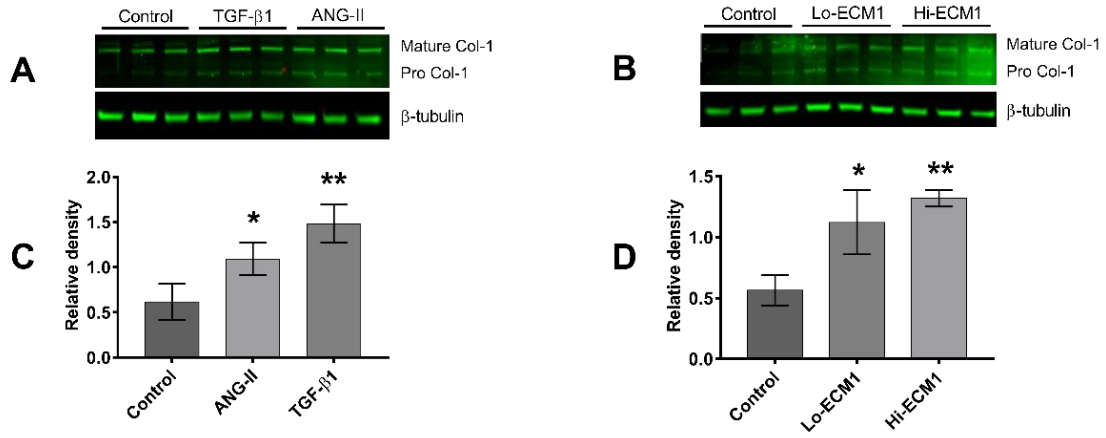

Figure 2: Collagen-I is upregulated in primary cultured mouse cardiac fibroblasts in response to ECM1, TGF-β1 and ANG-II. Collagen-I protein expression was analysed in primary mouse cardiac fibroblast cells cultured under standard conditions (control), and in response to 48 h of treatment with recombinant TGF-β1 (10 ng/ml), ANG-II (100 nM), low-dose ECM1 ('Lo-ECM1'; 20ng/ml), or high-dose ECM1 ('Hi-ECM1'; 200ng/ml) (n=3 each group). (A/B) Immunoblots of mature dimerised collagen-I protein (~270kDa), and pro-collagen-I protein (~170kDa) expression after treatment with recombinant TGF-β1 (A), ANG-II (A), or ECM1 (B) including β-tubulin (~55kDa) as a loading control. (C/D) Average relative band density analysed as combined mature dimerised collagen-I, and pro-collagen-I bands from the corresponding immunoblot for cells treated with TGF-β1 (C), ANG-II (C), or ECM1 (D); data is normalised against β-tubulin expression. All data is expressed as mean ± SD. * $p < 0.05$; ** $p < 0.01$.

12.16 Justification of the research question and novelty value

The diseased heart is subject to dramatic cellular and molecular changes in response to tissue damage. This leads to acute and/or prolonged inflammatory responses, ECM remodelling and fibrotic tissue formation, but the precise molecular mechanisms underpinning these events remain incompletely understood. Due to the clear importance of

inflammation in setting the stage for wound healing, particularly post-MI, therapeutics to target inflammation broadly, and specific inflammatory pathways, were an attractive approach to improve the mortality rates associated with MI. Unfortunately, since the 1960s clinical trials in this space have been either conflicting, inconsistent, unsuccessful, or unsafe. Similarly, a few treatments have successfully modified cardiac fibrosis itself, most probably due to indirect, secondary effects, and have become the cornerstones of current heart failure therapy. Despite this, the morbidity and mortality from heart disease remains high and alternative therapies are desperately needed to reduce the burden heart disease places on health care systems worldwide. As such, new research is direly needed.

A cornerstone of cardiovascular research is investigation of novel proteins and mechanisms which underpin cardiac wound healing. One novel mechanism is the inflammation-fibrosis crosstalk in wound healing post-MI. This novel axis of inflammation-fibrosis crosstalk may be why uni-directional therapies which target fibrosis or inflammation alone have failed to dramatically reduce the mortality associated with fibrotic cardiac diseases (10). As we have outlined, ECM1 interacts with many ECM proteins (16), acts as a structural basement membrane protein, and regulates inflammatory cell function (17-19). Further, the only study previously conducted on ECM1 in the heart, by Ramirez et al., 2012, identified an association with *ECM1* mRNA expression and left ventricular inflammation. In keeping with this literature, our preliminary results suggest that ECM1 plays a role in cardiac inflammation, ECM remodelling and fibrosis associated with MI. Thus, ECM1 could play a key role in both the inflammatory response and the development of fibrosis, or even facilitate inflammatory-fibrosis crosstalk in cardiac wound healing too. ECM1 shows promise and may prove to be an ideal therapeutic target for treatment of fibrosis associated with cardiac disease, particularly MI.

12.17 Aim and hypothesis of the dissertation

This project aims to characterise the cellular origins, expression patterns, and mechanistic role of ECM1 in the diseased heart undergoing inflammatory and fibrotic responses.

Hypothesis:

ECM1 regulates ECM remodelling and fibrosis after myocardial infarction by mediating signalling between inflammatory cells and fibroblasts.

My dissertation/thesis tested this hypothesis through the following aims:

1. **Define the cellular origin of ECM1 in the heart.** I have shown that ECM1 is expressed in the adult mouse heart at baseline, and is upregulated with age and in the infarct zone following MI. However, we did not detect ECM1 expression in fibroblasts cultured *in vitro*. Aim 1 will determine the cellular origin of ECM1 expression in the healthy and diseased heart.

2. **Define the expression of ECM1 in healthy human hearts and human heart disease.** Via the collaboration established through my dually awarded doctoral degree with UON and the Medical University of Graz, Austria (MUG), I will use a large human tissue bank available at MUG to characterise the expression of ECM1 ischaemic and dilated human heart failure patient tissue. This will allow us to confirm the relevance of my findings collected in animal models and inform us to what level my findings in the mouse model are translatable to humans.

3. **Investigate the signalling pathways involved in ECM1-dependent upregulation of cardiac fibroblast collagen-I expression.** We have shown that ECM1 increases the production of collagen-I in cardiac fibroblasts *in vitro*. However, the receptors/binding partners and intracellular signalling pathways that mediate this response remain unknown. Aim 3 is to define the underlying signalling pathways and thus potential therapeutic targets in our cardiac fibroblast primary cell culture model. In brief, cardiac fibroblasts will be cultured, treated with recombinant ECM1, and screened for intracellular signalling pathway changes in comparison to control (media alone treated) cells via phosphoproteomics and mass spectrometry approaches, and other biochemical techniques such as western blotting, qPCR, and wound healing assays.

12.18 Limitations of the research topic

The research topic addressed here focusses on cardiac fibrosis in the setting of experimentally induced MI in mice, and ischemic and dilated human heart failure. The methods of this thesis are pre-clinical and were designed to provide the first description of the spatiotemporal cellular origins of ECM1 in healthy and diseased human and mouse hearts, as well as ECM1 dependent human cardiac fibroblast (HuCFb) signalling mechanisms. The data presented in this thesis provides a fundamental cellular and molecular knowledge base for future work to determine the potential of therapeutically targetting ECM1 to ameliorate wound healing with fibrotic cardiac diseases. As such, the results presented in this thesis have the limitation of not directly addressing the translation of our findings to a clinical setting. However, here we describe the expression of ECM1 in human heart failure patient tissue, which is a crucial first step towards clinical translation. Finally, this study is limited by a lack of experiments utilising *in vivo* ECM1 genetic knockout/overexpression in the setting of experimentally induced MI in mice; as well as in human cell culture models. We note this as a critical next step for future research, and we have carried out the foundational work towards this goal by creating an ECM1 genetic knockout mouse model, and providing the first phenotyping data of these mice.

Despite limitations, the design and progression of experiments in my thesis was carefully planned, and provides a knowledge base of crucial descriptive and mechanistic data for future pre-clinical (using ECM1 genetic knockout/overexpression), and translational/clinical experiments to build on.

13. Materials and methods

13.1 Mouse studies and ethics

As published (1), male C57Bl/6 mice were used for all experiments, except for bone marrow cell (BMC) experiments where both male and female mice were used; young mice were 2-3 months old, aging mice were 18 months old. Mice were used with approval from the University of Newcastle's animal care and ethics committee (ACEC, approval numbers A-2014-409 & A-2014-435), and according to the NIH guidelines and the guidelines of the

Institutional Animal Care and Use Committee of UCSF the University of California. All experimental procedures conducted on mice were in strict accordance with the Australian Code of Practice for the Care and Use of Animals for Scientific Purposes. Animals were anesthetized with 5% isoflurane, and sacrificed via 5% isoflurane anaesthesia followed by exsanguination. All efforts were made to minimise animal suffering.

13.2 Human studies, ethics, and patient characteristics

As published (1), for the use of human right atrial appendage tissue, all patients provided written informed consent for tissue collection for experimental purposes, and all protocols were conducted in strict accordance with the Australian National Statement on Ethical Conduct in Human Research 2007 and approved by the University of Newcastle's Human Research Ethics Committee (HREC); approval number H-2014-0390. Written consent was obtained, and right atrial appendage tissue was collected from ischemic heart disease patients undergoing coronary artery bypass grafting procedure.

The use of human left ventricle tissue and biomaterials was approved by the Ethics committee of the Medical University of Graz (20-277 ex 08/09, 26-355 ex 13/14, 28-508 ex 15/16) and conformed to all pertaining regulations and the principles of the Declaration of Helsinki. Left ventricular cardiac samples were collected from ischemic cardiomyopathy (ICM), dilated cardiomyopathy (DCM) and non-failing (NF) controls (n=8/group) for immunoblotting at the time of cardiac explant. All ICM and DCM patients were male, NF included two females. The average age was 63.3 ± 1.8, 58.9 ± 3.0 and 64.4 ± 4.2 years, respectively (ICM, DCM, NF). The average ejection fraction was 27.5 ± 2.6%, 19.4 ± 1.9% and 61.9 ± 1,6%, respectively (ICM, DCM, NF). Left ventricular cardiac samples used for immunohistochemistry (IHC) were collected from heart disease patients at autopsy (n=12; 75% male; 66± 4.16 years, ICM n=8, NF n=4), all failing hearts with ischemic heart disease in clinical and pathological history. Ethics committee of the Medical Universitsy of Graz (31-288 ex 18/19). The ethical committee waived the requirement for informed consent when human tissue originated from deceased persons, all other persons provided written informed consent.

13.3 Analysis of published single-cell and single-nuclei RNA-sequencing data

Published single-cell (sc) RNA-Sequencing (RNA-seq) data of murine cardiac interstitial cells of ventricles from sham and MI hearts, from the Farbehi, Patrick (73) publication, are available from ArrayExpress (www.ebi.ac.uk/arrayexpress) under accession codes E-MTAB-7376. Briefly, 8-12 weeks old male C57Bl/6J mice were anaesthetised, intubated, hearts exposed, and the left anterior descending coronary artery ligated permanently. Hearts were harvested at 3- or 7-days post-surgery. Sham-operated mice were subject to the same procedure without ligation and cells isolated from sham or MI hearts were profiled for scRNAseq using the 10x Genomics Chromium system. Published mouse single-cell RNA-sequencing data post-MI scRNAseq data (ArrayExpress www.ebi.ac.uk/arrayexpress, accession codes E-MTAB-7376) were reanalysed using the Seurat R package 26, with UMAP dimensionality reduction calculated on the top 25 principal components. Cell labels were assigned using previous characterisations (Farbehi et al., 2019). Differentially expressed genes were calculated using the Seurat FindMarkers program with MAST testing 27, with a gene defined as DE if it obtained a Bonferroni-adjusted p-value < $1x10^{-05}$ and an absolute log fold-change difference > 0.25. For gene expression correlation analyses with Ecm1, Spearman correlation was calculated using the R cor.test function on log-normalised counts. For comparison of Ecm1 expression with ligand-receptor connections, we used a previous approach for modelling ligand-receptor communication between cell populations in scRNAseq data (Farbehi et al., 2019). Briefly, using a curated set of ligand-receptor pairs 28, a communication weight between a source (ligand-expressing) and target (receptor-expressing) cell type is calculated according to the fold-change difference of the ligand and receptor expression for the source and target cell populations, respectively, with reference to protein-protein association scores in the STRING database 29. Ecm1 expression was correlated (Spearman's Rho) with the number of outbound high-weighted paths (weight > 1.5) for each cell type.

Processed and annotated human heart single nuclei (sn)/scRNA-seq data (https://www.heartcellatlas.org), from the Litviňuková, Talavera-López (121) publication, was loaded in the Seurat R package for further analysis. A normalized gene expression score per cell base for ECM1 was extracted using the *AddModuleScore* function.

13.4 Preliminary studies: Inducing MI and pressure-overload in mice

As published (1), MI was surgically induced by performing left anterior descending (LAD) ligation surgery (122), as we have previously described in young mice. Briefly, mice were anesthetized, intubated, and placed supine on a heat mat to maintain their temperature at 37°C. For induction of MI, a thoracotomy was performed, and the LAD ligated using a 7-0 prolene suture. For induction of pressure-overload cardiomyopathy, a 6-0 polypropylene suture was tied around a 27G needle placed over the aortic arch, and the needle was removed. For both LAD-ligation and TAC, the chest was then closed, and the animal allowed to recover to day-3 or day-28 post LAD-ligation.

13.5 Tissue preparation and analysis

As adapted from publication (1), mice used in our preliminary studies were humanely euthanized as previously described (123) and whole hearts were surgically removed and perfused with 0.5 mL saline through the aorta, and the LV was snap frozen and stored at -80°C. For MI tissue, LV tissue was separated into three distinct zones prior to snap freezing depending on distance from the site of infarct: infarct zone, border zone, and remote zone. Protein was extracted from primary mouse and human CFbs and the following commercially sourced human cardiac cell lines: HuCFbs (Sigma Aldrich), coronary artery endothelial and smooth muscle cells (HCAEC & HCAESMC respectively; Sigma Aldrich), and human cardiac cardiomyocytes (HCM; PromoCell); n=1 technical replicates/cell line. BMCs for the below mRNA fluorescent in-situ hybridization (mRNA-FISH) protocol were extracted as described by Liu and Quan (124). BMCs were analysed whole (n=3) or separated in mononuclear and granulocyte cell fractions (n=4) with Ficoll-Paque PREMIUM 1.084 (GE Healthcare) as per the manufacturer protocol. Frozen tissue sections (day-3 post-MI) to be used in mRNA-FISH were sectioned at 8µm using a Leica CM1950 cryostat at -20°C, as per the manufacturer protocol.

Human samples were snap frozen in liquid nitrogen upon explantation and stored at -80°C. mRNA and protein were extracted from human samples and HuCFb cells, and subject to immunoblotting and/or qPCR analysis, as we have outlined below and as previously described (125, 126).

Extracted protein and mRNA was subject to western blotting and quantitative polymerase chain reaction (qPCR) analysis respectively, as we have outlined below and as previously described (125, 126). All *ECM1* mRNA expression data is expressed as fold-change in delta delta threshold cycle (ΔΔCt) relative to control *ECM1* mRNA expression and normalized to *Tpt-1* housekeeping gene or both *Tpt1* and *β-actin*. All mRNA expression data is expressed as ΔΔCt, relative to control mRNA expression, and normalised to *tpt1* housekeeping gene. All immunoblot protein expression data was normalised to either GAPDH, β-tubulin (55kDa) or β-actin (42kDa) as the loading control for relative band density analysis, but in the case of phosphoproteins and active β-catenin, data was normalised as a ratio of the active or phosphorylated form/total (non-phosphorylated). For specific methods of protein isolation and quantification, RNA isolation and quantification, SDS-PAGE, immunoblot, qPCR, IHC, *in situ* hybridisation (RNAscope), and our list of qPCR primer sequences see below; qPCR primer sequences are listed in Table 1 (1), and Table 2.

13.6 Protein extraction and quantification

As published (1), to isolate total protein for use in SDS-PAGE, samples were suspended in RIPA lysis buffer containing Roche cOmplete™, Mini, EDTA-free protease inhibitor and PhosSTOP™ phosphatase inhibitor cocktail (Sigma-Aldrich®) and homogenised using a Precellys®24 high-throughput tissue homogeniser as per the manufacturer's protocol. The concentration of protein lysate was quantified via BCA assay using a Pierce™ BCA Protein Assay Kit (ThermoFisher Scientific) as per the manufacturer's protocol.

13.7 RNA isolation and analysis

As published (1), for **Fig 1**, RNA isolation was conducted using TRIzol® Plus RNA purification reagents (Life Technologies) as per the manufacturer protocol. RNA samples were subject to DNase I treatment using a DNase I, Amplification Grade Kit (ThermoFisher scientific) as per the manufacturer protocol. The NCBI Primer-BLAST program was used to identify exon-spanning primers specific to each gene of interest to avoid any amplification of genomic DNA. Primers which satisfied the set parameters were screened using 'Primer3' software version 2.3.7 (127, 128). All forward and reverse primer sequences, amplicon length, and

accession numbers are outlined in **Table 1**. Reverse transcription PCR (RT-PCR) reactions for complementary DNA (cDNA) synthesis were conducted using a GeneAmp® PCR System 9700 (Applied Biosystems). Reverse transcription (RT) and cDNA synthesis was conducted with 200ng of RNA each from each individual sample using Oligo (dT)18 primers (Bioline), dNTP (Bioline) and a SuperScript® III (Invitrogen) First Strand Synthesis System for RT-PCR. All target and reference genes from cDNA transcripts were measured using quantitative real-time polymerase chain reaction (qPCR), with SYBR™ Green Master Mix (Life Technologies) reagents; amplification reactions were run using an Applied Biosystems® 7500 Real-Time PCR System (Applied Biosystems) instrument; 7500 Software v2.3 (Applied Biosystems). mRNA levels were quantified using the 2(-ΔΔct) method, normalized to Tpt-1 (for mouse mRNA) and β-actin (for human mRNA).

For **Fig 11B**, cells were treated with ECM1 (20ng/ml) in starving media or were untreated control cells (starving media alone) for either 3 h, 6 h or 16 h, as per the Cell culture procedures in main document. Cells were harvested/collected in 900 µl Trizol (LS Reagent, Ambion) and disrupted with mechanical forces. RNA was extracted with Trizol (LS Reagent, Ambion) and purified using RNeasy Mini Kits from Qiagen, including gDNA elimination steps as per the manufacturer's protocol. One µg of RNA was used for the synthesis of cDNA utilizing QuantiTect Reverse Transcription kits (Qiagen) and qPCR was performed with Advanced Universal SYBR Green Supermix (BIO RAD). The primers used are listed in **Table 2**.

Table 1: As published (1), qPCR target and reference gene primer specifications.

Gene	Forward Primer	Reverse Primer
Mouse ECM1	TAGTCCTGCCCGTGATGAGT	CCCTTCCACTTCCACAGAGC
Mouse Tpt-1	ATGACGAGCTGTTCTCCGAC	AACACCGGTGACTACTGTGC
Human ECM1	CTGCTGTGACCTGCCATTTC	TCCCCAGGACTCAGGTAACA
Human β-Actin	AGAGCTACGAGCTGCCTGAC	AGCACTGTGTTGGCGTACAG

Table 2: Human primers and their sequences used for HuCFb cell qPCR experiments

Gene	FW primer	REV primer

Human *Tpt1*	GGC ATG GTT GCT CTA TTG GA	ATT TCC CCT CCA CGG CTC AA
Human *Tgfb1*	ATT CCT GGC GAT ACC TCA GC	ATT TCC CCT CCA CGG CTC AA
Human *Tgfb2*	GAG AGG AGC GAC GAA GAG TA	TGA GCC AGA GGG TGT TGT
Human *CXCL1*	CAC CCC AAG AAC ATC CAA AG	CTT AAC TAT GGG GGA TGC AGG
Human *Wnt5a*	CTT TGG GGA TGG CTG GAA G	GGG TTA TTC ATA CCT AGC GAC
Human *ACTA2*	AGC GTG GCT ATT CCT TCG TT	CCC ATC AGG CAA CTC GTA ACT
Human *IL6*	TTC GGT CCA GTT GCC TTC TC	GTG AGT GGC TGT CTG TGT GG
Human *Col1a*	TCA GAA CAT CAC CTA CCA CTG	CCC CAT TCA TTT GTC TTT TTA
Human *IL1b*	GAT AAG CCC ACT CTA CAG CTG	GGC AGA CTC AAA TTC CAG CTT
Human *CCL2*	AGC AGC AAG TGT CCC AAA GA	GTG GAG TGA GTG TTC AAG TC
Human *TRAF2*	GCT GAC TTG GAG CAG AAG GT	GGA GAA GAT GGC GGG TAT G

Assays were validated by generating standard curves to evaluate the efficiency of each primer set. The specificity of PCR products was analysed via melt curve and gel electrophoresis. All target and reference genes from cDNA transcripts were measured using quantitative real-time polymerase chain reaction (qPCR), performed on a BIO RAD CFX384 and results were analysed using the CFX Manager Software. mRNA quantities were normalised using two housekeeping genes Tpt1 and β-actin, and final values calculated using the ΔΔCt method.

13.8 SDS-PAGE and immunoblot

As published (1), for fluorescent immunoblotting, SDS-PAGE was performed under reducing conditions. SDS sample buffer (MiliQ H_2O supplemented with 8% SDS, 30% Glycerol, 0.02% Bromophenol Blue, 0.25m Tris-HCl; pH8) and Bolt™ sample reducing agent (Life Technologies) was added to total protein lysate solution. Samples were then reduced at 90 °C for 10 min, and 30 µL total volume loaded into each well of Precast Bolt™ 4-12% Bis-Tris Plus Gels (ThermoFisher Scientific). Gels were then placed in a Mini Gel Tank (Life

Technologies) electrophoresis system containing Bolt™ MES SDS Running Buffer (Life Technologies), and 150V (constant volt) was applied for approximately 1h at room temp, or until the blue sample buffer had sufficiently run out of the gel casing. Gels were then transferred to nitrocellulose membranes. Membranes were blocked with Casein blocking buffer (Li-Cor Biosciences) for 1 hour at RT and incubated for 2 hours at RT or overnight at 4°C with primary antibodies in Casein Blocking buffer. Membranes were washed in PBS supplemented with 0.01% tween-20 (w/v) (PBS-T) then incubated with IRDye 800CW Donkey anti-rabbit (1:15,000) and IRDye 680LT Donkey anti-mouse (1:20,000, Li-Cor Biosciences 926-68022) secondary antibodies in Casein blocking buffer for 1 hour at RT. Membranes were washed PBS-T and PBS and imaged using a Li-Cor Odyssey CLx imaging system. Immunoblots were analysed using ImageJ software (version 1.49) to return a numerical value based on band density/intensity, to be used for quantification of protein expression as previously described (129, 130). All washing and incubation steps were performed on agitation. All casein blocking buffer used for dilution of antibodies was supplemented with 0.01% Tween-20 (w/v).

For chemiluminescent immunoblotting, SDS-PAGE was performed under reducing conditions. BioRad™ 4x XT sample buffer (BioRad) and 20x sample reducing agent (Life Technologies) was added to total protein lysate solutions, to a total volume of 30 µL. Samples were then reduced at 90 °C for 10 min and loaded into each well of Precast Bolt™ 4-12% Bis-Tris Plus Gels (ThermoFisher Scientific). Gels were then placed in a Mini-Gel Tank (Life Technologies) electrophoresis system containing Bolt™ MES SDS Running Buffer (Life Technologies), and 150V (constant volt) was applied for ~1 h at room temperature (RT), or until the blue sample buffer had sufficiently run out of the gel casing. Gels were then transferred to nitrocellulose membranes. Membranes were blocked with 5% skim milk powder suitable for microbiology (Sigma-Aldrich) in TBS supplemented with 0.01% tween-20 (w/v) (TBS-T) for 1 h at RT. Membranes were then washed once with TBS-T and incubated for 2h at RT or overnight at 4°C with primary antibody (Table S2) in 0.5% skim milk in TBS-T. Membranes were washed 3 times in TBS-T then incubated with IRDye 800CW Donkey anti-rabbit (1:15,000) and IRDye 680LT Donkey anti-mouse (1:20,000, Li-Cor Biosciences 926-68022) secondary antibodies in 0.5% skim milk in TBS-T for 1 h at RT. Membranes were

washed twice with TBS-T, once with TBS, and then imaged using a ChemiDoc™ Touch Imaging System (Bio-Rad). Immunoblots were analysed using Image Studio software (Lite version 5.2) to return a numerical value based on band density/intensity, to be used for quantification of protein expression. All washing and incubation steps above were performed on agitation.

Table 3: Primary antibodies used.

Antibody Name	**Cat#**	**Company**	**Concentration**
ECM1 for fluorescent immunoblotting	H-300	SantaCruz®	1:300
ECM1 for human Immunohistochemistry	ab126629	Abcam	1:100
ECM1 for chemiluminescent immunoblotting	HPA027241	Sigma-Aldrich	1:500
Erk1/2	4696S	Cell signalling technology	1:2000
Phospho-Erk1/2	4370S	Cell signalling technology	1:1000
P38	9212S	Cell signalling technology	1:2000
Phospho-P38	9216S	Cell signalling technology	1:500
AKT	40D4	Cell signalling technology	1:2000
Phospho-AKT	S473	Cell signalling technology	1:500
Collagen-I	ab21286	Abcam	1:250
β-tubulin	Ab6046	Abcam	1:1000
β-Actin	A3854	Sigma-Aldrich®	1:20,000
β-catenin	13-8400	ThermoFisher	1:1000
Active β-catenin	05-665	Sigma Aldrich	1:500
Total-MYPT	PA5-17164	ThermoFisher	1:1000
Phospho-MYPT (Thr696)	5163	Cell signalling technology	1:500
JNK1+JNK2+JNK3	ab179461	Abcam	1:1000

Phospho-JNK1+JNK2+JNK3 (phospho Y185 + Y185 + Y223)	ab76572	Abcam	1:1000
IkB alpha	MA5-15132	ThermoFisher	1:500
NF-κB p65	8242S	Cell signalling technology	1:2000
Phospho-NF-κB p65 (Ser468)	3039S	Cell signalling technology	1:500

13.9 RNAscope and Immunohistochemistry (IHC) in human heart failure tissues

Formalin-fixed paraffin-embedded (FFPE) tissue sections to be used in IHC were cut between 2-4µm, mounted onto microscopy slides, and allowed to dry overnight at 37°C.

RNAscope® was conducted according to the RNAscope 2,5 HD Detection Kit (Red) manual, with/without the "Target Retrieval solution" for 15 min (n=2 no retrieval, n=1 retrieval; n=3 total).

For IHC, tissue sections were de-waxed in xylene (2x 10 min), followed by incubation in absolute alcohol for 5 min. Tissue was then rehydrated in a series of 90, 80, 70 and 50% alcohol, followed by one wash in phosphate buffered saline (PBS, pH 7.3) for 5 min. Antigen was unmasked/retrieved by treating with 0.1% Sodium-Citrate-Puffer (pH 6.0) for 40 min at 150 watt in a microwave. Tissue sections were cooled in the antigen retrieval solution for 20 min at RT. Tissue sections were then washed well in 2 changes of distilled water (5 min each) and transfer to PBS. Endogenous peroxidase staining was blocked using 3% H_2O_2 in methanol for 15 min at RT. Sections were washed 3 times in PBS for 3 min each. Antibody was then applied to tissue sections in 1:50 in Dako antibody diluent (cat# S2022) and incubated for 60 min at RT. Tissue sections were washed 3 times in PBS for 3 min each. UltraVision Large Volume Detection Kit was then applied to tissue (Thermo Scientific TL-125-HL) and incubated for 30 min at RT. Sections were then washed 3 times in PBS for 3 min each. Staining was visualised by applying AEC Substrate Chromogen (Ready to use, Dako cat# K3464) and incubated for 10 min at RT. Sections were washed 3 times in PBS for 3 min each and nuclei were counterstained with Mayer´s haematoxylin for 30 sec. Slides were washed in 2 changes of in tap water at 3 min each, and slides mounted with coverslips in Aquatex (Merck cat# 1.08562.0050).

13.10 Cell culture

As adapted from publication (1), specific primary mouse CFb and primary human CFb cell culture methods are outlined below. Briefly, mouse primary CFbs were serum starved for 24 h, followed by treatment with either recombinant angiotensin-II (Ang-II; 100 nM), transforming growth factor β1 (TGF-β1; 10 ng/ml) or Complete CFb Media alone, for 48 h. Primary human CFb cells were cultured under standard conditions. Cell culture of commercially sourced HuCFb, HCM, HCAEC and HCASMC cell lines were performed with recommended reagents as per the manufacturer's protocols. However, the "starving media" formulation, used also with HuCFb cells, was of DMEM/F-12 GlutaMAX™ (ThermoFisher, cat# 31331028) supplemented with 0.5% fetal bovine serum (FBS, ThermoFisher, cat# 10099141).

Briefly, HuCFbs (Sigma Aldrich, cat# 306-05A) cells were cultured to 70% confluence, growth media replaced with starving media for 16 h, followed by treatment with recombinant proteins in starving media at the following concentrations: ECM1 (20 ng/ml; R&D systems, cat# 3937-EC), and TNF-α (20 ng/ml; Gibco™, cat# PHC3011). Cells were treated at various time-points (as detailed in results) to investigate cell signalling pathway activation and collagen-I expression. Protein and mRNA were extracted from cells for use in SDS-PAGE, Western Blot, and qPCR. Alternatively, MTT Cell Proliferation Kit I (Roche, Cat# 11 465 007 001) and wound healing assays were performed on live HuCFb cells in culture; methods are specified below. Protein lysates from cultured HuCFb cells were also used for phosphoproteomics, and his-tag dependent pull-down of ECM1 protein-protein binding partners followed by mass spectrometry (in-gel digestion workflow). For specific methods see below. All mass spectrometry proteomics data have been deposited to the ProteomeXchange Consortium via the PRIDE (131) partner repository with the dataset identifier PXD027626.

13.11 Mouse primary cardiac fibroblast cell culture

As published (1), LVs were minced in 1x Digestion Media (200 U/mL Collagenase II, 400 µg/mL Trypsin in HBSS) and incubated at 37°C for 5 min. The first digestion supernatant was

discarded, and the following 8 digestions were collected, filtered (100µm), diluted 1:2 in Complete Fibroblast Media (1x High Glucose DMEM supplemented with 10% foetal bovine serum, 2mM L-glutamine, 1mM sodium pyruvate, 100 U/mL Penicillin, 100 µg/mL Streptomycin), and centrifuged (300g, 10 min, 4°C). The pellet was resuspended in fresh media and plated for 2 hours to allow fibroblast adherence. Fresh media was applied, and cultures maintained in a humidified incubator at 37°C with 5% CO_2. Cardiac fibroblast cells were cultured to passage 3 and stored at -80 °C in fibroblast storage media. For this project, cells were revived from passage 3, placed immediately into Complete Fibroblast Media, and cell suspension was transferred to Cellstar® 6-well cell culture plates (Greiner bio-one) at 100,000 live cells/well, and incubated at 37 °C with 5% CO_2. Media was changed every 2 days until cells reached 80% confluence. Cells were passaged once, allowed to reach 80% confluence, then incubated with serum-free media for 24 h at 37 °C with 5% CO_2, followed by treatment with either recombinant angiotensin-II (Ang-II; 100 nM), transforming growth factor β1 (TGF-β1; 10 ng/ml) diluted accordingly in complete fibroblast media, for 48 h. To estimate live cell numbers, all cells were counted with a Countess™ Automated Cell Counter (Invitrogen™) as per the manufacturer protocol.

13.12 Human primary cardiac fibroblast cell culture

As published (1), explant primary culture was conducted on right atrial appendage tissue. Briefly, tissue was minced and incubated with agitation in 1X Digestion Media (200 U/mL Collagenase II (Cat# 17101-015, ThermoFisher Scientific) and 400 mg/mL Trypsin (Cat# 27250018, ThermoFisher Scientific) in HBSS (Cat# 14025092, Life Technologies) at 37°C for 30 min. 1X Digestion Media was quenched with Complete Fibroblast Media (DMEM/F12, Cat#11320033, Life Technologies) media supplemented with 20% foetal bovine serum (Cat#SFBS-F, Bovogen Biologicals), 1 mM sodium pyruvate (Cat# 11360070, Life Technologies), and Pen/Strep (100 U/mL Penicillin, 100 mg/mL Streptomycin, Cat# 15070063, Life Technologies). Tissue was plated and incubated in fresh Complete Fibroblast Media to allow cardiac fibroblasts to exit. Cultures were maintained in a humidified incubator at 37°C with 5% CO2. Cells were further expanded, and protein extracted.

13.13 mRNA-FISH

As published (1), oligonucleotide mRNA FISH probes were sourced from LGC Biosearch Technologies (Stellaris) for both 'Ship Ready' Mouse GAPDH, and custom Stellaris made Mouse *ECM1*; *ECM1* and GAPDH probe sets were conjugated with Quasar 670 dye. mRNA-FISH was conducted on fresh extracted BMCs, and cryostat-sectioned 8 µm frozen tissue sections as per the Stellaris 'Cells in Suspension' and 'Frozen Tissue' RNA FISH protocols. Cells and tissue were imaged using fluorescence microscopy (Zeis; Axio Imager M2) under DAPI and Cy5 channels to detect nuclear stain 4',6-Diamidino-2-Phenylindole, Dihydrochloride (DAPI) and Quasar 670 dye, respectively.

13.14 Flow cytometry

As published (1), bone marrow cells were collected from 4 mice. Cells were blocked with Fc block (anti-CD16/32) for 30 min and stained with the antibodies depicted in Table 4. Staining and washing steps were performed with FBS stain buffer (554656, BD Biosciences). Samples were acquired on a BD LSR Fortessa X-20 flow cytometer.

Table 4. As published (1), flow cytometry antibody specifications.

Antibody	Catalogue #	Clone	Fluorophore	Assay dilution	Source
Rat Anti-Mouse I-A/I-E (MHC2)	563414	M5/114.15.2	BV711	1/1000	BD Biosciences
Rat Anti-CD11b	562287	M1/70	PE-CF594	1/750	BD Biosciences
Rat Anti-Mouse F4/80	565635	T45-2342	BV480	1/100	BD Biosciences
Rat Anti-Mouse CD117	563399	2B8	BV650	1/200	BD Biosciences
Hamster Anti-Mouse CD11c	560584	HL3	PerCP-Cy5.5	1/100	BD Biosciences
Rat Anti-Mouse CD3	564010	17A2	BV786	1/50	BD Biosciences
Rat Anti-Mouse Ly-6C	562727	AL-21	BV421	1/200	BD Biosciences

Rat Anti-Mouse CD45	552848	30-F11	PE-Cy7	1/1000	BD Biosciences
Rat Anti-Mouse Ly-6G	561105	1A8	FITC	1/100	BD Biosciences
Hamster Anti-Mouse FcεRI-α	134308	MAR-1	PE	1/400	Biolegend

As published (1), flow cytometry data were analysed using FlowJo (version 10). Cells were gated using FSC-A vs SSC-A, and single-cells identified using FSC-A vs FSC-H. Of these populations, 50,000 cells from each animal were downsampled and concatenated to one .fcs file. t-distributed stochastic neighbour embedding (tSNE) analysis was performed on the concatenated sample containing the gated populations from all four samples combined. For this, all compensated channels were assessed (FITC, PerCP-Cy5.5, BV421, BV510, BV650, BV711, BV786, PE, PE-CF594, PE-Cy7, APC) under the following tSNE settings: Iteration 1000, Perplexity 20, Eta 200, Theta 0.5. Histograms established from the same plot show the differential expression of the cell markers in ECM1+ and ECM1- cells.

Similarly, for standard flow cytometry presented in **Fig 13C**, bone marrow cells were collected from 3 WT mice, and 3 ECM1Δ2 homozygous knockout mice. Cells were blocked with Fc block (anti-CD16/32) for 30 min and stained with the antibodies depicted in Table 4 with the addition of Siglec-F (1/25 dilution, BD Biosciences cat# 565183, fluorophore APC-R700, clone E50-2440). Staining and washing steps were performed with FBS stain buffer (554656, BD Biosciences). Samples were acquired on a BD LSR Fortessa X-20 flow cytometer. Flow cytometry data was exported as .fcs files and analysed with the program FlowJo (BD Biosciences, versions 10.6 and 10.7). Individual populations were identified with the gating strategy indicated in **Table 5**. Gating strategies for each cell population were identified and kept constant throughout different experiments for comparable results. No changes were made to any gates within the same experimental group of samples acquired on the same day. Data were then exported to Microsoft Excel and converted to a proportion (%) of the total number of leukocytes present in the bone marrow. This was done by normalising leukocyte sub-populations to the number of total CD45+ leukocytes counted (e.g., total neutrophil number/total $CD45^+$ cell number).

Table 5. Flow cytometry gating strategy for Fig 13C.

Cell type	Gating strategy
Neutrophils	CD45+, Ly6G+, F4-80-
Mast cells	CD45+, Ly6G-, CD117+, Ly6C-, Fcer1a+
Monocytes	CD45+, Ly6G-, Ly6C+, CD3-, CD11b+, MHC2-, CD11c-, F4-80+
Macrophages (Ly6C High)	CD45+, Ly6G-, SiglecF-, Ly6C+, F4-80+, CD3-, FSC/SSC, Ly6C high
Macrophages (Ly6C Low)	CD45+, Ly6G-, SiglecF-, Ly6C+, F4-80+, CD3-, FSC/SSC, Ly6C low
B cells	CD45+, lymphocytes, CD3+, Ly6G-, SiglecF-, Fcer1a-, F4-80-, MHC2+
T cells	CD45+, lymphocytes, CD3+, Ly6G-, SiglecF-, Fcer1a-, F4-80-, MHC2-
NK-cells	CD45+, lymphocytes, Ly6G-, MHC2-, CD11b+, CD3-
Dendritic cells	CD45+, MHC2+, CD11b+, CD11c+
Eosinophils	CD45+, SiglecF+, CD11c- (Eosinophils). Further gating for CD3-, MHC2-, Ly6G-, F4-80+ was conducted to produce a cleaner population.

13.15 Phospho-proteomics

Cells were lysed in lysis buffer (6M guanidine hydrochloride, 10 mM Tris(2-carboxyethyl)phosphine hydrochloride, 40 mM 2-chloroacetamide in 100 mM Tris-HCl pH 8.5) using a sonication probe at 90% amplitude (counting to 1500 J), reduced, and alkylated for 10 min at 95 °C and centrifuged for 30 min at 3500x*g* and 4 °C to remove cell debris. Protein was precipitated with acetone, resuspended in 4% sodium deoxycholate (w/vol) in 100mM Tris-HCl (pH=8.5) and estimated using the PierceTM BCA Protein Assay. One mg protein was digested with Promega modified trypsin, followed by phosphopeptide enrichment according to (132) using Venator Sachtopore NP TiO2 beads (SNX 010S003, 3 µm - 100Å, #11110007). Half of each sample was measured in duplicate by nano-HPLC (Dionex Ultimate 3000) equipped with an Aurora Series Emitter nanocolumn with CSI fitting (C18, 1.6 µm, 120 Å, 250 x 0.075 mm; IonOpticks, Melbourne, Australia). Separation was carried out at 50 °C at a flow rate of 300 nL/min using the following gradient, where solvent A was 0.1 % formic acid in water and solvent B was acetonitrile containing 0.1 % formic acid: 0-18 min: 2% B; 18-160 min: 2-25% B; 160-167 min: 25-35% B, 167-168 min: 35-95% B; 168-178 min: 95% B, 178-178 min: 95-2% B; 178-193 min: 2% B. Peptides were detected on

a Thermo Orbitrap velos pro mass spectrometer operated in positive ion mode by alternating full scan MS (m/z 300 to 2,000, 60,000 resolution) and MS/MS by HCD of the 10 most intense peaks in the ICR cell with dynamic exclusion enabled. The MS/MS data were analysed for protein identification and label free quantification using MaxQuant 1.6.2.10 against the public database Swissprot with taxonomy *Homo sapiens* and common contaminants (downloaded on 16.04.2019, 20,482 sequences). Carbamidomethylation on Cys was entered as fixed modification, oxidation on Met and phosphorylation on Ser/Thr as variable modifications. Detailed search criteria were used as follows: trypsin, max. missed cleavage sites: 2; search mode: MS/MS ion search with decoy database search included; precursor mass tolerance +/- 4.5 ppm; product mass tolerance +/- 20 ppm; acceptance parameters for identification: 1 % PSM FDR; 1% protein FDR and 1% site decoy fraction. In addition, label free quantitation including the match between runs feature of MaxQuant was performed (133), requiring a minimum of 2 ratio counts of quantified razor and unique peptides. Data processing was performed using Perseus software version 1.6.5.0, following the proposed workflow for label-free phosphoproteomic data (134); http://www.coxdocs.org/doku.php?id=perseus:user:use_cases:modifications (last accessed 30/08/2021). Contaminants and reverse phosphorylation sites created during database searches were removed. Intensities were log2 transformed to lower the effect of the outlier values, filtered for a localization probability of >75% and 6 valid values in at least one group, respectively. Missing intensities were replaced with random values taken from the Gaussian distribution of values using default parameters (width of 0.3 and downshift of 1.8), to simulate an intensity value for those low abundant phosphosites. Two-sample t-test with subsequent multiple testing correction by Permutation-based FDR method were used to identify altered phosphorylation sites (s0 = 0.1, FDR = 0.05 with reported q-value and 250 randomizations). For the calculation of signalling scores of averaged group ratios, PHOTON (135) implemented in Perseus version 1.6.5.0 was used, on our ECM1 treated HuCFb phosphoproteomics data as a ratio of ECM1/control with a two-sided PHOTON test, following tutorial data on GitHub (https://github.com/jdrudolph/photon). Protein network data for *Homo sapiens* (v11.0) was downloaded from string database (136). For all additional gene ontology (GO) enrichment analysis, the GOnet/DICE online tool was used (GOBP, GOCC or GOMF; q-value threshold ≤ 0.05), developed and described by (137).

13.16 Gene ontology testing

For all additional gene ontology (GO) enrichment analysis, “GOnet”/”DICE” online tool was used (GOBP, GOCC or GOMF; q-value threshold ≤ 0.05), developed and described by (137).

13.17 His-tag dependent pull-down of ECM1 protein-protein binding partners

A purified HuCFb membrane/membrane-associated protein lysate was prepared using a Mem-PER™ Plus Membrane Protein Extraction Kit (ThermoFisher, cat# 89842), as per the manufacturer’s protocol. Twenty ug of purified membrane/membrane associated HuCFb lysate were used per sample. One set of membrane/membrane-associated HuCFb lysate samples (20 ug) were made up to a total volume of 200 µl with either Mem-PER™ Plus Membrane Protein Extraction Kit solubilisation buffer at the supplied concentration (1x detergent samples). A second set of membrane/membrane associated HuCFb lysate samples (20 ug) were made up to 200 µl with a mixture of solubilisation buffer and salt buffer to achieve a 1 in 4 diluted detergent concentration (1/4x detergent samples); the salt buffer formulation was 300 mM NaCl, 50 mM Na_3PO_4, pH 7.4. One mg (25 ul) of Dynabeads™ His-Tag Isolation and Pulldown (ThermoFisher, cat# 10103D) were used per sample and prepared by first washing beads once with His-IP lysis buffer (50 mM Na_3PO_4, 300 mM NaCl, 0.01% Tween-20, 1% Triton x-100, 1x protease inhibitor [Roche, ref# COEDTAF-RO], pH 8) by pipetting beads up and down in solution, followed by placing tubes on a magnetic rack for 1 min to pellet Dynabeads™ and allow aspiration of wash supernatant. All following bead wash steps were conducted in this manner; similar to the Dynabeads™ His-Tag Isolation and Pulldown manufacturer’s protocol. Washed Dynabeads™ were then incubated with His-IP lysis buffer containing 500 ng recombinant human ECM1 protein (ECM1 samples; R&D Systems, # 3937-EC-050), or buffer without recombinant ECM1 protein (control/CT samples) for 10 min at RT on constant rotation/inversion. ECM1 and control (no protein) bound beads were then washed 3 times with His-IP wash buffer (50 mM Na_3PO_4, 300 mM NaCl, 0.01% Tween-20, 1x protease inhibitor [Roche, ref# COEDTAF-RO], pH 8) and then incubated with either our previously prepared 1x detergent samples or our 1/4x detergent samples of purified membrane/membrane-associated HuCFb protein lysate, for 45 min at RT on constant rotation/inversion. After 45 min, protein-protein interactions

were covalently crosslinked by adding 2.88 µl of a 12.5 mM BS3 (ThermoFisher, cat# 21580) solution (in milli-q H_2O) to the bead-HuCFb lysate sample solution (a ~20x molar excess of BS3, relative to HuCFb protein, was used). The resulting BS3-bead-HuCFb sample solutions were allowed to incubate for 30 min at RT on constant rotation/inversion to achieve protein-protein crosslinking. BS3 crosslinking reactions were then quenched by addition of 8.2 µl of 0.5 M Tris (in milli-q H_2O, pH 7.5) to achieve a final concentration of 20 mM and were incubated for 15 min at RT on constant rotation/inversion. Beads were then washed 3 times in His-IP wash buffer. The resulting purified crosslinked protein-protein complexes were then eluted from Dynabeads™ by resuspending beads in 30 µl of electrophoresis sample buffer containing BioRad™ XT sample buffer (BioRad) and XT sample reducing agent (Life Technologies), followed by reducing at 90 °C for 10 min. Eluted samples in reduced buffer were then aspirated off Dynabeads™ and directly loaded into Precast Bolt™ 4-12% Bis-Tris Plus Gels (ThermoFisher Scientific), in a Mini Gel Tank (Life Technologies) electrophoresis system containing Bolt™ MES SDS Running Buffer (Life Technologies). 150 V (constant volt) was applied until the blue Coomassie dye front had migrated sufficiently into the tip 1-2cm of the gel. Gel bands containing gel filtered BS3 crosslinked protein-protein binding complexes were then carefully cut out (below the foot of the loading well but above the Coomassie dye front) and stored in 20% ethanol in milli-q H_2O (w/v) at -20 until in-gel digestion for proteomics.

13.18 In-gel proteomics digestion and mass spectrometry of samples from His-tag dependent pull-down of ECM1 protein-protein binding partners

Gel bands from the 12% Bis-Tris Plus Gel were reduced, alkylated and digested with Promega modified trypsin according to the method of (138). Resulting Peptides were acidified with formic acid (final concentration of 0.1%) and analysed by nano-HPLC (Dionex Ultimate 3000) equipped with an Aurora (Ionoptics) nanocolumn (C18, 1.6 µm, 250 x 0.075 mm). Separation was carried out at 50 °C at a flow rate of 300 nL/min using the following gradient, where solvent A is 0.1% formic acid in water and solvent B is acetonitrile containing 0.1% formic acid: 0-18 min: 2% B; 18-100 min: 2-25% B; 100-107 min: 25-35% B, 107-108 min: 35-95% B; 108-118 min: 95% B, 118-118 min: 95-2% B; 118-133 min: 2% B. A maXis II ETD mass spectrometer (Bruker) was operated with the captive source in positive

mode with following settings: mass range: 200-2,000 m/z, 4 Hz, capillary 1,600 V, dry gas flow 3 L/min with 150 °C, nanoBooster 0.2 bar, precursor acquisition control top20 (CID). The LC-MS/MS data were analysed using Data analysis software (Bruker) with the Sum Peak algorithm, and by MaxQuant 1.6.1.0 by searching the public Swissprot database with taxonomy *Homo sapiens* and common contaminants (downloaded on 16.04.2019, 20482 sequences). Carbamidomethylation on Cys was entered as a fixed modification and oxidation of methionine as a variable modification. Detailed search criteria were used as follows: trypsin, max. missed cleavage sites: 2; search mode: MS/MS ion search with decoy database search included; precursor mass tolerance +/- 0.006 Da; product mass tolerance +/- 80 ppm; acceptance parameters for identification: 1% PSM FDR; 1% protein FDR. Data processing was performed using Perseus software version 1.6.6.0. Contaminants and reverse protein sequences created during database search were removed. Intensities were log2 transformed to lower the effect of the outlier values, filtered for 3 valid values in at least one condition and normalised on the median of each column (by subtraction). For protein groups missing values an imputation step was performed. Briefly missing values were replaced with random values taken from a shifted Gaussian distribution of all valid values (width of 0.3 and downshift of 1.8 separately for each column), to simulate an intensity value for those low abundant protein groups. For statistical analysis, a Two-sample t-test was performed to identify significantly enriched proteins in the ECM1 bound samples (p-value ≤ 0.05); the p-value was not adjusted by multi-testing correction (since otherwise no significant results were left). Following this, significantly bound ECM1 proteins from 1x detergent sample and 1/4x detergent sample lists were compared in a Venn diagram, and common proteins taken as our final high confidence list of ECM1-HuCFb binding partners (**Supplementary table 14**).

13.19 MTT assay

Cell Proliferation Kit I (Roche, Cat# 11 465 007 001) MTT assay was conducted on HuCFbs cultured in Greiner CELLSTAR® 96-well plates (cat# M0562) performed as per the manufacturer's protocol with readout time-points of 24, 48 and 72 hours; starving media was supplemented with 0.5% FBS instead of 10% FBS.

13.20 Wound healing assay

HuCFbs wound healing assays were cultured in Ibidi® culture-inserts (cat# 80369), inserted into each well of a 12-well cell culture plate (ThermoFisher, cat# 150628). Cells were incubated with starving media for 16 h, Ibidi® culture-inserts removed, media aspirated, and replaced with starving media containing recombinant human ECM1 (20 ng/ml), or starving media with no recombinant human ECM1 (control). Phase contrast images of the cell gap were acquired hourly at 5x with a Zeiss Cell Observer microscope. Collected images were analysed where the mean of all 4 positions per well were plotted, and rate of migration per each hour calculated. An equation was fitted over the plotted functions and the inclination (slope) during the 24-hour active migration phase was calculated and compared between control and ECM1 treated groups. For visualisation, analysis was also conducted on group dependent differences in the change in rate of migration over time between control and ECM1 using two-way ANOVA by first normalising the growth rate of all replicates/samples to be equal at time zero.

13.21 Statistical analysis

All datasets were assessed for normalcy of distribution (parametric distribution) using Shapiro-Wilk tests. Parametric data were represented as mean ± standard deviation and were analysed using t-tests for two groups, ANOVA for more than two groups. Non-parametric data were analysed using appropriate alternative non-parametric test equivalents (e.g., Mann-Whitney tests, Kruskal-Wallis). All tests were conducted with an assigned significance level of $p<0.05$. Statistical analysis of scRNAseq and proteomics experiments are provided above in methods.

14. Results

14.1 ECM1 is expressed in BMCs and infiltrating cells in the infarct zone post-MI

Our preliminary study suggested that primary mouse CFbs do not express ECM1 protein under standard culture conditions, nor when stimulated with recombinant TGF-β1 (10

ng/ml) or ANG-II (100 nM) (**Fig 2**) (1). Thus, the cellular origin of ECM1 observed in LV samples remained unknown.

All data presented from this point onward were generated during my PhD candidature. As published (1), we investigated if ECM1 originated from other resident cardiac cells or infiltrating inflammatory cells (leukocytes) in the heart. We cultured each of the major resident cell types in the heart separately to assess ECM1 expression: primary human CFbs (1°CFb), and cell lines of human cardiac fibroblasts (HuCFb), human cardiac cardiomyocytes (HCM), human coronary artery endothelial cells (HCAEC), human coronary artery smooth muscle cells (HCASMC) and differentiated-HCASMC cells. No ECM1 protein was detected from any cell type (**Fig 3A**). To investigate the possibility that ECM1 is of inflammatory cell origin in the heart, bone marrow cells (BMCs) were then extracted from young healthy mice. ECM1 protein was highly expressed in BMCs, and when separated into monocyte and granulocyte cell fractions, there was significantly more ECM1 expression in the granulocyte fraction of BMCs (**Fig 3A**). *ECM1* mRNA-FISH was then conducted on BMCs to confirm mRNA expression (**Fig 3B**), followed by mRNA-FISH on frozen LV tissue sections from day-3 post-MI animals to further investigate the cellular origin of ECM1 (**Fig 3C**). *ECM1* mRNA was highly localized to the dense inflammatory cell infiltrate of the infarct and border zones. Only minor expression of *ECM1* was seen surrounding cardiomyocytes of the remote zone, with no *ECM1* expression seen within cardiomyocytes.

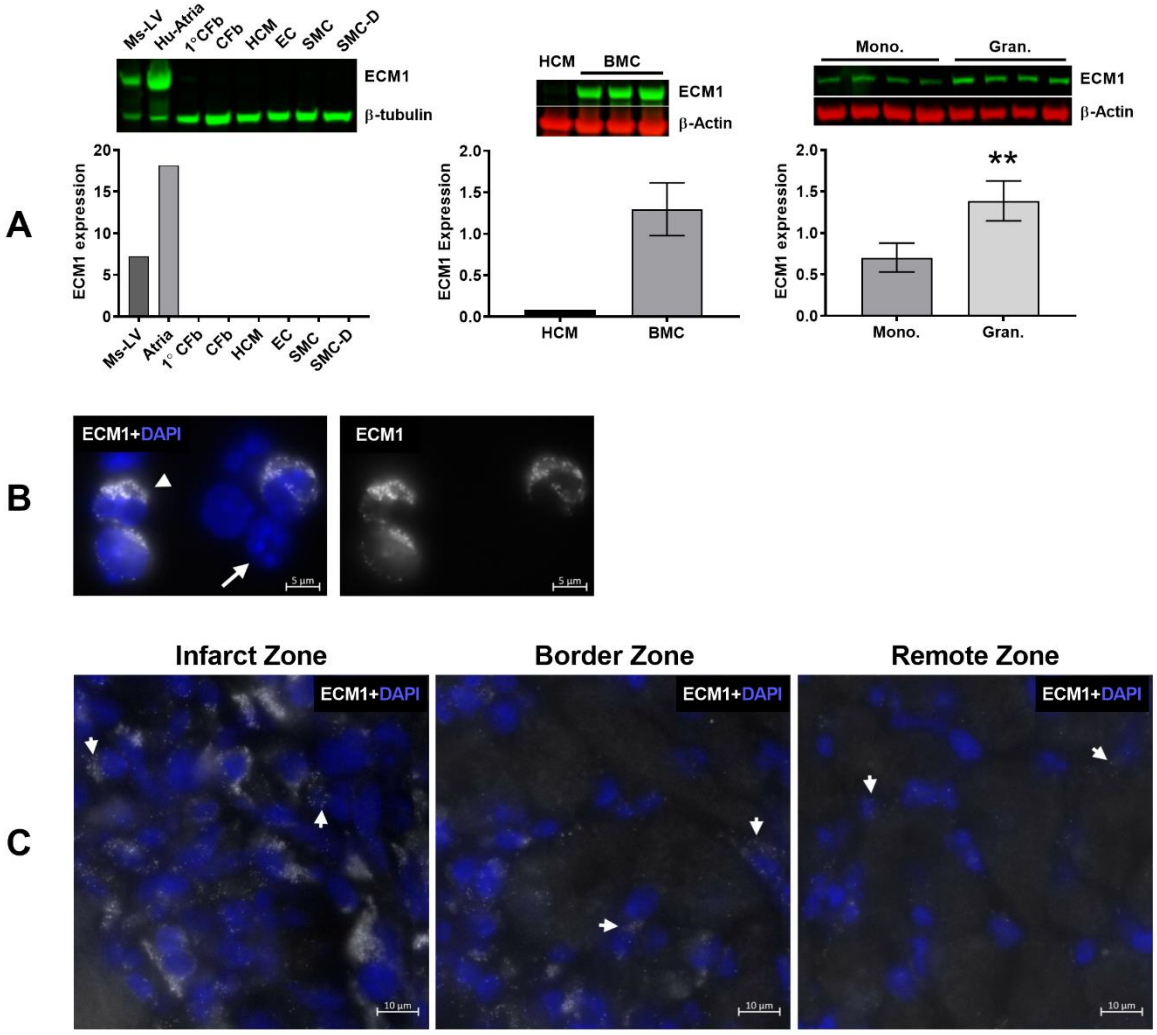

Figure 3: Reproduced from Hardy, Mabotuwana (1) with permission of the publisher (PLOS ONE). ECM1 is not expressed by resident cardiac cells, but is highly expressed in bone marrow cells (BMCs) and cells in the infarct zone day-3 post-MI. A) Immunoblot of ECM1 protein expression (~75kDa) in primary human CFbs, and cell lines: human cardiac fibroblasts (CFb), human cardiomyocytes (HCM), human coronary artery EC (EC), SMC (SMC) and SMC differentiated (SMC-D) cell lines (Left). No ECM1 protein expression is seen in any cell type; positive controls show ECM1 expression in mouse LV (Ms-LV), and human atrial appendage (Hu-Atria), all data was normalized to β-tubulin expression as a loading control (~55kDa). Immunoblot of ECM1 protein expression in BMCs from young healthy mice (middle, n=3, HCM serve as a negative control), and in BMCs separated into mononuclear and granulocyte fractions by Ficoll-Paque gradient density centrifugation (right, n=4). A high level of ECM1 expression in BMCs, with a significantly higher level of ECM1 expression in granulocytes (gran.), compared to monocytes (mono., p=0.005 analysed by Student's T-test); all data was normalized to β-Actin expression as a loading control (~42kDa). B) mRNA-FISH of *Ecm1* mRNA (white), conducted on BMCs in suspension; DAPI nuclear stain was used to visualize cell nuclei (Blue). *ECM1* mRNA is expressed in some BMCs (arrowhead), and not in other BMCs (full-arrow). C) mRNA-FISH of *ECM1* mRNA conducted on day-3 post-MI LV tissue, showing positive *ECM1* expression as areas of sharp and punctate Cy5 fluorescent dots; example areas

indicated by arrowheads, DAPI nuclear stain was used to visualize cell nuclei (Blue). High *ECM1* mRNA expression is seen in the infarct zone, some expression in the border zone, and little expression in the remote zone, consistent with inflammatory cell infiltrate. In Fig 3A, positive controls and resident cardiac cells (right) n=1 technical replicates/group, BMCs n=3/group, BMC monocytes and granulocytes n=4/group. **p<0.01 relative to control.

14.2 ECM1 is expressed by granulocytes and/or macrophages in the healthy mouse bone marrow

As published (1), to further investigate the cellular source of ECM1+ cells, multicolour FISH-flow cytometry was conducted on mouse bone marrow cells, which had been tagged with an ECM1 mRNA-FISH probe, alongside fluorescently labelled antibodies specific to the following cell surface markers: Ly-6G, CD11c, Ly-6C, F4/80, CD117, MHC2, CD3, FcεrI-α, CD11b and CD45. following tSNE analysis, ECM1+ cells demonstrated expression (to varying levels) for CD45, CD11b, CD11c, F4/80, Ly6-C, Ly-6G, and FcεrI-α, (**Fig. 4**). Further, when visualising side scatter (SSC) versus forward scatter (FSC) for ECM1+ cells, it is clear that ECM1+ cells are highly granular and moderate to large in size, indicative of granulocytes (e.g., neutrophils, eosinophils) or large cells such macrophages. Taken together, these results suggest that ECM1 is constitutively expressed in granular bone marrow cells but not in smaller CD3+ or MHC II+ cells. Further, post-MI ECM1+ leukocytes may be recruited to the infarct zone of the LV to contribute to post-inflammatory fibrosis.

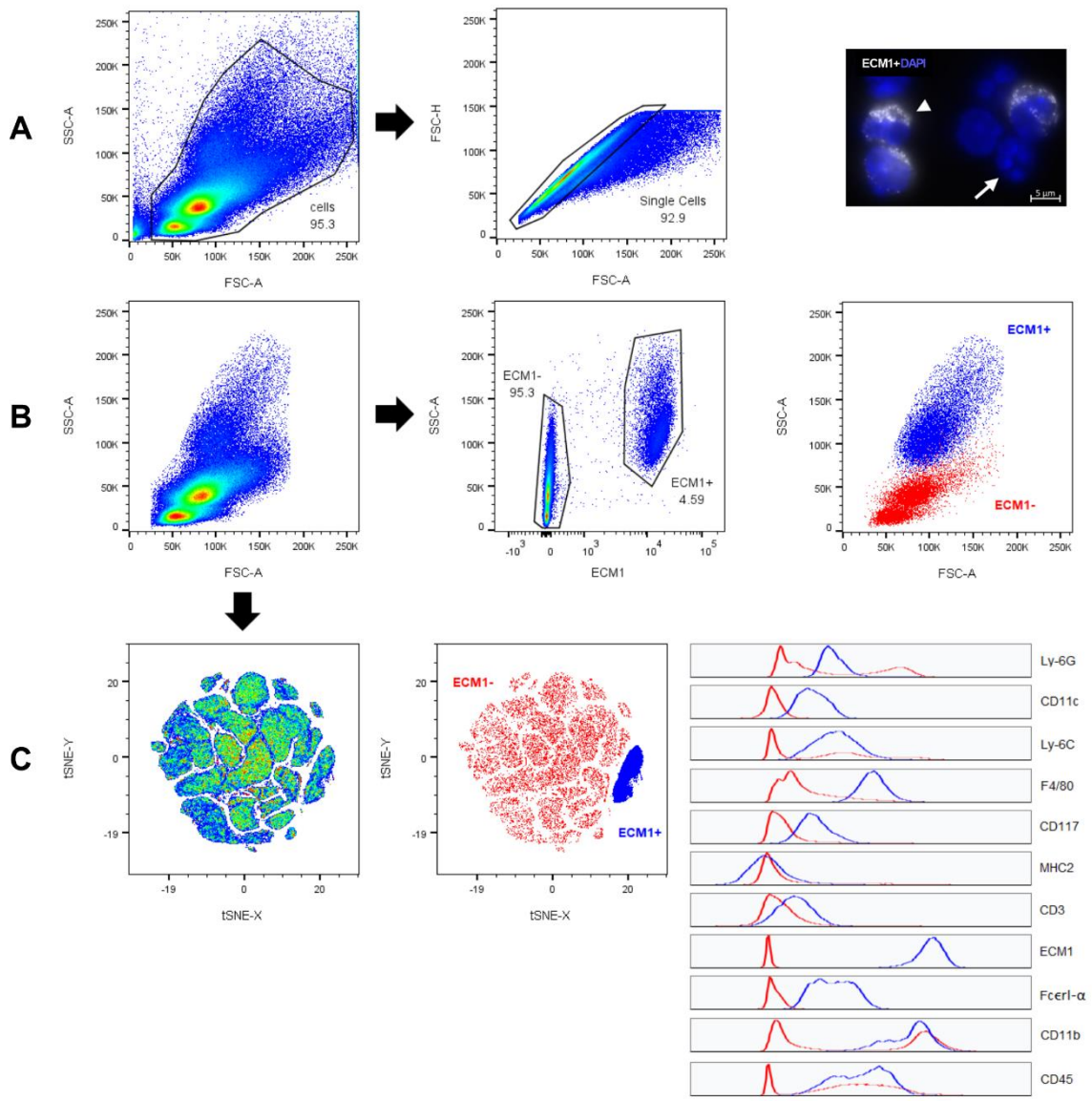

Figure 4: Reproduced from Hardy, Mabotuwana (1) with permission of the publisher (PLOS ONE). ECM1 FISH-Flow cytometry. ECM1 mRNA-FISH was coupled with flow cytometry to identify the cell surface marker profile of ECM1 positive (ECM1+) cells in young healthy mouse bone marrow. A) Forward scatter area (FSC-A; x-axis) versus side scatter area (SSC-A; y-axis) pseudocolour plot, demonstrating the gating strategy used to define our "cells" population, in order to exclude debris; left graph. Forward scatter area (FSC-A; x-axis) versus forward scatter height (FSC-H; y-axis) pseudocolour plot, demonstrating the gating strategy used to define "single cells" population, in order to exclude cell doublets; middle graph. An image of mRNA-FISH of *Ecm1* mRNA (white), conducted on BMCs in suspension; DAPI nuclear stain was used to visualize cell nuclei (Blue); right image. B) FSC-A versus SSC-A pseudocolour plot of the defined "single cells" population (left graph), and ECM1 (APC area channel) versus SSC-A pseudocolour plot demonstrating the gating strategy used to define ECM1 positive (ECM1+) and ECM1 negative (ECM1-) cells (middle graph). Included is FSC-A versus SSC-A of the ECM1+ gate overlayed onto the "single cells" population. C) A pseudocolour plot of cell population clusters after tSNE analysis conducted on the concatenated sample containing the gated populations from all four

biological replicate samples combined (left graph; presented as tSNE x-axis versus tSNE y-axis). All compensated channels were assessed: FITC (Ly-6G), PerCP-Cy5.5 (CD11c), BV421 (Ly6C), BV510 (F4/80), BV650 (CD117), BV711 (MHC2), BV786 (CD3), APC (ECM1), PE (FcεRI-α), PE-CF594 (CD11b), and PE-Cy7 (CD45). Gates corresponding to ECM1+ (blue) and ECM- (red) cells from the concatenated sample was overlayed onto the tSNE pseudocolour graph (middle graph) to visualise expression levels of all cell surface markers investigated, as represented by the corresponding histograms (right graph); x-axis corresponds to expression level, y-axis corresponds to cells number.

14.3 ECM1 expression in healthy and failing human hearts

To translate our findings of ECM1 expression in mice to humans, we utilised the Medical University of Graz human cardiac tissue bank to investigate the expression of ECM1 in human ischaemic and dilated heart failure tissue samples. ECM1 protein expression was significantly upregulated in heart tissue from both ischemic and dilated heart failure patients (**Fig 5A**). To visualise the localisation of ECM1 expression we conducted ECM1 IHC and *in situ* hybridisation in human non-failing (NF) and ischemic (ICM) heart failure patients. ECM1 expression was predominantly interstitial, localised to fibrotic, inflammatory, and peri-vascular areas (**Fig 5B**)**.** *In situ* hybridisation confirmed that ECM1 was locally transcribed in these areas (**Fig 5C**).

During the later course of our research, two key scRNAseq datasets emerged which elegantly charactered the cellular mRNA expression profile of stromal cells and leukocytes in the healthy human heart (generated by Litviňuková, Talavera-López (121)), and the mouse heart over the time-course of wound healing post-MI (generated by Farbehi, Patrick (73)). This provided an excellent platform to build on our previous work and demonstrate the *in vivo* cellular sources of ECM1 in the healthy and diseased heart. For this purpose, we collaborated with both these groups and new analyses specific to ECM1 expression were conducted on these datasets.

First, we analysed ECM1 expression in single cell and single nuclei RNA sequencing (sc/snRNAseq) in healthy human heart donors in the dataset generated by Litviňuková, Talavera-López (121). Cells expressing ECM1 in the human heart were predominantly fibroblasts, leukocytes, and vascular cells (**Fig 5D & Fig 6**). A small number of ECM1+ leukocytes was identified in this data due to low leukocyte cell numbers in healthy hearts,

relative to the diseased hearts (**supplementary table 1**). The cell type with the highest ECM1 expression level of all cells was “FB5_ECM-organising” (23.15% ECM1+) - these are ventricular fibroblasts enriched for ECM production, remodelling and degradation genes (**Fig 5E**); see **supplementary table 2** for detailed cell characteristics, and **supplementary table 3-4** for detailed data. The leukocyte sub-population with the highest number of ECM1+ cells were LYVE1+ tissue-resident macrophages (LYVE1+MØ1), which are enriched in clathrin and cathepsin genes associated with cardiovascular remodelling (139). Interestingly, PC1_vent had the overall highest number of ECM1+ cells in the dataset and was the most abundant cell type with 50,095 cells, nearly double the 2nd most abundant cell type, FB1_VT-canonical (26,632 cells). PC1_vent are pericytes enriched for adhesion molecules NCAM2, CD38 and the microvascular morphogenesis and endothelial cell crosstalk gene CSPG4.

Together, these data reveal spatio-cellular ECM1 expression in healthy human hearts that is amplified in failing human hearts. Fibroblast and leukocyte (macrophage) subsets as well as pericytes are the predominant cellular ECM1 sources.

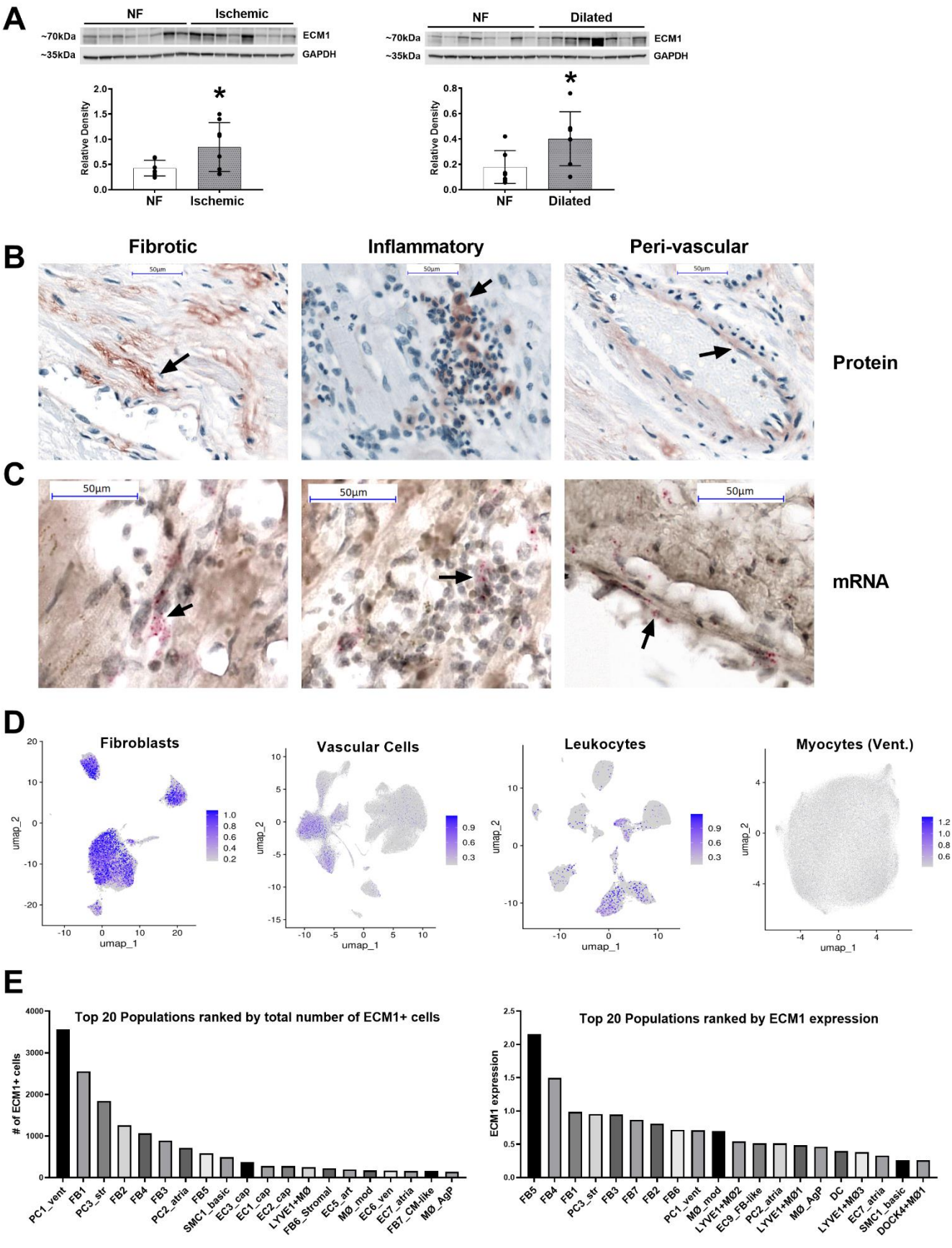
A
NF
Ischemic
~70kDa
~35kDa
ECM1
GAPDH
Relative Density
NF
Ischemic
Dilated
B
Fibrotic
Inflammatory
Peri-vascular
Protein
C
mRNA
50µm
D
Fibroblasts
Vascular Cells
Leukocytes
Myocytes (Vent.)
umap_1
umap_2
E
Top 20 Populations ranked by total number of ECM1+ cells
# of ECM1+ cells
PC1_vent
FB1
PC3_str
FB2
FB4
FB3
PC2_atria
FB5
SMC1_basic
EC3_cap
EC1_cap
EC2_cap
LYVE1+MØ
FB6_Stromal
EC5_art
MØ_mod
EC6_ven
EC7_atria
FB7_CM-like
MØ_AgP
Top 20 Populations ranked by ECM1 expression
ECM1 expression
FB5
FB4
FB1
PC3_str
FB3
FB7
FB2
FB6
PC1_vent
MØ_mod
LYVE1+MØ2
EC9_FB-like
PC2_atria
LYVE1+MØ1
MØ_AgP
DC
LYVE1+MØ3
EC7_atria
SMC1_basic
DOCK4+MØ1

Figure 5. ECM1 is upregulated in human failing hearts, and is localised to fibrotic tissue, leukocytes, and endothelia. **A**) Western blotting shows ECM1 protein is upregulated in ischemic and dilated human heart failure patients, analysed by Student's T-test (n=8/group); NF = non-failing. **B**) Immunohistochemistry of ECM1 protein expression in the human heart (n=4 NF, n=8 heart failure) shows ECM1 expression is predominantly interstitial, localised to fibrotic, inflammatory, and peri-vascular areas (40x magnification); scale bars = 50µm. **C**) mRNA *in-situ* hybridisation (n=3) confirms transcription of ECM1 in these areas (40x magnification zoomed in); scale bars = 50µm. **D**) Sc/snRNAseq dataset identifies ECM1 expression by fibroblasts, leukocytes, and vascular cells in the healthy human heart (all cells = grey, ECM1+ cells = blue overlay). **E**) The top 20 ECM1 expressing cell sub-populations ranked by total number of ECM1+ cells, and by ECM1 expression level (expressed as a Log2 average). *$p<0.05$.

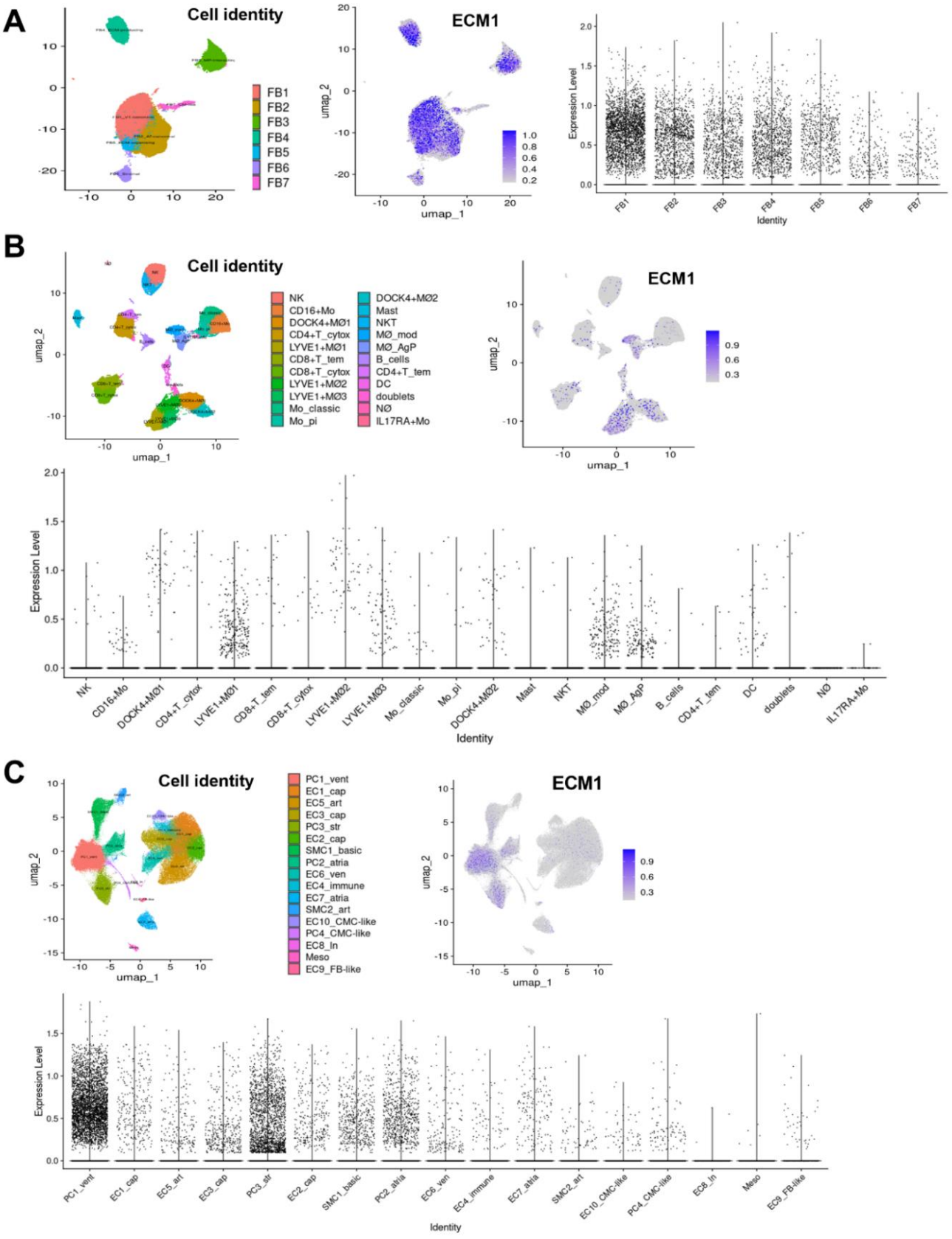

Figure 6. Analysis of ECM1 expression in sc/snRNA-seq of cardiac interstitial cells from healthy human hearts (121). UMAP and violin plots of ECM1 expression levels in specific cardiac cell-sub populations: fibroblasts (**A**),

leukocytes (**B**), and vascular cells (**C**). ECM1 positive cells are displayed as a blue overlay on grey total cell identity UMAP coordinates.

14.4 Dynamic ECM1 expression patterns post-MI

Next, to investigate the origin of ECM1 in the heart and its dynamic cellular expression changes following myocardial infarction, we analysed ECM1 expression in the mouse scRNAseq dataset of interstitial cells post-MI generated by Farbehi, Patrick (73). Consistent with our analysis in human heart tissue (**Fig 5 & 6**), ECM1 was expressed most abundantly by fibroblasts and monocytes/macrophages (Mo/MΦ, **Fig 7A-C**). Further, we found a dynamic shift of ECM1 cellular expression between fibroblasts and Mo/MΦ's over the time-course of wound healing post-MI. In the uninjured sham-operated heart, the number of ECM1+ cells were highest in unactivated F-SL and F-SH fibroblasts (which express genes either enriched for cell adhesion [F-SH] or cell secretion and cell signalling processes [F-SL]). At day-3 post-MI, ECM1 expression was highest in M1MΦ's, with expression also in M1Mo's, F-Act, MAC8, and interferon-inducible cell (IFNIC) MΦ's. At day-7 post-MI ECM1 expression significantly increased in activated fibroblasts (F-Act), myofibroblasts, and M2MΦ's, which are involved in inflammation resolution and repair (**Fig 7D-F)**; see **supplementary table 5** for detailed cell characteristics, and **supplementary table 6** for detailed data. ECM1 was also expressed by some vascular mural cells, which encompass pericytes and endothelial cells (ECs), however ECM1+ cell numbers decreased after MI. Little ECM1 expression was observed in lymphoid cell populations at all time-points. Of note, although leukocyte numbers were present at small numbers in sham-operated hearts, tissue-resident MΦ's (MAC-TR) had the highest ECM1+ cell number of all leukocyte sub-populations, consistent with our data in the human heart (**Fig 5 & 6**).

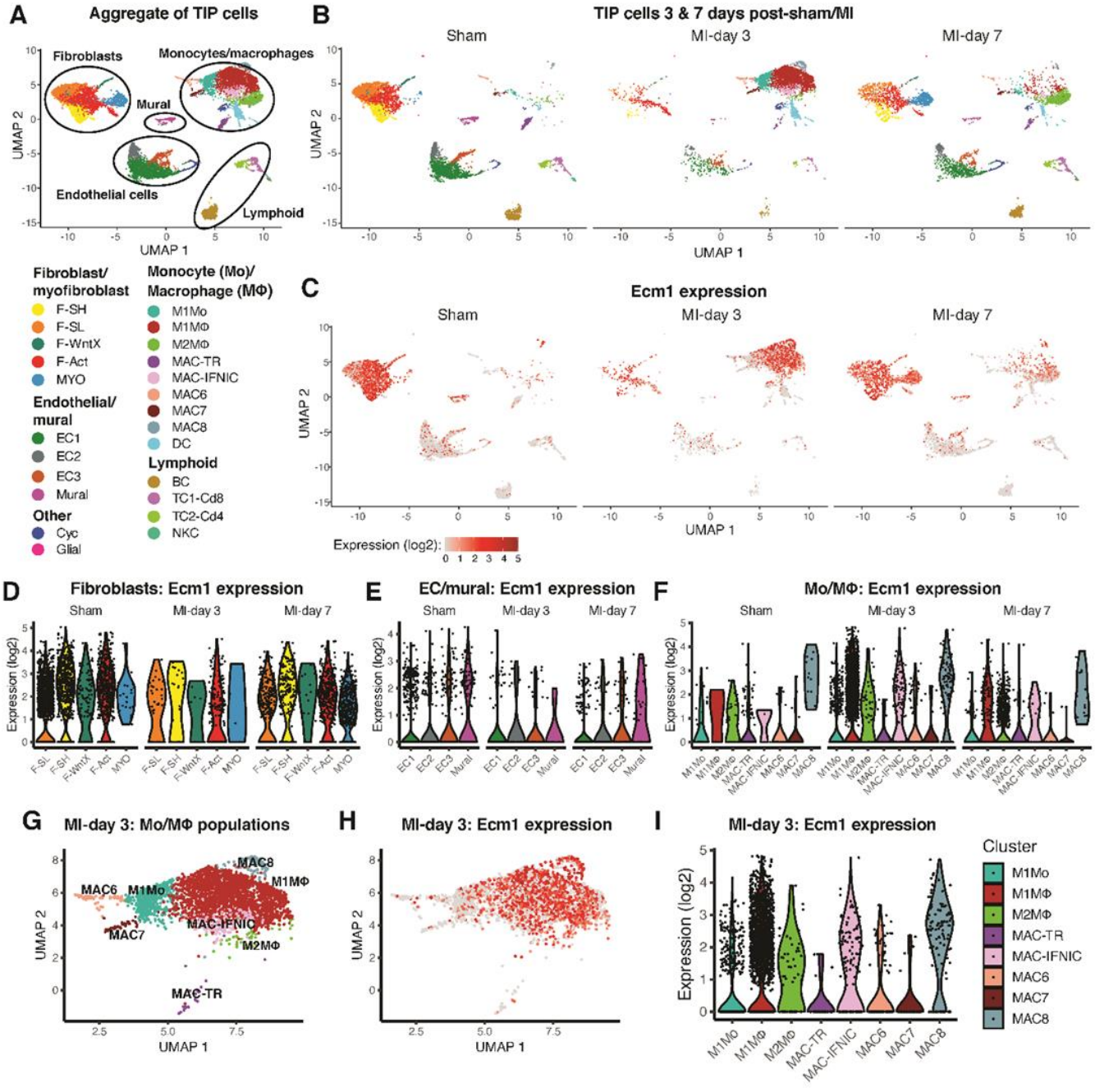

Figure 7. Expression of *Ecm1* in cardiac interstitial cells before and after myocardial infarction. A) UMAP plot showing cell populations in scRNA-seq of cardiac interstitial cells from sham-operated and MI hearts combined, and (**B**) facetted according to condition. **C**) Ecm1 expression on UMAP coordinates according to condition. **D-F**) Violin plots of Ecm1 expression according to condition for cell sub-populations in (**D**) fibroblasts, (**E**) endothelial and mural cells and (**F**) monocyte (Mo) and macrophage (MΦ) populations. (**G**) UMAP plot of Mo/MΦ cell populations at day-3 post-MI. **H, I**) Ecm1 expression in day-3 post-MI Mo/MΦ cells on (**H**) UMAP coordinates and (**I**) in violin plots.

To gain unbiased insights into the function of ECM1 in the heart post-MI, we next correlated ECM1 expression levels with all genes in the Farbehi, Patrick (73) dataset. We also assessed differentially expressed genes (DEGs) between ECM1+ and ECM1- cells (per specific cell population). ECM1 expression most positively correlated with inflammatory and tissue remodelling genes Galectin 1 (Lgals1) and Low density lipoprotein receptor-related protein-1 (Lrp1) (140, 141). Gene Ontology Biological Process (GOBP) enrichment analysis of correlated genes (e.g., Tissue inhibitor of metalloproteinases 2 (Timp2), Fibulin-1 (Fbln1), and Collagen type I alpha 1 chain (Col1a1)) showed ECM1 expression was most significantly associated with ECM and collagen organisation, cell adhesion, and developmental processes, (**Fig 8A & 8C**, **supplementary table 7 & 8**).

DEG analysis and GOBP enrichment showed genes upregulated in ECM1+ F-Act and F-SH fibroblasts were over-represented for extracellular structure and ECM organisation (**Fig 8D, supplementary table 9 & 10)**. Further, the two cellular adhesion proteins Ccdc80 and Fbln1 were commonly upregulated in ECM1+ F-Act, F-SH, and F-SL fibroblasts (**Fig 8E**). Upregulated DEGs in ECM1+ M1MΦs showed over-representation of chemotactic, and migration associated processes (**Fig 8D, supplementary table 11)**. Finally, via new analysis of the Farbehi, Patrick (73) cell-cell communication data, we identified a strong correlation between ECM1 expression levels and the number of significant outbound ligand-receptor connections (**Fig 8B**), suggesting a functional association between ECM1 expression and intercellular signalling crosstalk.

Together, these data reveal that cellular expression patterns of ECM1 shift between fibroblasts and MΦ post-MI, supporting a key role for ECM1 in fibroblast-MΦ crosstalk in wound healing. ECM1 expression is functionally associated with ECM and collagen organisation/remodelling, cardiac inflammation, cell-cell/cell-matrix adhesion, cell migration, and intercellular signalling crosstalk.

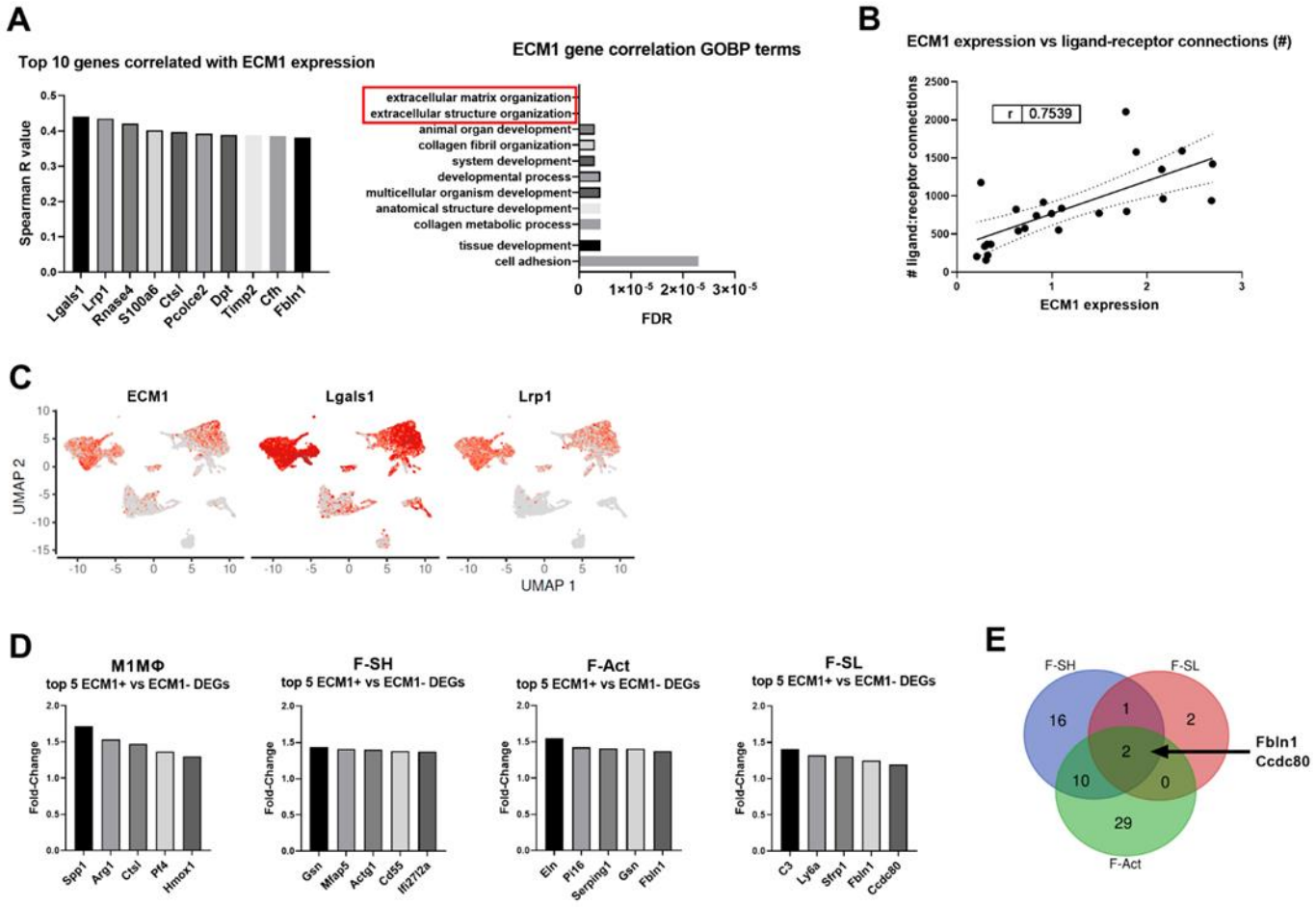

Figure 8. ECM1 expression strongly correlated with the number of outbound ligand-receptor interactions between cells, ECM organisation, and cell adhesion genes. A) Per-cell Spearman correlation analysis of ECM1 expression against all genes in the mouse scRNAseq dataset (73); all p-values <0.0001. The top 10 positively correlated genes (x-axis) are shown as column graphs of Spearman r-value (y-axis). The top ECM1 correlated genes (with Spearman r $\geq$ 0.3) were subject to GOBP enrichment analysis via the GOnet/DICE online tool. The top 10 GOBPs are presented as a bar chart ranked by FDR p-value. **B**) The average ECM1 expression level (Log2) of each cell sub-population is positively correlated with the number of significant outbound ligand-receptor connections (r = 0.75), analysed by Spearman correlation. **C)** ECM1, Lgals1 and Lrp1 expression overlayed on the UMAP plot of cardiac interstitial cells from sham and MI (as shown in Fig 2A), to compare the cellular expression profile of the top 2 ECM1 correlated genes. **D**) Differentially expressed genes (DEGs) between ECM1+ and ECM1- cells (per cell sub-population) within the major ECM1 expressing cell sub-populations were assessed via MAST. Only M1MΦ, F-Act, F-SH and F-SL returned lists of significant DEGs, and the top 5 upregulated genes in ECM1+ cells (x-axis) are shown in column graphs as fold-change in gene expression (y-axis). **E**) All upregulated DEGs for M1MΦ, F-Act, F-SH and F-SL were subject to Venn diagram analysis. No genes were commonly upregulated in all 4 cell types, however Fbln1 and Ccdc2 were commonly upregulated in ECM1+ F-Act, F-SH, and F-SL cells.

14.5 ECM1 stimulates collagen production from cardiac fibroblasts via activation of ERK1/2 and AKT

As we have clearly identified an association of ECM1 in fibrotic cardiac disease, and identified the cellular sources of ECM1, we then explored whether ECM1 contributes to the observed fibrosis using human CFb cell lines cultured *in vitro*.

As published (1), recombinant ECM1 was added to HuCFbs in culture and was sufficient to increase collagen production (p=0.004, **Fig 9**). To investigate the mechanism of collagen-I expression, we assessed several key signalling pathways involved in fibrosis (AKT, ERK1/2 & p38). Recombinant ECM1 significantly upregulated HuCFb ERK1/2 activation (Thr202/Tyr204; p<0.0001) and AKT activation (Ser473) at 10 minutes (p<0.0001), and significantly downregulated AKT activation at 50 minutes (p=0.02) compared to untreated control HuCFbs (**Fig 9**). No significant difference in p38 activation (Thr180/Tyr182) was seen at any time-point. This data confirms our preliminary results and suggests ECM1 has pro-fibrotic effects on CFbs during cardiac wound healing.

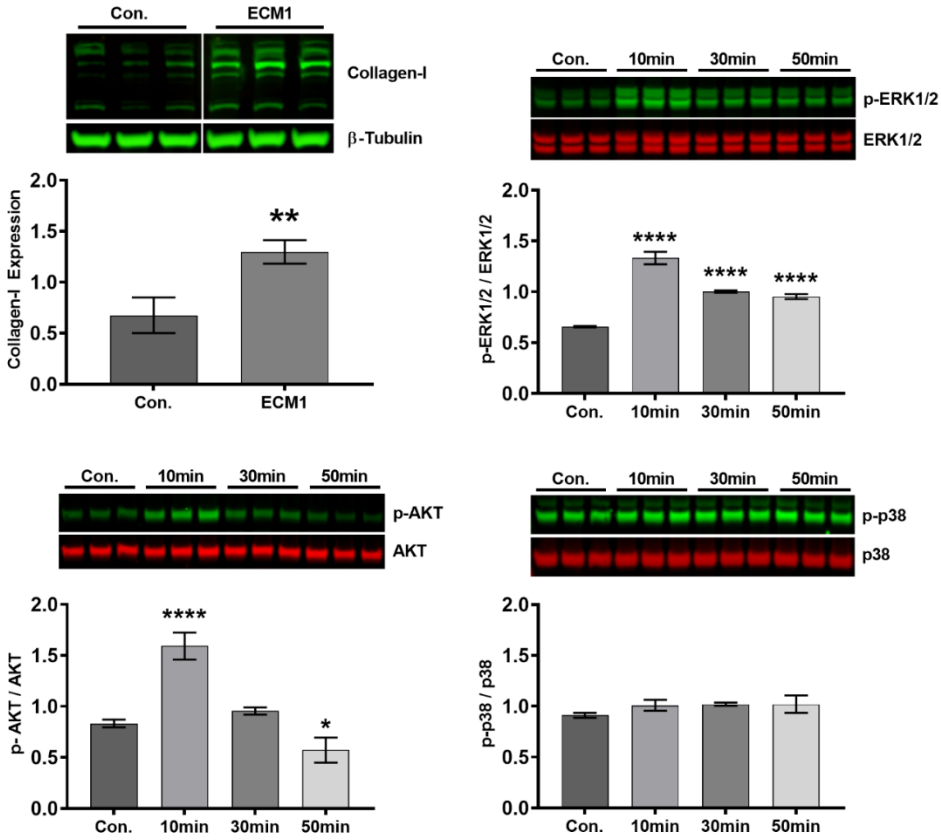

Fig 9: Reproduced from Hardy, Mabotuwana (1) with permission of the publisher (PLOS ONE). ECM1 stimulates collagen-I expression and ERK1/2 and AKT pathway activation in cardiac fibroblasts. Collagen-I protein expression was increased in human cardiac fibroblasts (HuCFbs) in response to 48 h of treatment with recombinant ECM1 (20 ng/ml) relative to untreated control (Con.) cells (top left); data normalized to β-tubulin expression (~55kDa) and analysed by Student's T-test. Immunoblots of ERK1/2 and p-ERK1/2 at Thr202/Tyr204 (top right), AKT and p-AKT at Ser473 (bottom left), and p38 and p-p38 at Thr180/Tyr182 (bottom right) expression in HuCFbs treated with recombinant ECM1 (20 ng/ml) for 10, 30 or 50 minutes. Shows significant ERK1/2 activation at 10, 30 and 50min, and AKT activation at 10min. Data is represented as phosphorylated/non-phosphorylated protein and analysed by ordinary one-way ANOVA with Dunnett's multiple comparisons post-hoc test. The blot image in top left figure was cropped only to re-arrange the order of control lanes of the same blot. All data is expressed as mean ± SD, with n=3 technical replicates/group. *p<0.05, **p<0.01, ****P<0.0001 relative to control.

14.6 ECM1-dependent human cardiac fibroblast cell signalling

Next, to understand the effect of ECM1 more deeply in wound healing and fibrosis post-MI, we investigated potential signalling cascades associated with ECM1 on human cardiac fibroblasts (HuCFb) using unbiased phosphoproteomics mass spectrometry (serine/threonine). We identified 38 differentially phosphorylated proteins in ECM1 treated HuCFbs, relative to control cells treated with media alone (**Fig 10A**); for full data see **supplementary table 12**. MAP1B was the most highly phosphorylated protein relative to controls (27.3-fold, q-value <0.0001). Interestingly, most proteins (28 proteins) were dephosphorylated in the ECM1 treatment group, with only 8 proteins (10 including multiple p-sites) increasing in phosphorylation relative to controls: MAP1B, ARHGEF11, ANAPC4, MYO9B, CETN2, SURF2, PTPN12, and KIFAP3. Of note, ARHGEF11, MYO9B and PTPN12, have significant influence over Rho protein/Rho GTPase signal transduction, e.g., PTPN12 dephosphorylates CTNND1 and controls cell motility via alterations to CTNND1 dependent Rho protein signal transduction (142). Analysis of GOBPs using Fisher's exact test complemented this, showing over-representation of calcium-dependent cell-cell adhesion, Rho protein signal transduction, cell polarity, microtubule-based transport, and Mo/MΦ chemotaxis processes (**supplementary table 13**). GO Cellular Compartment (GOCC) locations associated with microtubule rich cellular projections and non-motile primary cilia were also over-represented. PHOTON pathway analysis identified 18 proteins with significant signal functionality scores (≥ 6) in the "greater" direction (i.e., increased

phosphorylation with ECM1 treatment), including CDC42, RAC1, S100a10, LRP8, and RELN; this indicates involvement in active mediation of ECM1 dependent signal transduction. ANAT reconstruction of this ECM1 network shows ECM1 signalling through TIMP3 and TP53 to influence pathways including Rho GTPase mediators CDC42 and RAC1 (**Fig 10B**).

To complement phosphoproteomics, ECM1 binding partners were pulled down from a purified HuCFb membrane protein lysate. This was done using recombinant human ECM1 protein which was pre-bound ("ECM1" sample) to His-Tag Isolation Dynabeads ("control" sample Dynabeads had no ECM1 pre-bound). With this approach, we identified 4 potential ECM1 binding proteins: CTNND1, HK1, DYNC1I2, and DHX9. CTNND1 is of particular interest as it is the only one of these 4 proteins specifically shown to be localised to the cell membrane; others are proposed intracellular organelle, cytoskeleton or cytosol associated.

Together, our unbiased mass spectrometry (MS)-based experiments suggest that ECM1 binds CTNND1 on the cardiac fibroblast cell surface/membrane and induces phosphorylation of proteins associated with Rho protein signalling, cell-cell adhesion, cell polarity, microtubule dynamics, and chemotaxis in HuCFbs.

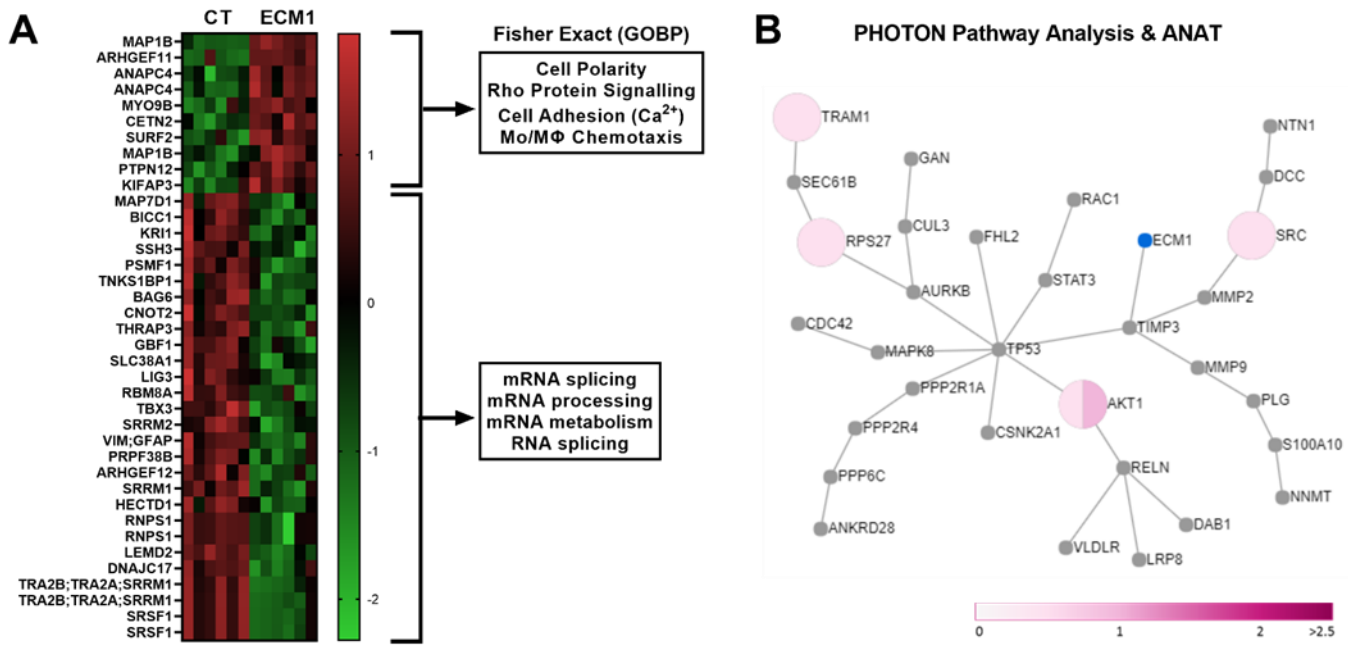

Figure 10. ECM1 triggers significant alterations in HuCFb cell signalling pathways associated with Rho protein signalling, cell-cell adhesion, cell polarity, microtubule dynamics, and cell chemotaxis. A) HuCFb cells were treated with ECM1 (20 ng/ml) for 10min and subject to phosphoproteomics (Ser/Thr) mass spectrometry (titanium dioxide workflow; n=6 /group). Thirty-eight proteins with significantly different phosphorylation level were identified between control (CT; media alone) and ECM1 treated cells, assessed via Student's T-test with Permutation-based FDR; data is presented as the Log2 difference (CT-ECM1) in phosphorylation level; green = downregulated, red = upregulated. Note that proteins measured multiple times represent different phosphosites within these proteins. Fisher's exact enrichment testing was conducted on significantly upregulated and downregulated phosphorylation sites in ECM1 treated samples (separately), and 4 of the most over-represented GO biological processes (GOBP) are shown. **B**) Our list of differential phosphorylation sites in ECM1 treated HuCFbs was then subjected to PHOTON pathway analysis (two-sided) with reconstruction ANAT (ECM1 as the response source) to visualise the ECM1 dependent signalling network. The ANAT network for ECM1 signalling in the "greater" PHOTON analysis direction (signalling score ≥ 6) is shown with ECM1 highlighted in blue. All proteins shown in the network represent involvement in active mediation of ECM1 dependent signal transduction. Pink pie charts represent fold-changes of measured phosphorylation sites (see scale bar), with multiple phosphorylation sites represented by a pie chart divided by the number of phosphorylation sites measured.

14.7 ECM1 stimulates inflammatory, fibrotic, and non-canonical Wnt-signalling pathways in human cardiac fibroblasts

Next, based on our sc/snRNAseq and MS data, we aimed to test ECM1's impact on fibroblast functionality. Wound healing assay showed ECM1 significantly reduced the rate of HuCFb migration *in vitro* over 24-hours, relative to control cells treated with media alone (**Fig. 11A**). ECM1 had no direct effect on cell proliferation (MTT assay).

We then used qPCR and immunoblotting to investigate the influence of ECM1 over inflammatory and fibrotic pathways, chemotactic pathways (*CCL2* [*MCP-1*]*)*, and *Wnt5a* which modulates non-canonical Wnt signalling, Rho protein signalling, cell/microtubule architecture organisation, cell adhesion, and cell chemotaxis. ECM1 significantly upregulated mRNA expression of *Wnt5a*, *IL-1β* and *IL-6* at 3 hours post-treatment, and downregulated *CCL2* mRNA expression, relative to control (**Fig 11B**). ECM1 significantly upregulated *TGF-β1* and *TGF-β2* expression at 3 hours post-treatment, followed by an upregulation of *Col1a2* expression at 16 hours.

Finally, we used immunoblotting to assess the activation of canonical and non-canonical Wnt pathways, and canonical NFκB signalling pathways (**Fig 11C**). ECM1 treatment increased JNK1/2/3 and MYPT1 phosphorylation (markers of non-canonical Wnt PCP and Wnt Ca^{2+} pathways, respectively). ECM1 had no effect on β-catenin protein levels at any time (canonical Wnt pathway activation), nor did it influence canonical NF-κB signalling at any time (**Fig 12**).

Taken together, these data demonstrate that ECM1 inhibits HuCFb cell migration, and regulates inflammatory, fibrotic, and non-canonical Wnt pathways.

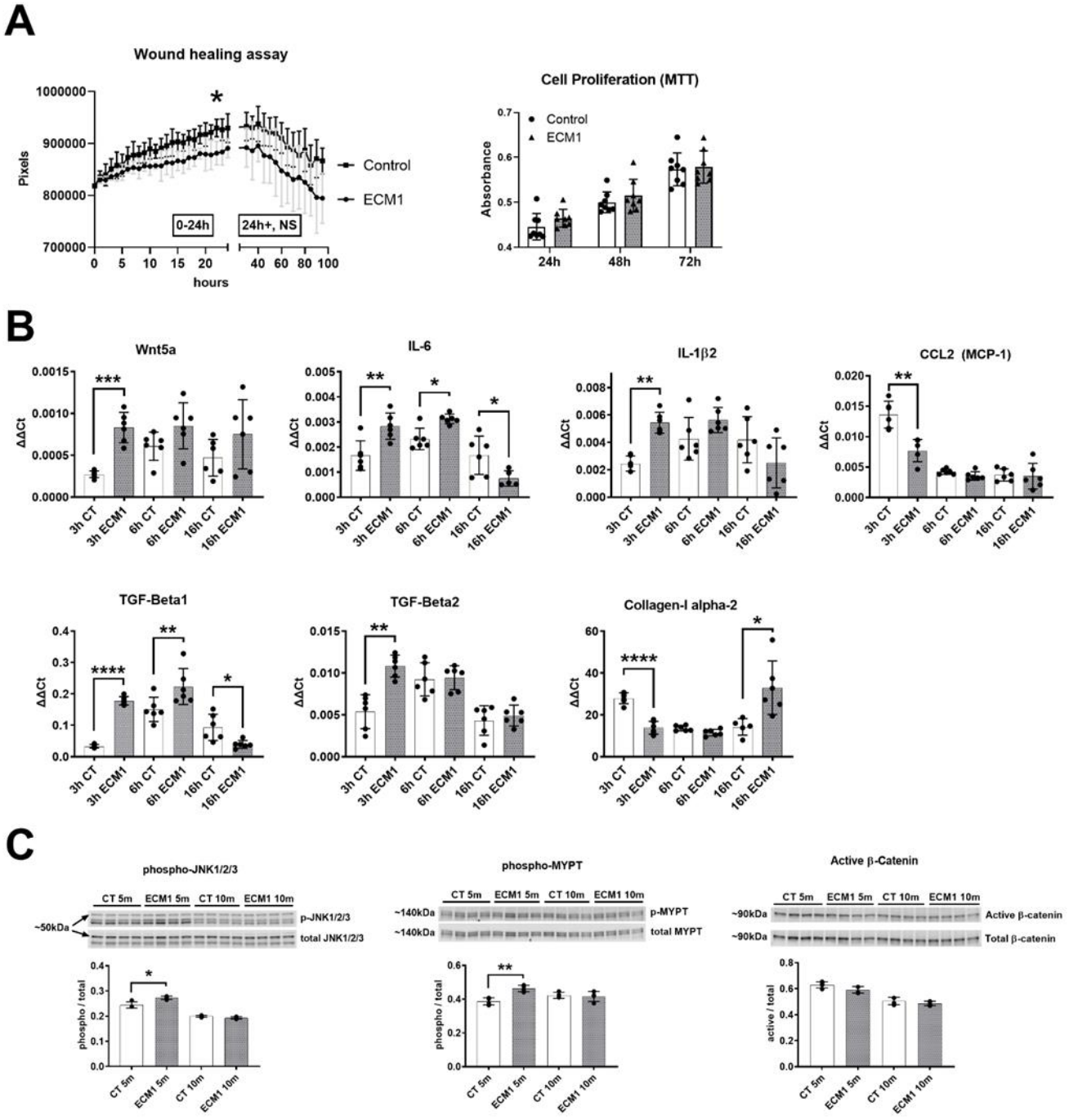

Figure 11. ECM1 inhibits HuCFb cell migration in culture and activates inflammatory, fibrotic, and non-canonical Wnt-signalling pathways. A) ECM1 treatment (20 ng/ml) significantly reduced the migration rate of HuCFb cells over 24-hours relative to controls (n=4/group), assessed via both two-way ANOVA ($p = 0.044$, no post-hoc test applied), and inclination of the linear equation of growth rate via Student's T-test ($p = 0.027$). ECM1 had no effect on cell proliferation assessed via MTT assay after 24, 48 or 72 hours of treatment, assessed via Student's T-test. **B)** HuCFbs were treated with ECM1 (20 ng/ml) or media alone (CT = control) for 3, 6 or 16 hours and assessed via qPCR for mRNA expression of Wnt5a, IL-1β2, IL-6, CCL2, TGF-β1, TGF-β2, and Col1a2 (a one-way ANOVA analysis with Šídák's multiple comparisons post-hoc test including all 3 time-points

was used for each gene); expression of all genes are presented as the delta-delta threshold cycle (ΔΔCt) relative to Tpt1 housekeeping gene expression, n=6/group. **C)** HuCFbs were treated ECM1 (20 ng/ml) or media alone (CT) for 5 or 10 minutes and assessed via immunoblotting for changes in the ratio of phosphorylated/total protein expression of canonical and non-canonical Wnt signalling pathway markers JNK1/2/3, MYPT, and β-catenin (assessed as the ratio of active/total); assessed via Student's T-test n=4/group. *p<0.05; **p<0.01; ***p<0.001; ****p<0.0001.

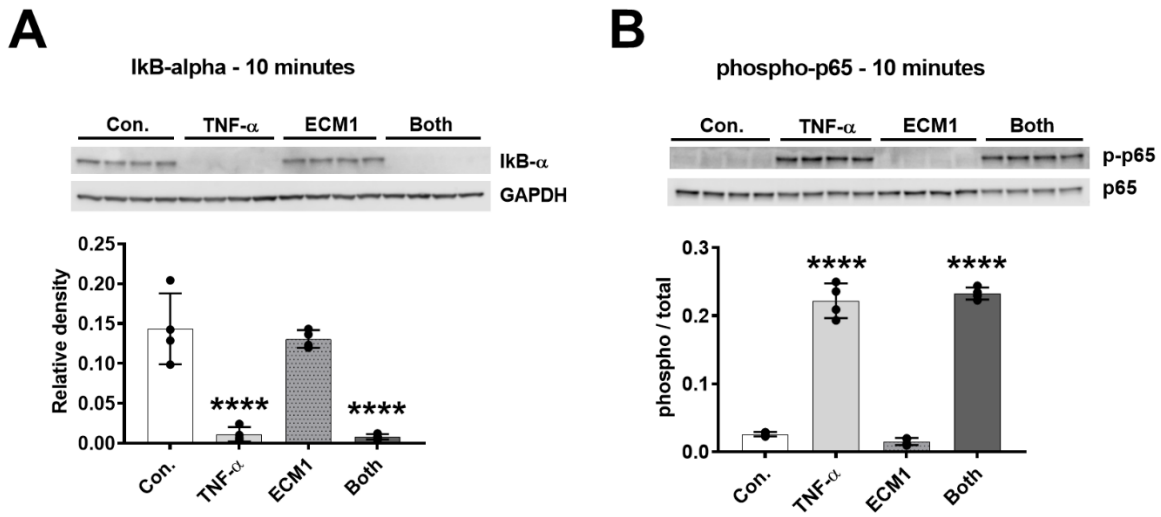

Figure 12. ECM1 does not activate canonical NF-kB pathways in HuCFb cells. ECM1 (20 ng/ml) did not result in IkB-alpha degradation (**A**), or p65 phosphorylation (**B**), after 10 min of treatment; the positive control TNF-α (20 ng/ml) achieved both. Co-treatment with both ECM1 and TNF-α did not inhibit or alter the effect of TNF-α. All data assessed via Student's T-test n=4/group. ****p<0.0001.

14.8 Development of an ECM1 genetic knockout murine model

Next, we aimed to develop an ECM1 genetic knockout mouse model using CRISPR-Cas9 technology. Via collaboration with Australian BioResources (ABR) at the Garvan Institute of Medical Research (Moss Vale, Australia), we generated 3 variations of a total body ECM1 genetic knockout mouse on a C57BL/6 background. We named these ECM1Δ1, ECM1Δ2 and ECM1Δ7 (see **below** for DNA mutation sequences; all sequencing was conducted by Australian BioResources (ABR) at the Garvan Institute of Medical Research (Moss Vale, Australia)). The ECM1Δ1 and ECM1Δ2 animals both had small deletions in Exon 1 (slightly different between the two) that cause frame shift mutations just after the signal sequence.

The ECM1Δ7 animal involved a frame shift mutation in Exon 7 that shifts the reading frame after amino acid #162, resulting in a stop codon ~40aa later. We decided to discontinue ECM1Δ1 and ECM1Δ7 lines and use the ECM1Δ2 line. We chose the ECM1Δ2 animals, as they presented a frameshift mutation from an early point in the ECM1 genetic sequence (exon 1) to encode a shortened, non-functional protein of only 32aa. We deemed this an acceptable level of ECM1 protein loss-of-function, and the homozygous animals displayed a clear phenotype difference to WT animals. As such, all experiments to follow were conducted on ECM1Δ2 mice.

Alignment of ECM1 (DNA sequence) Exon 1 with WT on top and Ecm1Δ1 GMO on the bottom

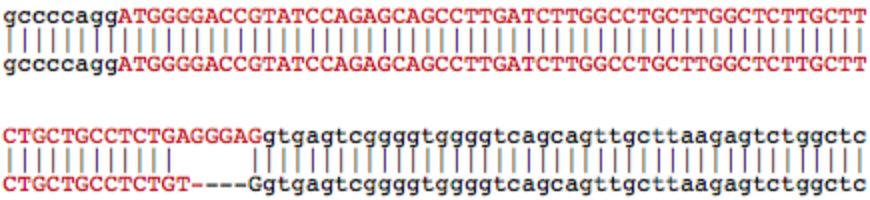

Alignment of ECM1 (DNA sequence) Exon 1 with WT on top and Ecm1Δ2 GMO on the bottom

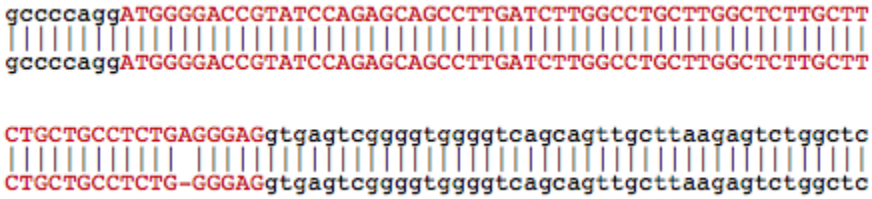

Alignment of (DNA sequence) Exon 7 with WT on top and Ecm1Δ7 GMO on the bottom

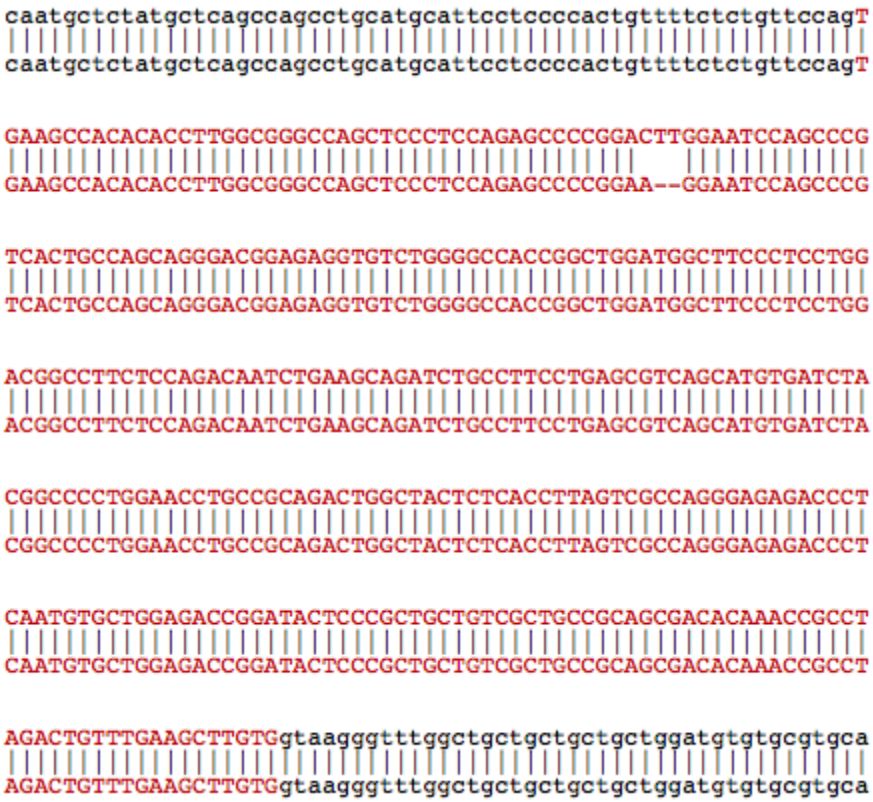

Homozygous ECM1 knockout mice ($ECM1^{-/-}$) displayed lower weight, smaller overall body size, and a significantly lower rate of survival over the first 16 weeks of life relative to WT mice (**Fig 13A**). Heterozygous ECM1 knockout mice ($ECM1^{+/-}$) showed no adverse phenotype, nor any change in rate of survival. The age at which $ECM1^{-/-}$ survival began to decline was ~7-8 weeks. ECM1-/- mice had significantly lower ratio of heart weight to tibia length (mm), and lung weight to tibia length, relative to WT (**Fig 13B**). There was no change in ratio of heart to body weight (g) or total BMC count. Flow cytometry revealed the composition of leukocytes in the bone marrow was largely the same, with only a significant decrease seen in the proportion of T cells, and a significant increase in the proportion of NK cells in young 'healthy' bone marrow of $ECM1^{-/-}$ mice, relative to WT (**Fig 13C**).

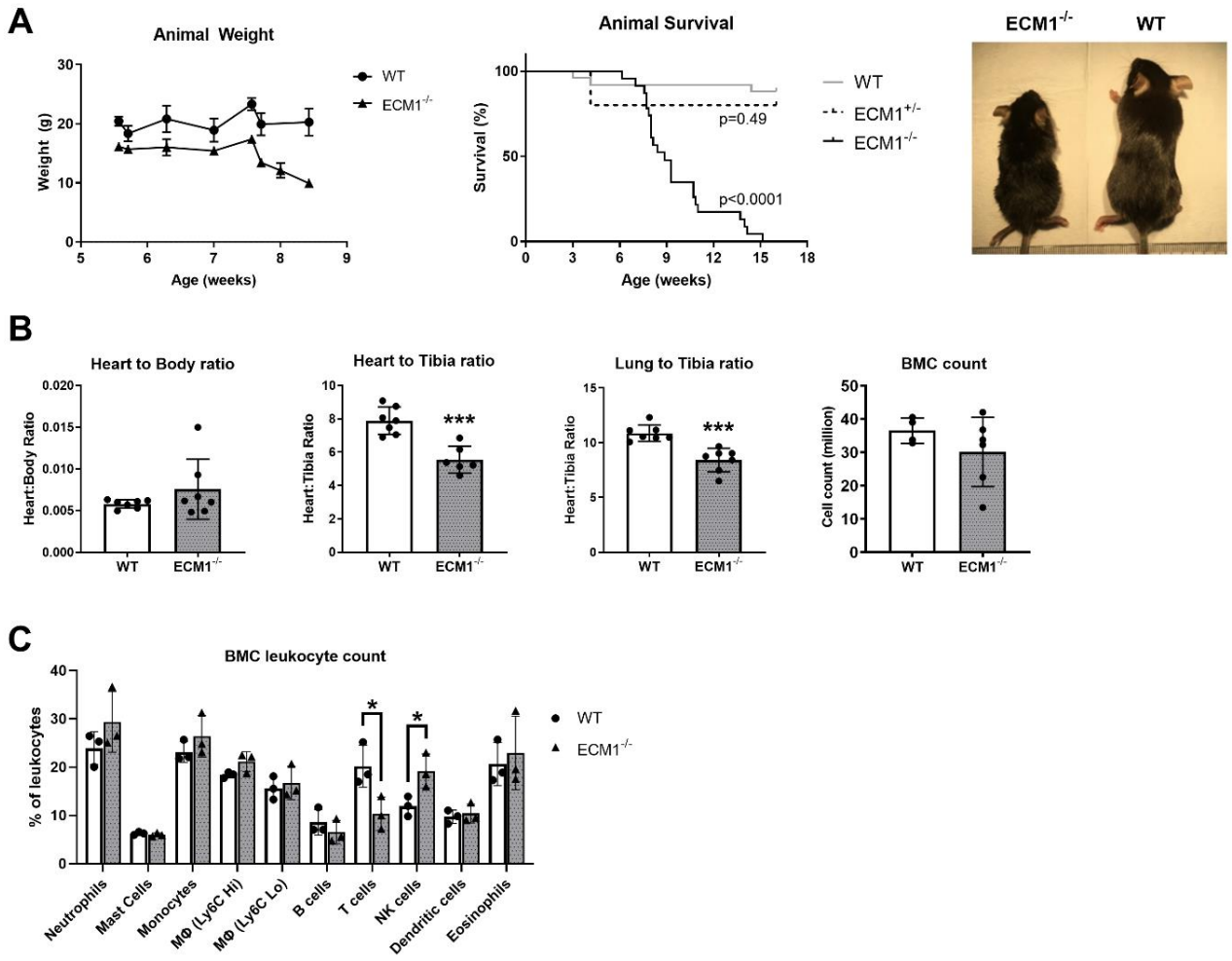

Figure 13. ECM1 knockout mouse model. A) A line graph plotting mouse weight (g) against age (weeks) of WT and ECM1$^{-/-}$ mice, no statistical testing was applied. A Kaplan-Meier curve showing significantly reduced survival rate of ECM1$^{-/-}$ mice over the first 16 weeks of life relative to WT, assessed via Mantel-Cox test ($p<0.0001$). A representative image showing ECM1$^{-/-}$ mice are smaller than WT mice is included. **B)** Ratio of heart to body weight (g), heart weight to tibia length (mm; $p=0.0003$), lung weight to tibia length ($p=0.0003$), and total BMC count of WT and ECM1$^{-/-}$ mice (minimum n=4), assessed via Student's T-test. **C)** multicolour flow cytometry identified the proportion % of major leukocyte populations present in young 'healthy' WT and ECM1$^{-/-}$ mice BMCs (n=3/group). ECM1$^{-/-}$ mice have significantly more NK cells ($p=0.037$), and significantly fewer T cells ($p=0.038$) in the bone marrow relative to WT mice, assessed via Student's T-test; to aid visualisation of data side-by-side, all values except neutrophils were multiplied to increase numerical value and should not be considered a true value of % of total leukocytes present in the bone marrow.

15. Discussion

15.1 Overview and clinical implications

Cardiac aging, wound healing and tissue remodelling are complex dynamic processes. Wound healing with MI in particular involves mass recruitment of leukocytes to areas of tissue damage, and intrinsically relies upon tightly coordinated cell-cell signalling, interaction with the ECM, and dynamic collaboration between leukocytes (particularly macrophages) and fibroblasts (8, 143). This ensures that a mature scar is developed throughout the course of wound healing to prevent cardiac rupture (8). These processes need to preserve global cardiac function, but often lead to excessive and detrimental scarring which impairs cardiac structure, function, and promotes the progression of heart failure (5, 8). As treatment options for fibrosis are limited and have failed to dramatically reduce the mortality associated with cardiac disease in the past (both anti-inflammatory and anti-fibrotic), new therapeutic options are desperately needed. Since anti-inflammatory and anti-fibrotic therapies were first trialed to treat cardiac disease and MI in the 1960s, we had dramatic technological advances, and have uncovered unprecedented opportunity in the form of novel mechanisms and pathways in wound healing which could potentilly be leveraged to ameliorate the pathogenesis of cardiac fibrosis. One such mechanism is the novel inflammation-fibrosis crosstalk that we now appreicate has significant influence over the progression of wound healing. Some researchers even think that this newly accepted importance for inflammation-fibrosis crosstalk in wound healing may explain why “uni-directional” therapies to target inflammation or fibosis alone have failed to provide the clinical results we had hoped in the past (10).

In this study we suggest for the first time that ECM1 plays both a pro-fibrotic and pro-inflammatory role in fibrotic cardiac disease, and unlike most fibrotic factors, ECM1 is expressed by both fibroblasts and leukocytes, and is impliated in intracellular signalling crosstalk. Thus, ECM1 may facilitate a novel form of inflammation-fibrosis crosstalk in wound healing, and may be an ideal therapeutic target to improve wound healing with cardiac disease. The research presented here provides clinical relevance of ECM1 to human heart failure and a basis for future research to test the viability of ECM1 as a therapeutic target to improve wound healing in cardiac disease. Further, as scarring and fibrosis is a

universal response to injury in many organs, the work presented here has potential implications beyond cardiac disease (e.g., lung fibrosis).

15.2 Preliminary data: ECM1 plays a role in cardiac disease, fibrosis, or inflammation in wound healing post-MI

As published (1), our published preliminary results characterised the expression of ECM1 in aging and cardiac disease in mice. We also investigated the effect of recombinant ECM1 protein on mouse cardiac fibroblasts cultured *in vitro* (not published). Aging has been associated with cardiac fibrosis as the result of a multitude of factors including cellular senescence, cell death and inflammation due to age-associated immunoinflammatory dysregulation (35, 144-146). We identified an increase in ECM1 expression in both aging mouse LV tissue, and at day-3 post-MI in young mice during the inflammatory phase, selectively in the infarct zone. Day 1-3 post-MI is associated with acute inflammation involving infiltration of leukocytes including neutrophils, macrophages, lymphocytes, eosinophils, to the site of infarct (4, 62, 70, 147); the above discussion paragraph was adapted from Hardy, Mabotuwana (1). Further, CFbs cultured *in vitro* do not express ECM1 protein under standard culture conditions, nor when stimulated with recombinant TGF-β1 (10 ng/ml) or ANG-II (100 nM). However ECM1 appeared to have pro-fibrotic effets on primary mouse CFbs at both a low (20 ng/ml) and high dose (200 ng/ml); to an extent comparable to TGF-β1 and ANG-II. As such, ECM1 may have pro-fibrotic effects, and ECM1 expression in the heart may originate from leukocytes and/or other resident cardiac cells. The present study discussed below, conducted throughout my PhD candidature, aimed to define the cellular origins of ECM1 in the heart, convert our preliminary findings in mice to human tissue, and investigate the cellular signalling mechansims that ECM1 influences in CFbs.

15.3 ECM1 is upregulated in human heart disease and is expressed predominantly by fibroblasts and macrophages

Our preliminary studies confirmed that ECM1 is upregulated with aging and fibrotic cardiac disease post-MI and suggest that ECM1 has pro-fibrotic effects, but primary mouse CFbs

cultured *in vitro* do not express ECM1 protein themselves. Therefore, the experiments that followed firstly aimed to identify the cellular origins of ECM1 in the healthy and diseased heart, and to translate our data in mice to human cells and heart failure patient tissue.

Via the use of the Division of Cardiology's human cardiac tissue bank, we successfully confirmed our mouse data (1) and showed that ECM1 expression is upregulated in the human heart in both ischaemic and dilated heart failure. Further, ECM1 expression in the human heart was localised in the interstitium to areas of inflammatory cell infiltrate as well as fibrotic and peri-vascular areas. These results strongly suggest a role for ECM1 in wound healing with inflammatory and fibrotic cardiac disease with clinical relevance to human ischaemic and dilative heart failure.

To investigate the cellular origins of ECM1, we first tested if ECM1 originated from the major resident cardiac cells (fibroblasts, cardiomyocytes, endothelial cells and smooth muscle cells) or infiltrating inflammatory cells (leukocytes) in the heart. Via western blotting, we did not detect ECM1 protein expression in commercially sourced human cell lines of resident cardiac cells cultured *in vitro*, but saw high ECM1 expression in mouse bulk BMC protein lysates, with a significantly higher level of ECM1 expression in granulocytes compared to monocytes when separated by Ficoll-Paque gradient density centrifugation. Multicolour mRNA FISH-Flow cytometry revealed ECM1+ mouse bone marrow cells are granular, of medium to large size, and are: Ly-6G-intermediate, CD11c-low, Ly-6C-intermediate, F4/80+, CD117-/low, MHC2-, CD3-, FcεrI-α+, CD11b+ and CD45+. Based on our findings, it appeared that ECM1+ cells in the bone marrow of healthy, young mice are macrophages and/or granulocytes (e.g. neutrophils, eosinophils, mast cells) and likely not lymphocytes.

To this point, our results suggested that ECM1 expression in the heart is of inflammatory cell origin, either cardiac-resident leukocytes and/or infiltrating leukocytes. No previous studies have been conducted on ECM1+ cells in bone marrow of young healthy animals, however literature has identified significant ECM1 expression in T_H2 lymphocytes (at day-3 post antigen presentation) in allergic airway inflammation, and macrophages in the colon (12, 14). Although our findings are indicative of macrophages and granulocytes, cells residing in the bone marrow may have different expression of both ECM1, as well as cell surface markers (e.g. MHC2), compared to cells which have migrated to the infarct zone of the heart. This is plausible as migration and phenotype shift of BMCs and other leukocytes to

the site of infarct during the inflammatory phase early post-MI is well established (62, 63). For this reason, it is was important for us to further investigate the cellular origins of ECM1 in the mouse and human heart *in vivo*.

The publication of the Litviňuková, Talavera-López (121) and Farbehi, Patrick (73) scRNAseq publications provided us with an unprecedented new platform to accurately investigate the *in vivo* spatiotemporal expression patterns of ECM1 in the mouse and human heart. Our new ECM1 specific analysis of these existing datasets clearly showed that fibroblasts, macrophages, and pericytes/vascular mural cells are the predominant cellular sources of ECM1 in both mice and humans. Specifically, in the healthy human heart (121), ECM1 was most abundant in a fibroblast subset with high expression of genes involved in the production, remodelling and degradation of ECM (FB5), and fibroblasts with high expression of genes responsive to TGFβ signalling (e.g. POSTN and TNC). Alongside our analysis of the Farbehi, Patrick (73) dataset, we now show that the cellular origin of upregulated ECM1 in the inflammatory phase at day 3 post-MI is mostly recruited M1MΦ macrophages. Later, ECM1 expression is sustained by M2MΦ's involved in inflammation resolution and wound repair, and fibroblast subsets such as myofibroblasts, activated fibroblasts (F-Act), fibroblasts enhanced for secretion and cell signalling (F-SL), and cell adhesion (F-SH). Thus, ECM1 clearly has potential to play a pivotal, dynamic role in both inflammation and fibrosis, or novel crosstalk between the two in post-MI wound healing. When considered alongside our human ECM1 western blotting, IHC and *in-situ* hybridisation (discussed above), it is plausible to extrapolate that these are the sources of ECM1 that we observed in fibrotic, inflammatory and peri-vascular areas in the diseased human heart.

Herein we have used cutting edge scRNAseq technologies to refine our published findings (1), and demonstrate the specific cells of origin in the heart throughout MI, namely macrophages and fibroblasts. Researchers have shown ECM1 to control M1MΦ polarisation in the colon with inflammatory bowel disease (14), highlighting the importance for ECM1 in MΦ-dependent inflammation. It is noteworthy to address that in our previous work (1) we did not detect ECM1 protein expression in fibroblasts cultured *in vitro*. This is likely due to technical reasons, for example antibody quality and/or sensitivity of antibodies; opposed to the accuracy of RNAseq. However, an alternative explanation may be the environmental differences between cell culture and the heart *in vivo*. Another, is with regard to protein

isolation procedures. In our previous work, cultured cells were washed twice with PBS before being subject to protein isolation buffers and procedures (1). As ECM1 has been proposed as a largely secreted protein (11, 109, 120), these technical procedures may have resulted in significant ECM1 protein loss, and the negative signal via western blotting that we observed. Also of note, a distinct neutrophil population was not defined in our scRNAseq analysis data in mice post-MI (73). This may be in part due to the fact that neutrophil cell numbers in the heart peak at day-1 post-MI, and may be largely cleared by day-3 MI (8, 71). However, the MAC-6 population encompassed cells that showed upregulation of neutrophil (Ly6g), granulocyte (S100a9 and Csf3r), and eosinophil markers (Siglecf), but none showed a noteworthy level of ECM1 positivity. Also notable, in the healthy human heart sc/snRNAseq dataset (121) there was an over-representation of PC1_vent cells, and the most populous ECM1+ cell type was PC1_vent. This PC1_vent over-representation is possibly due to cell-specific sensitivity of cell/nuclei isolation methods used, as was discussed before (121). For instance, PC1 had a much lower percentage of ECM1+ cells (7.11%) relative to FB5_ECM-organising (23.15% ECM1+).

Subsequent gene correlation analyses (and GOBP enrichment) of the Farbehi, Patrick (73) mouse scRNAseq dataset indicated that the role of ECM1 cellular expression in the heart post-MI was in ECM and collagen organisation (or remodelling), cell-cell/cell-matrix adhesion, cell migration and cardiac inflammation; fittingly, we confirmed that ECM1 influences HuCFb cell migration in vitro via wound healing assay and a corresponding downregulation of CCL2 (MCP-1) mRNA expression, as discussed later. We found a strong positive correlation between ECM1 expression and the number of outbound ligand-receptor connections in cells, suggesting a functional association between ECM1 expression and intercellular signalling crosstalk. Our analysis (and GOBP enrichment) of DEGs between ECM+ and ECM1- cell populations demonstrated a close functional relationship between ECM1 expression, M1MΦ cell migration, and fibroblast (F-Act and F-SH) dependent extracellular structure and/or ECM organisation. We also identified that the two cellular adhesion proteins Ccdc80 and Fbln1 were commonly upregulated in ECM1+ F-Act, F-SH, and F-SL fibroblasts, further supporting that ECM1 expression is associated with cell-cell/cell-ECM adhesion processes. Indeed, Fbln1 and these other processes also have prominent

roles in pulmonary fibrosis, which may be important areas of future investigations for ECM1 (148).

Our proposed functions of ECM1 are strongly supported by a recent study, which showed upregulation of genes associated with cell adhesion, ECM organisation and cell migration in ECM1 siRNA silenced dermal fibroblasts (107); indeed the authors also showed that "ECM1 knockdown fibroblasts exhibited a marked delay in cell migration and gel contraction". Several other previous studies are in line with our results suggesting that ECM1 has pro-inflammatory effects in IBD (14), influences migration and invasion of cancer cells (120), is a structural basement membrane protein that binds many ECM proteins (Fbln1, Fibronectin, Fibulin-3, Laminin 332, IGF, EGF and MMP-9), and is essential for the maintenance of ECM and overall structural integrity of the skin (11). ECM1 gene mutation is a major cause of the skin disorder lipoid proteinosis (149); these studies gave rise to the description of ECM1 as a multifunctional binding core or a scaffolding protein.

Collectively, our results show that ECM1 is upregulated in human heart disease and expressed predominantly by fibroblasts and macrophages. Our deeper analysis of the Farbehi, Patrick (73) dataset indicated that ECM1 plays a role in ECM structural integrity, inflammation, cell migration, cell/matrix adhesion, and perhaps facilitates intracellular signalling crosstalk. This is plausible as leukocytes, especially macrophages play a pivotal role in inflammation-fibrosis crosstalk, orchestrating ECM remodelling and fibrosis in ischaemic wound healing in the infarct zone (10, 62, 68, 70, 74, 147, 150). Further, macrophages are shown to carry out fibrotic tissue depostion (collagen) themselves (78, 79), and even adopt a "fibroblast-like phenotype post-MI (80). However, to test if ECM1 plays a role in inflammation-fibrosis crosstalk in the heart, we needed to more deeply investigate the effect of ECM1 on CFbs.

15.4 ECM1 is pro-fibrotic, effects fibroblast cell migration, and may facilitate inflammation-fibrosis crosstalk

To first confirm our *in vitro* preliminary results and translate the findings to human cells, we investigated the effect of ECM1 on cultured human CFbs. As published (1), recombinant

ECM1 elicited a rapid activation of ERK1/2 and AKT in HuCFbs, as well as a later increase in collagen-I production. This is the first report of ECM1 dependent HuCFb cell signalling, and demonstrates that ECM1 stimulates cardiac fibroblast proliferative and pro-fibrotic pathways (AKT, ERK1/2, collagen-I), which may contribute to fibrotic tissue formation with aging, and cardiac disease (151-155). Since we know ECM1 is expressed by fibroblasts and cardiac infiltrating macrophages post-MI, our results now strongly suggest that ECM1 plays a role in contributing to cardiac fibrosis, and ECM1 may be a novel intermediary facilitating inflammation-fibrosis crosstalk in wound healing post-MI.

Further unbiased assessment via phosphoproteomics identified that ECM1 also affects pathways associated with Rho protein signalling, cell-cell adhesion, cell polarity, microtubule dynamics, and cell chemotaxis in HuCFbs; some of which are directly in line with our ECM1 scRNAseq correlation analysis. Rho GTPases are small molecular switches that control an array of signal transduction pathways such as cell polarity, microtubule/actin cytoskeleton dynamics, and membrane transport pathways (156). Of interest, we identified 4 differentially phosphorylated proteins involved in Rho protein signalling: ARHGEF11 (157, 158) and ARHGEF12 (159) which are Rho guanine nucleotide exchange factors (RhoGEFs) associated with adherens/tight junctions, cell motility, and Rho protein signalling; the Rho GTPase activator MYO9B involved in cell motility (160); and PTPN12, which is a core controller of both Rho GTPase activity, fibroblast cell motility, actin cytoskeleton remodelling, and cell adhesion (161-163). PHOTON pathway analysis was supportive of this, showing that the Rho GTPase regulator proteins CDC42 and RAC1 are involved in active mediation of ECM1 dependent HuCFb signal transduction (156). In line with these results, Gómez-Contreras, Ramiro-Díaz (108) showed ECM1 is essential in the regulation of cell architecture and microtubule organisation in triple-negative breast cancer cells, and that siRNA against ECM1 significantly distorted cellular architecture. They suggested that the calcium-binding protein s100a4 and/or Rho-family GTPases (Rho A) are the main effectors of these ECM1-dependent cytoskeletal changes. Another recent study suggested a similar influence of ECM1 over AKT/FAK/Rho/cytoskeleton signalling in cancer cells (109).

Our protein-protein binding MS data further implicate ECM1 in Rho protein signal transduction and cell adhesion, showing that ECM1 binds to CTNND1 (also known as p120

catenin) on the HuCFb cell surface/membrane. CTNND1 is a key regulator of cell-cell adhesion, cell/adherens junctions, cell migration and cytoskeletal dynamics via controlling Rho family GTPase activity (143, 164, 165). Mutations in CTNND1 lead to several cardiac abnormalities in humans including ventricular septal defects and mitral valve stenosis (166). Interestingly, PTPN12 (identified in our phosphoproteomics) specifically targets and de-phosphorylates CTNND1, thereby controlling CTNND1's Rho GTPase activity and effects on cell motility (142, 162); as well as restricting CTNND1 subcellular distribution to the leading edge of actin/microtubule-rich cell projections. Studies also show that CTNND1 localises to and has control over actin-rich cell projections (142, 167). These cell signalling locations (GOCCs) were over-represented in our phosphoproteomics dataset and are directly supported by a study in breast cancer cells which showed that ECM1 is expressed at the cytomembrane and the basal region of membrane protrusions, and is essential for invadopodia (actin-rich protrusions of the plasma membrane) formation (168). Thus, our data fits with and extends existing literature on ECM1 control of Rho GTPases and cell morphology to now include this process in heart tissue. Future studies should further investigate the link between ECM1-CTNND1 binding and PTPN12-Rho protein signalling with *in vivo* and genetic knockout models.

Contrary to our proposed function for ECM1 in the heart, a study in the liver suggested that ECM1 has anti-fibrotic properties via sequestering TGFβ in its latent form in the ECM (98). This study showed that ECM1 expression decreases with increasing severity of liver disease in both mice and human patients. The reason for the discrepancy is possibly due to differences in injury models (chronic liver disease *vs* acute MI injury), and/or in inflammatory and fibrotic responses between the liver as a regenerative organ (169), and the adult heart which is non-regenerative (7). Regardless, considering our published study (1) alongside our unbiased scRNAseq cellular expression profile of ECM1 in the mouse and human heart, it appears that ECM1 does not have an overall anti-fibrotic effect in the heart; consistent with that, ECM1 has also been identified as a biomarker for fibrosis in the development of fibrostenotic Crohn's disease (170). Future *in vivo* studies in ECM1 genetic knockout mice will be required to prove this.

Next, we investigated the downstream effects of ECM1 on HuCFbs. We found that ECM1 inhibited the rate of HuCFb migration in wound healing assays and led to a downregulation of the chemotactic gene *CCL2* (*MCP*-1) mRNA expression. Incidentally, Espejo, Jeng (142) showed that PTPN12 knockdown increased cell motility via altering CTNND1 phosphorylation and cellular distribution. Thus, it is enticing to speculate that this effect of ECM1 on HuCFb cell migration is achieved through a CTNND1/PTPN12/*CCL2* axis, however further studies are needed to confirm this. Notably, although ECM1 clearly influences cell migration *in vitro,* these effects may be micro-environment specific and different *in vivo* (171). This may explain why our results contradict previous studies in breast cancer cells showing that ECM1 increases cell migration and invasion in this setting (120).

Next, to follow up our data thus far implicating ECM1 in inflammation-fibrosis crosstalk, we investigated the effect of ECM1 on mRNA expression of inflammatory, fibrotic, and non-canonical Wnt genes. ECM1 stimulated mRNA upregulation of pro-inflammatory genes *IL-1β* & *IL-6*, pro-fibrotic genes *TGF-β1*, *TGF-β2* (3-hours) and *Col1a2* (16 hours), and non-canonical Wnt gene *Wnt5a.* This further indicates that ECM1 induces both inflammatory and fibrotic processes in HuCFbs, in line with our published study (1); and the Zhang, Li (14) in terms of pro-inflammatory effects. Wnt5a acts as a non-canonical Wnt ligand through β-catenin independent signalling pathways, including the planar cell polarity Wnt pathway (Wnt PCP pathway) and the calcium-/ROCK-dependent Wnt pathway to influence microtubule organisation & stability, cell architecture, and cell adhesion properties (172-174). A recent study identified that Wnt5a directly activates Rho GTPase CDC42 and reinforces coupling between adherens junctions and the actin cytoskeleton via these non-canonical Wnt signalling pathways (174). This functionality is consistent with our phosphoproteomics, pathway analysis, and ECM1-CTNND1 binding data. We therefore followed up on this finding, and showed that ECM1 upregulates both JNK1/2/3 phosphorylation (a marker of non-canonical Wnt PCP pathway that also signals through RhoA/Rac GTPases (173)), and MYPT1 phosphorylation (a marker of Wnt Ca^{2+}/ROCK dependent pathways (175)).

Together, our findings indicate that ECM1 is predominantly expressed by fibroblasts and macrophages, and strongly suggest that ECM1 has both inflammatory and fibrotic effects in cardiac disease. ECM1 may facilitate inflammatory-to-fibrotic signalling via traditional pro-

inflammatory and pro-fibrotic pathways, as well as through Rho protein dependent and non-canonical Wnt signalling pathways; thereby regulating cell adhesion, cell migration, and cell cytoskeletal/morphogenic properties. Thus, ECM1 represents a novel mechanism in facilitating inflammation-to-fibrosis crosstalk in the heart post-MI, through a macrophage-fibroblast cell signalling axis.

15.5 Development of an ECM1 genetic knockout murine model

Next, we generated a total body ECM1 genetic knockout mouse on a C57BL/6 background. We assessed 3 different ECM1 knockout stategies, and found the ECM1Δ2 mutation the most appropriate; a frameshift mutation in exon 1 to encode a shortened, non-functional 32aa protein. Homozygous ECM1Δ2 mice ($ECM1^{-/-}$) displayed a phenotype of lower body weight, smaller overall body size, and a significantly lower rate of survival; survival rates decline at ~7-8 weeks of age. Further, we saw a lower ratio of both heart weight to tibia length, and lung weight to tibia length in $ECM1^{-/-}$ mice, suggesting smaller heart and lung size. Our results of $ECM1^{-/-}$ surival are in line with Fan, Liu (98) who also report increased mortality in their $ECM1^{-/-}$ mice at 6-8 weeks of age. This implies a similar phenotype between our ECM1 genetic knockout model and the model generated by Fan, Liu (98). Fortunately, our $ECM1^{+/-}$ mice showed no overt adverse phenotype, nor any change in rate of survival, allowing us to easily and ethically breed these $ECM1^{+/-}$ mice to generate a sustainable colony for future experiments.

Our other phenotyping experiments revealed a significant decrease in the proportion of T cells, a significant increase in the proportion of NK cells in young 'healthy' bone marrow of $ECM1^{-/-}$ mice. This may indicate that ECM1 KO leads to immune alterations. However, it is difficult to interpret these results with regard to the control of ECM1 immune function, and future studies are needed to clarify the phenotype of these animals and define the cause of early death. Future phenotyping studies should include quantification of fibrotic tissue area (i.e., via Masson's trichrome staining) and level of inflammatory cell infiltrate throughout the heart (e.g., via haemotoxylin and eosin [H&E] stain, or May Grunwald-Giemsa [MGG] stain, immunofluorescence and flow cytometry), and assessment of MMP enzymatic activity in LV tissue (zymography). Ideally, this should be conducted on age-matched WT and $ECM1^{-/-}$ mice at 6-weeks of age, prior to the 7-8 week time-point of reduced animal health and

survival; or alternatively in 8-12 week old ECM1$^{+/-}$. However, of highest priority to future work should be mechanistic studies utilising this mouse model.

15.6 Limitations and suggestions for further work

Here we have characterised the expression patterns of ECM1 in both mouse and human cardiac disease for the first time (quantitative, spatial, temporal and cellular), and explored the effect of ECM1 on cardiac fibroblast cells on several levels. We show that ECM1 is upregulated in cardiac disease in both mice and humans. ECM1 expression originates from fibroblasts, macrophages and pericytes/vascular mural cells, with expression predominantly interstitial, localised to fibrotic, inflammatory, and peri-vascular areas in the healthy and diseased heart. ECM1 stimulates collagen-I protein, the expression of fibrotic and inflammatory genes, is implicated in intracellular signalling crosstalk, and induces phosphorylation of Rho and *Wnt5a*/non-canonical Wnt signalling proteins in HuCFbs. Thus, ECM1 influences both inflammatory and fibrotic pathways in cardiac disease, and may represent a novel mechanism in facilitating inflammation-to-fibrosis crosstalk in wound healing post-MI.

Our study has several limitations. One limitation of our study is the lack of genetic knockout/overexpression models. Although we have successfully created an ECM1 KO mouse and conducted initial phenotyping experiments, it is imperitive for future studies to utilise this ECM1 genetic knockout model, alongside viral overexpression/rescue of ECM1 (e.g., AAV), in experiments of surgically induced MI (LAD-ligation). These experiments should compare animal survival, inflammatory cell infiltrate and precise cellular profile (day-3 post-MI, e.g., via flow-cytometry), infarct size (day-28 post-MI), level of MMP enzymatic activity (various time-points, e.g., via zymography), and follow up/validate signalling pathways described in this thesis; detailed further below. Such studies will provide important mechanisctic, physiological, and survival data to determine if modulating ECM1 expression therapeutically can improve wound healing, and meaningfully reduce the mortality associated with cardiac disease and MI. As such, these future experiments will be important to assess translational and clinical potential. Further, these future experiments should be done alongside *in vitro* ECM1 knockout/overexpression experiments of fibroblast and macrophage cell culture. Such studies will provide mechanistic depth, and further proof,

into the cell specific fibrotic and inflammatory roles of ECM1 (i.e., anti-/pro-fibrotic in fibroblasts, or pro-/anti-inflammatory in macrophages?). Incidentally, another limitation of our study, is that due to our focus on fibrosis, all *in vitro* experiments were conducted on cardiac fibroblast cells. Future work should extrapolate our findings and study the effect of ECM1 on macrophages in culture. These studies should utilise fibroblast-macrophage co-culture technique, to allow investigation into our proposed role for ECM1 dependent inflammation-fibrosis cellular crosstalk; this may also help delineate the cell specific roles of ECM1 in fibroblasts and macrophages.

The limitations of our work also provide an excellent starting point for future studies. The cell signalling mechanisms we propose here, particularly ECM1-CTNND1 binding and regulation of PTPN12 and Rho protein signalling, should be of particular focus for the future work to prove the relevance of these mechanisms in ECM1 knockout/overexpression in mice post-MI, and in fibroblast and macrophage cell culture. Further, the large, unbiased datasets generated by our proteomics and ECM1 specific scRNAseq analysis, will provide a useful resource for future work. Our proteomics datasets have been made publicly available via the PRIDE database, allowing researchers in all fields to access and conduct further analysis on our data. This may have implications for research in adjacent areas such as cancer and pulmonary fibrosis. Similarly, our ECM1 specific scRNAseq analysis of the Farbehi, Patrick (73) dataset, provides a large amount of useful data for both future targetted research and hypothesis generation of other roles of ECM1 throughout disease. For example, as we presented here, Lgals1, Lrp1, Fbln1 and Ccdc80 should not be overlooked in future work regarding ECM1 dependent signalling post-MI in fibroblasts and macrophages. Further, with reference to **Fig 8E**, the DEGs upregulated in ECM1+ F-SH, F-Act, F-SL and M1MΦ cells, which are not commonly upregulated between these cell types (i.e., are specifically upregulated in F-SH or M1MΦ alone), may be useful indicators for specific cellular functionality with reference to ECM1. In this way, the data generated here will be useful in future studies focussing on the role of ECM1 throughout various organs/tissues thoughout the body.

16. Bibliography

1. Hardy SA, Mabotuwana NS, Murtha LA, Coulter B, Sanchez-Bezanilla S, Al-Omary MS, et al. Novel role of extracellular matrix protein 1 (ECM1) in cardiac aging and myocardial infarction. PloS one. 2019;14(2):e0212230.
2. Ertl G, Frantz S. Healing after myocardial infarction. Cardiovasc Res. 2005;66(1):22-32.
3. Amini M, Zayeri F, Salehi M. Trend analysis of cardiovascular disease mortality, incidence, and mortality-to-incidence ratio: results from global burden of disease study 2017. BMC Public Health. 2021;21(1):401.
4. Nah D-Y, Rhee M-Y. The Inflammatory Response and Cardiac Repair After Myocardial Infarction. Korean Circulation Journal. 2009;39(10):393-8.
5. Chen W, Frangogiannis NG. Fibroblasts in post-infarction inflammation and cardiac repair. Biochimica et biophysica acta. 2013;1833(4):945-53.
6. Kretzschmar K, Post Y, Bannier-Hélaouët M, Mattiotti A, Drost J, Basak O, et al. Profiling proliferative cells and their progeny in damaged murine hearts. Proceedings of the National Academy of Sciences. 2018;115(52):E12245.
7. Sadek H, Olson EN. Toward the Goal of Human Heart Regeneration. Cell Stem Cell. 2020;26(1):7-16.
8. Forte E, Furtado MB, Rosenthal N. The interstitium in cardiac repair: role of the immune–stromal cell interplay. Nature Reviews Cardiology. 2018;15(10):601-16.
9. Huang S, Frangogiannis NG. Anti-inflammatory therapies in myocardial infarction: failures, hopes and challenges. Br J Pharmacol. 2018;175(9):1377-400.
10. Van Linthout S, Miteva K, Tschope C. Crosstalk between fibroblasts and inflammatory cells. Cardiovascular research. 2014;102(2):258-69.
11. Oyama N, Merregaert J. The Extracellular Matrix Protein 1 (ECM1) in Molecular-Based Skin Biology. In: Farage MA, Miller KW, Maibach HI, editors. Textbook of Aging Skin. Berlin, Heidelberg: Springer Berlin Heidelberg; 2017. p. 91-110.
12. Li Z, Zhang Y, Liu Z, Wu X, Zheng Y, Tao Z, et al. ECM1 controls T(H)2 cell egress from lymph nodes through re-expression of S1P(1). Nature immunology. 2011;12(2):178-85.
13. He L, Gu W, Wang M, Chang X, Sun X, Zhang Y, et al. Extracellular matrix protein 1 promotes follicular helper T cell differentiation and antibody production. Proc Natl Acad Sci U S A. 2018;115(34):8621-6.
14. Zhang Y, Li X, Luo Z, Ma L, Zhu S, Wang Z, et al. ECM1 is an essential factor for the determination of M1 macrophage polarization in IBD in response to LPS stimulation. Proceedings of the National Academy of Sciences. 2020;117(6):3083.
15. Ramirez TA, Jourdan-Le Saux C, Joy A, Zhang J, Dai Q, Mifflin S, et al. Chronic and intermittent hypoxia differentially regulate left ventricular inflammatory and extracellular matrix responses. Hypertens Res. 2012;35(8):811-8.
16. Olson EN, Schneider MD. Sizing up the heart: development redux in disease. Genes & development. 2003;17(16):1937-56.
17. Woodcock EA, Matkovich SJ. Cardiomyocytes structure, function and associated pathologies. The International Journal of Biochemistry & Cell Biology. 2005;37(9):1746-51.
18. Souders CA, Bowers SL, Baudino TA. Cardiac fibroblast: the renaissance cell. Circulation research. 2009;105(12):1164-76.
19. Baum J, Duffy HS. Fibroblasts and myofibroblasts: what are we talking about? Journal of cardiovascular pharmacology. 2011;57(4):376-9.
20. Kohl P, Gourdie RG. Fibroblast–myocyte electrotonic coupling: Does it occur in native cardiac tissue? Journal of Molecular and Cellular Cardiology. 2014;70:37-46.
21. Sadoshima J, Weiss JN. Cardiac fibroblasts: The good, the bad, the ugly, the beautiful. Journal of Molecular and Cellular Cardiology. 2014;70:1.

22. Tomasek JJ, Gabbiani G, Hinz B, Chaponnier C, Brown RA. Myofibroblasts and mechano-regulation of connective tissue remodelling. Nature reviews Molecular cell biology. 2002;3(5):349-63.
23. Serini G, Bochaton-Piallat M-L, Ropraz P, Geinoz A, Borsi L, Zardi L, et al. The Fibronectin Domain ED-A Is Crucial for Myofibroblastic Phenotype Induction by Transforming Growth Factor-β1. The Journal of Cell Biology. 1998;142(3):873-81.
24. Biernacka A, Frangogiannis NG. Aging and Cardiac Fibrosis. Aging and Disease. 2011;2(2):158-73.
25. Davis J, Molkentin JD. Myofibroblasts: Trust your heart and let fate decide. Journal of Molecular and Cellular Cardiology. 2014;70:9-18.
26. van den Borne SW, Diez J, Blankesteijn WM, Verjans J, Hofstra L, Narula J. Myocardial remodeling after infarction: the role of myofibroblasts. Nature reviews Cardiology. 2010;7(1):30-7.
27. Blankesteijn WM, Essers-Janssen YP, Verluyten MJ, Daemen MJ, Smits JF. A homologue of Drosophila tissue polarity gene frizzled is expressed in migrating myofibroblasts in the infarcted rat heart. Nature medicine. 1997;3(5):541-4.
28. Weber KT, Sun Y, Bhattacharya SK, Ahokas RA, Gerling IC. Myofibroblast-mediated mechanisms of pathological remodelling of the heart. Nature reviews Cardiology. 2013;10(1):15-26.
29. Cleutjens JP, Verluyten MJ, Smiths JF, Daemen MJ. Collagen remodeling after myocardial infarction in the rat heart. The American journal of pathology. 1995;147(2):325-38.
30. Filip DA, Radu A, Simionescu M. Interstitial cells of the heart valves possess characteristics similar to smooth muscle cells. Circulation research. 1986;59(3):310-20.
31. Calderone A, Bel-Hadj S, Drapeau J, El-Helou V, Gosselin H, Clement R, et al. Scar myofibroblasts of the infarcted rat heart express natriuretic peptides. Journal of cellular physiology. 2006;207(1):165-73.
32. Schuetze KB, McKinsey TA, Long CS. Targeting cardiac fibroblasts to treat fibrosis of the heart: Focus on HDACs. Journal of Molecular and Cellular Cardiology. 2014;70:100-7.
33. Willems IE, Havenith MG, De Mey JG, Daemen MJ. The alpha-smooth muscle actin-positive cells in healing human myocardial scars. Am J Pathol. 1994;145(4):868-75.
34. de Castro Bras LE, Toba H, Baicu CF, Zile MR, Weintraub ST, Lindsey ML, et al. Age and SPARC change the extracellular matrix composition of the left ventricle. BioMed research international. 2014;2014:810562.
35. Horn MA, Trafford AW. Aging and the cardiac collagen matrix: Novel mediators of fibrotic remodelling. Journal of Molecular and Cellular Cardiology. 2016;93:175-85.
36. Berk BC, Fujiwara K, Lehoux S. ECM remodeling in hypertensive heart disease. The Journal of clinical investigation. 2007;117(3):568-75.
37. Byron A, Humphries JD, Humphries MJ. Defining the extracellular matrix using proteomics. Int J Exp Pathol. 2013;94(2):75-92.
38. Burgess ML, McCrea JC, Hedrick HL. Age-associated changes in cardiac matrix and integrins. Mechanisms of Ageing and Development. 2001;122(15):1739-56.
39. de Souza RR. Aging of myocardial collagen. Biogerontology. 2002;3(6):325-35.
40. Yabluchanskiy A, Ma Y, Iyer RP, Hall ME, Lindsey ML. Matrix metalloproteinase-9: Many shades of function in cardiovascular disease. Physiology (Bethesda). 2013;28(6):391-403.
41. Shamhart PE, Meszaros JG. Non-fibrillar collagens: Key mediators of post-infarction cardiac remodeling? Journal of Molecular and Cellular Cardiology. 2010;48(3):530-7.
42. McCurdy S, Baicu CF, Heymans S, Bradshaw AD. Cardiac Extracellular Matrix Remodeling: Fibrillar Collagens and Secreted Protein Acidic and Rich in Cysteine (SPARC). Journal of molecular and cellular cardiology. 2010;48(3):544-9.
43. Ma Y, de Castro Brás LE, Toba H, Iyer RP, Hall ME, Winniford MD, et al. Myofibroblasts and the extracellular matrix network in post-myocardial infarction cardiac remodeling. Pflugers Archiv. 2014;466(6):1113-27.

44. Bishop JE, Greenbaum R, Gibson DG, Yacoub M, Laurent GJ. Enhanced deposition of predominantly type I collagen in myocardial disease. J Mol Cell Cardiol. 1990;22(10):1157-65.
45. Kong P, Christia P, Frangogiannis NG. The pathogenesis of cardiac fibrosis. Cellular and molecular life sciences : CMLS. 2014;71(4):549-74.
46. Stamenkovic I. Extracellular matrix remodelling: the role of matrix metalloproteinases. The Journal of pathology. 2003;200(4):448-64.
47. Parks WC, Wilson CL, Lopez-Boado YS. Matrix metalloproteinases as modulators of inflammation and innate immunity. Nat Rev Immunol. 2004;4(8):617-29.
48. Howard CM, Baudino TA. Dynamic cell–cell and cell–ECM interactions in the heart. Journal of Molecular and Cellular Cardiology. 2014;70:19-26.
49. Raffetto JD, Khalil RA. Matrix Metalloproteinases and their Inhibitors in Vascular Remodeling and Vascular Disease. Biochemical pharmacology. 2008;75(2):346-59.
50. Visse R, Nagase H. Matrix metalloproteinases and tissue inhibitors of metalloproteinases: structure, function, and biochemistry. Circulation research. 2003;92(8):827-39.
51. Kwak H-B. Aging, exercise, and extracellular matrix in the heart. Journal of exercise rehabilitation. 2013;9(3):338-47.
52. Brew K, Nagase H. The tissue inhibitors of metalloproteinases (TIMPs): An ancient family with structural and functional diversity. Biochimica et biophysica acta. 2010;1803(1):55-71.
53. Krenning G, Zeisberg EM, Kalluri R. The origin of fibroblasts and mechanism of cardiac fibrosis. J Cell Physiol. 2010;225(3):631-7.
54. Tian J, An X, Niu L. Myocardial fibrosis in congenital and pediatric heart disease. Experimental and Therapeutic Medicine. 2017;13(5):1660-4.
55. Menon SC, Eidem BW, Dearani JA, Ommen SR, Ackerman MJ, Miller D. Diastolic dysfunction and its histopathological correlation in obstructive hypertrophic cardiomyopathy in children and adolescents. Journal of the American Society of Echocardiography : official publication of the American Society of Echocardiography. 2009;22(12):1327-34.
56. de Boer RA, De Keulenaer G, Bauersachs J, Brutsaert D, Cleland JG, Diez J, et al. Towards better definition, quantification and treatment of fibrosis in heart failure. A scientific roadmap by the Committee of Translational Research of the Heart Failure Association (HFA) of the European Society of Cardiology. European journal of heart failure. 2019;21(3):272-85.
57. Shinde AV, Frangogiannis NG. Fibroblasts in myocardial infarction: A role in inflammation and repair. Journal of Molecular and Cellular Cardiology. 2014;70:74-82.
58. Thygesen K, Alpert JS, Jaffe AS, Chaitman BR, Bax JJ, Morrow DA, et al. Fourth Universal Definition of Myocardial Infarction (2018). Circulation. 2018;138(20):e618-e51.
59. Lusis AJ. Atherosclerosis. Nature. 2000;407(6801):233-41.
60. Swirski FK, Nahrendorf M. Cardioimmunology: the immune system in cardiac homeostasis and disease. Nature Reviews Immunology. 2018;18(12):733-44.
61. O'Rourke SA, Dunne A, Monaghan MG. The Role of Macrophages in the Infarcted Myocardium: Orchestrators of ECM Remodeling. Front Cardiovasc Med. 2019;6:101-.
62. Hofmann U, Frantz S. Role of lymphocytes in myocardial injury, healing, and remodeling after myocardial infarction. Circulation research. 2015;116(2):354-67.
63. Swirski FK, Nahrendorf M, Etzrodt M, Wildgruber M, Cortez-Retamozo V, Panizzi P, et al. Identification of Splenic Reservoir Monocytes and Their Deployment to Inflammatory Sites. Science. 2009;325(5940):612.
64. Duncan SE, Gao S, Sarhene M, Coffie JW, Linhua D, Bao X, et al. Macrophage Activities in Myocardial Infarction and Heart Failure. Cardiology research and practice. 2020;2020:4375127-.
65. Mescher AL. Macrophages and fibroblasts during inflammation and tissue repair in models of organ regeneration. Regeneration (Oxf). 2017;4(2):39-53.
66. Ortega-Gómez A, Perretti M, Soehnlein O. Resolution of inflammation: an integrated view. EMBO molecular medicine. 2013;5(5):661-74.

67. Liehn EA, Postea O, Curaj A, Marx N. Repair after myocardial infarction, between fantasy and reality: the role of chemokines. Journal of the American College of Cardiology. 2011;58(23):2357-62.
68. Okyere AD, Tilley DG. Leukocyte-Dependent Regulation of Cardiac Fibrosis. Frontiers in physiology. 2020;11:301-.
69. de Couto G. Macrophages in cardiac repair: Environmental cues and therapeutic strategies. Experimental & Molecular Medicine. 2019;51(12):1-10.
70. Horckmans M, Ring L, Duchene J, Santovito D, Schloss MJ, Drechsler M, et al. Neutrophils orchestrate post-myocardial infarction healing by polarizing macrophages towards a reparative phenotype. Eur Heart J. 2017;38(3):187-97.
71. Frodermann V, Nahrendorf M. Neutrophil–macrophage cross-talk in acute myocardial infarction. European Heart Journal. 2017;38(3):198-200.
72. Forte E, Skelly DA, Chen M, Daigle S, Morelli KA, Hon O, et al. Dynamic Interstitial Cell Response during Myocardial Infarction Predicts Resilience to Rupture in Genetically Diverse Mice. Cell Reports. 2020;30(9):3149-63.e6.
73. Farbehi N, Patrick R, Dorison A, Xaymardan M, Janbandhu V, Wystub-Lis K, et al. Single-cell expression profiling reveals dynamic flux of cardiac stromal, vascular and immune cells in health and injury. eLife. 2019;8:e43882.
74. Thomas TP, Grisanti LA. The Dynamic Interplay Between Cardiac Inflammation and Fibrosis. Frontiers in physiology. 2020;11:1133.
75. Jung M, Ma Y, Iyer RP, DeLeon-Pennell KY, Yabluchanskiy A, Garrett MR, et al. IL-10 improves cardiac remodeling after myocardial infarction by stimulating M2 macrophage polarization and fibroblast activation. Basic research in cardiology. 2017;112(3):33.
76. Suthahar N, Meijers WC, Silljé HHW, de Boer RA. From Inflammation to Fibrosis—Molecular and Cellular Mechanisms of Myocardial Tissue Remodelling and Perspectives on Differential Treatment Opportunities. Current Heart Failure Reports. 2017;14(4):235-50.
77. Hume RD, Chong JJH. The Cardiac Injury Immune Response as a Target for Regenerative and Cellular Therapies. Clinical Therapeutics. 2020;42(10):1923-43.
78. Simões FC, Cahill TJ, Kenyon A, Gavriouchkina D, Vieira JM, Sun X, et al. Macrophages directly contribute collagen to scar formation during zebrafish heart regeneration and mouse heart repair. Nat Commun. 2020;11(1):600.
79. Mouton AJ, DeLeon-Pennell KY, Rivera Gonzalez OJ, Flynn ER, Freeman TC, Saucerman JJ, et al. Mapping macrophage polarization over the myocardial infarction time continuum. Basic research in cardiology. 2018;113(4):26.
80. Haider N, Boscá L, Zandbergen HR, Kovacic JC, Narula N, González-Ramos S, et al. Transition of Macrophages to Fibroblast-Like Cells in Healing Myocardial Infarction. Journal of the American College of Cardiology. 2019;74(25):3124-35.
81. Zhang M, Zhang S. T Cells in Fibrosis and Fibrotic Diseases. Frontiers in Immunology. 2020;11(1142).
82. Daseke MJ, Valerio FM, Kalusche WJ, Ma Y, DeLeon-Pennell KY, Lindsey ML. Neutrophil proteome shifts over the myocardial infarction time continuum. Basic research in cardiology. 2019;114(5):37.
83. Bhalerao J, Tylzanowski P, Filie JD, Kozak CA, Merregaert J. Molecular cloning, characterization, and genetic mapping of the cDNA coding for a novel secretory protein of mouse. Demonstration of alternative splicing in skin and cartilage. The Journal of biological chemistry. 1995;270(27):16385-94.
84. Smits P, Ni J, Feng P, Wauters J, Van Hul W, Boutaibi ME, et al. The human extracellular matrix gene 1 (ECM1): genomic structure, cDNA cloning, expression pattern, and chromosomal localization. Genomics. 1997;45(3):487-95.
85. Philley JV, Kannan A, Griffith DE, Devine MS, Benwill JL, Wallace RJ, et al. Exosome secretome and mediated signaling in breast cancer patients with nontuberculous mycobacterial disease. Oncotarget. 2017;8(11):18070-81.

86. Deckers MM, Smits P, Karperien M, Ni J, Tylzanowski P, Feng P, et al. Recombinant human extracellular matrix protein 1 inhibits alkaline phosphatase activity and mineralization of mouse embryonic metatarsals in vitro. Bone. 2001;28(1):14-20.
87. Kong L, Tian Q, Guo F, Mucignat MT, Perris R, Sercu S, et al. Interaction between Cartilage Oligomeric Matrix Protein and Extracellular Matrix Protein 1 Mediates Endochondral Bone Growth. Matrix biology : journal of the International Society for Matrix Biology. 2010;29(4):276-86.
88. Patel S, Xi ZF, Seo EY, McGaughey D, Segre JA. Klf4 and corticosteroids activate an overlapping set of transcriptional targets to accelerate in utero epidermal barrier acquisition. Proceedings of the National Academy of Sciences of the United States of America. 2006;103(49):18668-73.
89. Fujimoto N, Terlizzi J, Brittingham R, Fertala A, McGrath JA, Uitto J. Extracellular matrix protein 1 interacts with the domain III of fibulin-1C and 1D variants through its central tandem repeat 2. Biochemical and biophysical research communications. 2005;333(4):1327-33.
90. Nasir M, Latif A, Ajmal M, Qamar R, Naeem M, Hameed A. Molecular analysis of lipoid proteinosis: identification of a novel nonsense mutation in the ECM1 gene in a Pakistani family. Diagn Pathol. 2011;6:69.
91. Sercu S, Zhang M, Oyama N, Hansen U, Ghalbzouri AE, Jun G, et al. Interaction of extracellular matrix protein 1 with extracellular matrix components: ECM1 is a basement membrane protein of the skin. J Invest Dermatol. 2008;128(6):1397-408.
92. Sercu S, Zhang L, Merregaert J. The extracellular matrix protein 1: its molecular interaction and implication in tumor progression. Cancer Invest. 2008;26(4):375-84.
93. Sercu S, Lambeir AM, Steenackers E, El Ghalbzouri A, Geentjens K, Sasaki T, et al. ECM1 interacts with fibulin-3 and the beta 3 chain of laminin 332 through its serum albumin subdomain-like 2 domain. Matrix biology : journal of the International Society for Matrix Biology. 2009;28(3):160-9.
94. Merregaert J, Van Langen J, Hansen U, Ponsaerts P, El Ghalbzouri A, Steenackers E, et al. Phospholipid Scramblase 1 Is Secreted by a Lipid Raft-dependent Pathway and Interacts with the Extracellular Matrix Protein 1 in the Dermal Epidermal Junction Zone of Human Skin. The Journal of biological chemistry. 2010;285(48):37823-37.
95. Mongiat M, Fu J, Oldershaw R, Greenhalgh R, Gown AM, Iozzo RV. Perlecan protein core interacts with extracellular matrix protein 1 (ECM1), a glycoprotein involved in bone formation and angiogenesis. The Journal of biological chemistry. 2003;278(19):17491-9.
96. Merregaert J, Van Langen J, Hansen U, Ponsaerts P, El Ghalbzouri A, Steenackers E, et al. Phospholipid scramblase 1 is secreted by a lipid raft-dependent pathway and interacts with the extracellular matrix protein 1 in the dermal epidermal junction zone of human skin. The Journal of biological chemistry. 2010;285(48):37823-37.
97. Lee KM, Nam K, Oh S, Lim J, Kim YP, Lee JW, et al. Extracellular matrix protein 1 regulates cell proliferation and trastuzumab resistance through activation of epidermal growth factor signaling. Breast Cancer Res. 2014;16(6):479.
98. Fan W, Liu T, Chen W, Hammad S, Longerich T, Hausser I, et al. ECM1 Prevents Activation of Transforming Growth Factor beta, Hepatic Stellate Cells, and Fibrogenesis in Mice. Gastroenterology. 2019;157(5):1352-67.e13.
99. Fujimoto N, Terlizzi J, Aho S, Brittingham R, Fertala A, Oyama N, et al. Extracellular matrix protein 1 inhibits the activity of matrix metalloproteinase 9 through high-affinity protein/protein interactions. Experimental dermatology. 2006;15(4):300-7.
100. Oyama N, Chan I, Neill SM, Hamada T, South AP, Wessagowit V, et al. Autoantibodies to extracellular matrix protein 1 in lichen sclerosus. The Lancet. 2003;362(9378):118-23.
101. Oyama N, Chan I, Neill SM, South AP, Wojnarowska F, Kawakami Y, et al. Development of antigen-specific ELISA for circulating autoantibodies to extracellular matrix protein 1 in lichen sclerosus. Journal of Clinical Investigation. 2004;113(11):1550-9.

102. Chan I. The role of extracellular matrix protein 1 in human skin. Clinical and experimental dermatology. 2004;29(1):52-6.
103. Wilson R, Norris EL, Brachvogel B, Angelucci C, Zivkovic S, Gordon L, et al. Changes in the Chondrocyte and Extracellular Matrix Proteome during Post-natal Mouse Cartilage Development. Molecular & Cellular Proteomics : MCP. 2012;11(1):M111.014159.
104. Haleem-Smith H, Calderon R, Song Y, Tuan RS, Chen FH. CARTILAGE OLIGOMERIC MATRIX PROTEIN ENHANCES MATRIX ASSEMBLY DURING CHONDROGENESIS OF HUMAN MESENCHYMAL STEM CELLS. Journal of Cellular Biochemistry. 2012;113(4):1245-52.
105. Kong L, Zhao YP, Tian QY, Feng JQ, Kobayashi T, Merregaert J, et al. Extracellular matrix protein 1, a direct targeting molecule of parathyroid hormone-related peptide, negatively regulates chondrogenesis and endochondral ossification via associating with progranulin growth factor. FASEB journal : official publication of the Federation of American Societies for Experimental Biology. 2016.
106. Su P, Chen S, Zheng YH, Zhou HY, Yan CH, Yu F, et al. Novel Function of Extracellular Matrix Protein 1 in Suppressing Th17 Cell Development in Experimental Autoimmune Encephalomyelitis. Journal of immunology (Baltimore, Md : 1950). 2016;197(4):1054-64.
107. Utsunomiya N, Utsunomiya A, Chino T, Hasegawa M, Oyama N. Gene silencing of extracellular matrix protein 1 (ECM1) results in phenotypic alterations of dermal fibroblasts reminiscent of clinical features of lichen sclerosus. Journal of Dermatological Science. 2020;100(2):99-109.
108. Gómez-Contreras P, Ramiro-Díaz JM, Sierra A, Stipp C, Domann FE, Weigel RJ, et al. Extracellular matrix 1 (ECM1) regulates the actin cytoskeletal architecture of aggressive breast cancer cells in part via S100A4 and Rho-family GTPases. Clinical & experimental metastasis. 2017;34(1):37-49.
109. Yin H, Wang J, Li H, Yu Y, Wang X, Lu L, et al. Extracellular matrix protein-1 secretory isoform promotes ovarian cancer through increasing alternative mRNA splicing and stemness. Nat Commun. 2021;12(1):4230.
110. Pauws E, Veenboer GJ, Smit JW, de Vijlder JJ, Morreau H, Ris-Stalpers C. Genes differentially expressed in thyroid carcinoma identified by comparison of SAGE expression profiles. FASEB journal : official publication of the Federation of American Societies for Experimental Biology. 2004;18(3):560-1.
111. Wang L, Yu J, Ni J, Xu XM, Wang J, Ning H, et al. Extracellular matrix protein 1 (ECM1) is over-expressed in malignant epithelial tumors. Cancer letters. 2003;200(1):57-67.
112. Ye H, Yu X, Xia J, Tang X, Tang L, Chen F. MiR-486-3p targeting ECM1 represses cell proliferation and metastasis in cervical cancer. Biomedicine & pharmacotherapy = Biomedecine & pharmacotherapie. 2016;80:109-14.
113. Wu Q, Li X, Yang H, Lu C, You J, Zhang Z. Extracellular matrix protein 1 is correlated to carcinogenesis and lymphatic metastasis of human gastric cancer. World journal of surgical oncology. 2014;12:132.
114. Meng XY, Liu J, Lv F, Liu MQ, Wan JM. Study on the correlation between extracellular matrix protein-1 and the growth, metastasis and angiogenesis of laryngeal carcinoma. Asian Pacific journal of cancer prevention : APJCP. 2015;16(6):2313-6.
115. Zhang Y, Wang H, Wang J, Bao L, Wang L, Huo J, et al. Global analysis of chromosome 1 genes among patients with lung adenocarcinoma, squamous carcinoma, large-cell carcinoma, small-cell carcinoma, or non-cancer. Cancer metastasis reviews. 2015;34(2):249-64.
116. Savore C, Zhang C, Muir C, Liu R, Wyrwa J, Shu J, et al. Perlecan knockdown in metastatic prostate cancer cells reduces heparin-binding growth factor responses in vitro and tumor growth in vivo. Clinical & experimental metastasis. 2005;22(5):377-90.
117. Chattopadhyay S, Shubayev VI. MMP-9 controls Schwann cell proliferation and phenotypic remodeling via IGF-1 and ErbB receptor-mediated activation of MEK/ERK pathway. Glia. 2009;57(12):1316-25.

118. Lee KM, Nam K, Oh S, Lim J, Lee T, Shin I. ECM1 promotes the Warburg effect through EGF-mediated activation of PKM2. Cellular signalling. 2015;27(2):228-35.
119. Wang Z, Zhou Q, Li A, Huang W, Cai Z, Chen W. Extracellular matrix protein 1 (ECM1) is associated with carcinogenesis potential of human bladder cancer. Onco Targets Ther. 2019;12:1423-32.
120. Steinhaeuser SS, Morera E, Budkova Z, Schepsky A, Wang Q, Rolfsson O, et al. ECM1 secreted by HER2-overexpressing breast cancer cells promotes formation of a vascular niche accelerating cancer cell migration and invasion. Laboratory Investigation. 2020;100(7):928-44.
121. Litviňuková M, Talavera-López C, Maatz H, Reichart D, Worth CL, Lindberg EL, et al. Cells of the adult human heart. Nature. 2020;588(7838):466-72.
122. Boyle AJ, Hwang J, Ye J, Shih H, Jun K, Zhang Y, et al. The Effects of Aging on Apoptosis Following Myocardial Infarction. Cardiovascular therapeutics. 2013;31(6):e102-e10.
123. Boyle AJ, Shih H, Hwang J, Ye J, Lee B, Zhang Y, et al. Cardiomyopathy of aging in the mammalian heart is characterized by myocardial hypertrophy, fibrosis and a predisposition towards cardiomyocyte apoptosis and autophagy. Experimental gerontology. 2011;46(7):549-59.
124. Liu X, Quan N. Immune Cell Isolation from Mouse Femur Bone Marrow. Bio-protocol. 2015;5(20):e1631.
125. Kim RY, Pinkerton JW, Essilfie AT, Robertson AAB, Baines KJ, Brown AC, et al. Role for NLRP3 Inflammasome-mediated, IL-1beta-Dependent Responses in Severe, Steroid-Resistant Asthma. American journal of respiratory and critical care medicine. 2017;196(3):283-97.
126. Ljubojević-Holzer S, Kraler S, Djalinac N, Abdellatif M, Voglhuber J, Schipke J, et al. Loss of autophagy protein ATG5 impairs cardiac capacity in mice and humans through diminishing mitochondrial abundance and disrupting Ca2+ cycling. Cardiovascular research. 2021.
127. Koressaar T, Remm M. Enhancements and modifications of primer design program Primer3. Bioinformatics (Oxford, England). 2007;23(10):1289-91.
128. Untergasser A, Cutcutache I, Koressaar T, Ye J, Faircloth BC, Remm M, et al. Primer3--new capabilities and interfaces. Nucleic acids research. 2012;40(15):e115.
129. Abràmoff MD, Magalhães PJ, Ram SJ. Image processing with ImageJ. Biophotonics international. 2004;11(7):36-42.
130. Schneider CA, Rasband WS, Eliceiri KW. NIH Image to ImageJ: 25 years of image analysis. Nature methods. 2012;9(7):671-5.
131. Perez-Riverol Y, Csordas A, Bai J, Bernal-Llinares M, Hewapathirana S, Kundu DJ, et al. The PRIDE database and related tools and resources in 2019: improving support for quantification data. Nucleic acids research. 2019;47(D1):D442-d50.
132. Humphrey SJ, Karayel O, James DE, Mann M. High-throughput and high-sensitivity phosphoproteomics with the EasyPhos platform. Nature protocols. 2018;13(9):1897-916.
133. Cox J, Hein MY, Luber CA, Paron I, Nagaraj N, Mann M. Accurate proteome-wide label-free quantification by delayed normalization and maximal peptide ratio extraction, termed MaxLFQ. Mol Cell Proteomics. 2014;13(9):2513-26.
134. Tyanova S, Temu T, Cox J. The MaxQuant computational platform for mass spectrometry-based shotgun proteomics. Nature protocols. 2016;11(12):2301-19.
135. Rudolph JD, de Graauw M, van de Water B, Geiger T, Sharan R. Elucidation of Signaling Pathways from Large-Scale Phosphoproteomic Data Using Protein Interaction Networks. Cell systems. 2016;3(6):585-93.e3.
136. Szklarczyk D, Gable AL, Lyon D, Junge A, Wyder S, Huerta-Cepas J, et al. STRING v11: protein-protein association networks with increased coverage, supporting functional discovery in genome-wide experimental datasets. Nucleic acids research. 2019;47(D1):D607-d13.
137. Pomaznoy M, Ha B, Peters B. GOnet: a tool for interactive Gene Ontology analysis. BMC Bioinformatics. 2018;19(1):470.
138. Shevchenko A, Wilm M, Vorm O, Mann M. Mass spectrometric sequencing of proteins silver-stained polyacrylamide gels. Analytical chemistry. 1996;68(5):850-8.

139. Lim HY, Lim SY, Tan CK, Thiam CH, Goh CC, Carbajo D, et al. Hyaluronan Receptor LYVE-1-Expressing Macrophages Maintain Arterial Tone through Hyaluronan-Mediated Regulation of Smooth Muscle Cell Collagen. Immunity. 2018;49(2):326-41.e7.
140. Seropian IM, González GE, Maller SM, Berrocal DH, Abbate A, Rabinovich GA. Galectin-1 as an Emerging Mediator of Cardiovascular Inflammation: Mechanisms and Therapeutic Opportunities. Mediators of Inflammation. 2018;2018:8696543.
141. Potere N, Del Buono MG, Mauro AG, Abbate A, Toldo S. Low Density Lipoprotein Receptor-Related Protein-1 in Cardiac Inflammation and Infarct Healing. Front Cardiovasc Med. 2019;6:51.
142. Espejo R, Jeng Y, Paulucci-Holthauzen A, Rengifo-Cam W, Honkus K, Anastasiadis PZ, et al. PTP-PEST targets a novel tyrosine site in p120 catenin to control epithelial cell motility and Rho GTPase activity. Journal of cell science. 2014;127(Pt 3):497-508.
143. Epifano C, Megias D, Perez-Moreno M. p120-catenin differentially regulates cell migration by Rho-dependent intracellular and secreted signals. EMBO reports. 2014;15(5):592-600.
144. Lu L, Guo J, Hua Y, Huang K, Magaye R, Cornell J, et al. Cardiac fibrosis in the ageing heart: Contributors and mechanisms. Clinical and Experimental Pharmacology and Physiology. 2017;44(S1):55-63.
145. Cieslik KA, Trial J, Crawford JR, Taffet GE, Entman ML. Adverse fibrosis in the aging heart depends on signaling between myeloid and mesenchymal cells; role of inflammatory fibroblasts. Journal of Molecular and Cellular Cardiology. 2014;70:56-63.
146. Cieslik KA, Taffet GE, Carlson S, Hermosillo J, Trial J, Entman ML. Immune-inflammatory dysregulation modulates the incidence of progressive fibrosis and diastolic stiffness in the aging heart. J Mol Cell Cardiol. 2011;50(1):248-56.
147. Toor IS, Rückerl D, Thomson A, Tang K, Newby DE, Rossi AG, et al. E Eosinophils have an essential role in cardiac repair following myocardial infarction. Heart. 2017;103(Suppl 5):A152.
148. Liu G, Cooley MA, Jarnicki AG, Borghuis T, Nair PM, Tjin G, et al. Fibulin-1c regulates transforming growth factor-β activation in pulmonary tissue fibrosis. JCI insight. 2019;5(16):e124529.
149. Hamada T, McLean WH, Ramsay M, Ashton GH, Nanda A, Jenkins T, et al. Lipoid proteinosis maps to 1q21 and is caused by mutations in the extracellular matrix protein 1 gene (ECM1). Human molecular genetics. 2002;11(7):833-40.
150. Walter W, Alonso-Herranz L, Trappetti V, Crespo I, Ibberson M, Cedenilla M, et al. Deciphering the Dynamic Transcriptional and Post-transcriptional Networks of Macrophages in the Healthy Heart and after Myocardial Injury. Cell Reports. 2018;23(2):622-36.
151. Rose BA, Force T, Wang Y. Mitogen-Activated Protein Kinase Signaling in the Heart: Angels Versus Demons in a Heart-Breaking Tale. Physiological reviews. 2010;90(4):10.1152/physrev.00054.2009.
152. Diez C, Nestler M, Friedrich U, Vieth M, Stolte M, Hu K, et al. Down-regulation of Akt/PKB in senescent cardiac fibroblasts impairs PDGF-induced cell proliferation. Cardiovascular research. 2001;49(4):731-40.
153. Gao Y, Chu M, Hong J, Shang J, Xu D. Hypoxia induces cardiac fibroblast proliferation and phenotypic switch: a role for caveolae and caveolin-1/PTEN mediated pathway. Journal of Thoracic Disease. 2014;6(10):1458-68.
154. Li L, Fan D, Wang C, Wang J-Y, Cui X-B, Wu D, et al. Angiotensin II increases periostin expression via Ras/p38 MAPK/CREB and ERK1/2/TGF-β1 pathways in cardiac fibroblasts. Cardiovascular research. 2011;91(1):80-9.
155. Luo S, Hieu TB, Ma F, Yu Y, Cao Z, Wang M, et al. ZYZ-168 alleviates cardiac fibrosis after myocardial infarction through inhibition of ERK1/2-dependent ROCK1 activation. Scientific Reports. 2017;7:43242.
156. Etienne-Manneville S, Hall A. Rho GTPases in cell biology. Nature. 2002;420(6916):629-35.
157. Itoh M, Tsukita S, Yamazaki Y, Sugimoto H. Rho GTP exchange factor ARHGEF11 regulates the integrity of epithelial junctions by connecting ZO-1 and RhoA-Myosin II signaling. Proceedings of the National Academy of Sciences. 2012;109(25):9905.

158. Mizuki Y, Takaki M, Sakamoto S, Okamoto S, Kishimoto M, Okahisa Y, et al. Human Rho Guanine Nucleotide Exchange Factor 11 (ARHGEF11) Regulates Dendritic Morphogenesis. International Journal of Molecular Sciences. 2017;18(1).
159. Lessey-Morillon EC, Osborne LD, Monaghan-Benson E, Guilluy C, O'Brien ET, Superfine R, et al. The RhoA guanine nucleotide exchange factor, LARG, mediates ICAM-1-dependent mechanotransduction in endothelial cells to stimulate transendothelial migration. Journal of immunology (Baltimore, Md : 1950). 2014;192(7):3390-8.
160. Hemkemeyer SA, Vollmer V, Schwarz V, Lohmann B, Honnert U, Taha M, et al. Local Myo9b RhoGAP activity regulates cell motility. The Journal of biological chemistry. 2020;296:100136.
161. Mansour M, Nievergall E, Gegenbauer K, Llerena C, Atapattu L, Hallé M, et al. PTP-PEST controls EphA3 activation and ephrin-induced cytoskeletal remodelling. Journal of cell science. 2016;129(2):277-89.
162. Lee K-J, Kim Y, Kim MS, Ju H-M, Choi B, Lee H, et al. CD99-PTPN12 Axis Suppresses Actin Cytoskeleton-Mediated Dimerization of Epidermal Growth Factor Receptor. Cancers. 2020;12(10):2895.
163. Young KA, Biggins L, Sharpe HJ. Protein tyrosine phosphatases in cell adhesion. Biochemical Journal. 2021;478(5):1061-83.
164. Anastasiadis PZ, Moon SY, Thoreson MA, Mariner DJ, Crawford HC, Zheng Y, et al. Inhibition of RhoA by p120 catenin. Nat Cell Biol. 2000;2(9):637-44.
165. Wildenberg GA, Dohn MR, Carnahan RH, Davis MA, Lobdell NA, Settleman J, et al. p120-catenin and p190RhoGAP regulate cell-cell adhesion by coordinating antagonism between Rac and Rho. Cell. 2006;127(5):1027-39.
166. Alharatani R, Ververi A, Beleza-Meireles A, Ji W, Mis E, Patterson QT, et al. Novel truncating mutations in CTNND1 cause a dominant craniofacial and cardiac syndrome. bioRxiv. 2019:711184.
167. Boguslavsky S, Grosheva I, Landau E, Shtutman M, Cohen M, Arnold K, et al. p120 catenin regulates lamellipodial dynamics and cell adhesion in cooperation with cortactin. Proceedings of the National Academy of Sciences of the United States of America. 2007;104(26):10882-7.
168. Wu Q, Chen D, Luo Q, Yang Q, Zhao C, Zhang D, et al. Extracellular matrix protein 1 recruits moesin to facilitate invadopodia formation and breast cancer metastasis. Cancer letters. 2018;437:44-55.
169. Mao SA, Glorioso JM, Nyberg SL. Liver regeneration. Transl Res. 2014;163(4):352-62.
170. Wu J, Lubman DM, Kugathasan S, Denson LA, Hyams JS, Dubinsky MC, et al. Serum Protein Biomarkers of Fibrosis Aid in Risk Stratification of Future Stricturing Complications in Pediatric Crohn's Disease. The American journal of gastroenterology. 2019;114(5):777-85.
171. Venhuizen J-H, Jacobs FJC, Span PN, Zegers MM. P120 and E-cadherin: Double-edged swords in tumor metastasis. Seminars in Cancer Biology. 2020;60:107-20.
172. Rodriguez-Trillo A, Mosquera N, Pena C, Rivas-Tobío F, Mera-Varela A, Gonzalez A, et al. Non-Canonical WNT5A Signaling Through RYK Contributes to Aggressive Phenotype of the Rheumatoid Fibroblast-Like Synoviocytes. Frontiers in Immunology. 2020;11:2727.
173. Lutze G, Haarmann A, Demanou Toukam JA, Buttler K, Wilting J, Becker J. Non-canonical WNT-signaling controls differentiation of lymphatics and extension lymphangiogenesis via RAC and JNK signaling. Scientific Reports. 2019;9(1):4739.
174. Carvalho JR, Fortunato IC, Fonseca CG, Pezzarossa A, Barbacena P, Dominguez-Cejudo MA, et al. Non-canonical Wnt signaling regulates junctional mechanocoupling during angiogenic collective cell migration. Elife. 2019;8.
175. Kawarazaki W, Fujita T. Role of Rho in Salt-Sensitive Hypertension. International journal of molecular sciences. 2021;22(6):2958.

17. Appendix

17.1 Supplementary Tables

Supplementary table 1: Percentage of major cell types which contribute to total interstitial cell number in human heart (excluding myocytes) (1).

Cell type	Percentage of total cells in dataset
Adi (adipocytes)	0.78
EC (endothelial cells)	20.69
FB (fibroblasts)	12.21
Total Leukocytes	8.41
Meso (meosthelial cells)	0.15
NC (neuronal cells)	0.81
PC (pericytes)	16.02
SMC (smooth muscle cells)	3.34

Supplementary table 2: Characteristics of the most prominent ECM1 expressing human cardiac cell populations. Cell characteristics are as described (1).

Fibroblast populations	
FB1 (VT-canonical)	regional enrichment in ventricles (left, right, apex and interventricular septum). Express canonical genes and define a basal, chamber-specific FB expression program FB1, FB4–FB6 are enriched in the ventricles
FB2 (AT-canonical)	regional enrichemtn in atria (left and right). FB2 cells express canonical genes and define a basal, chamber-specific FB expression program.
FB3 (macrophage/MP-interacting)	regional enrichemtn in atria (left and right). FB3 are less abundant in the left ventricle, have lower expression of ECM-related genes but higher expression of cytokine receptors such as OSMR and ILST643. These distinctive fibroblast gene programs probably govern stress-responsive cardiac remodelling and contribute to homeostasis. Also Enriched for oncostatin M pathway compared to other FB populations.
FB4 (ECM-producing)	Enriched in the ventricles (left, right, apex and interventricular septum). Less abundant in the right atrium than other regions. Express genes responsive to TGFβ signalling (for example, POSTN and TNC)
FB5 (ECM-organising)	Enriched in the ventricles (left, right, apex and interventricular septum). Less abundant in the right atrium than other regions. Have higher expression of genes involved in the production, remodelling and degradation of extracellular matrix (ECM).
Leukocyte populations	
LYVE1+MØ1	Cardiac monocyte-derived macrophages. Enriched in clathrin and cathepsin genes. Related to recently described tissue-resident macrophages associated with cardiovascular remodelling, although they are negative for TIMD4.
MØ_mod (monocyte derived macrophages)	Monocyte-derived macrophages. Express LYVE1 and FOLR2, monocyte-like markers CEBPB and S100A8, and chemoattractant cytokine genes CCL13 and CCL18.
MØ_AgP (antigen presenting macrophages)	Antigen-presenting macrophages are FOLR2−, LYVE1− and MERTK−, and enrich for HLA-DRA, HLA-DMA, HLA-DMB, HLA-DPA1 and TREM2 (described in lipid-associated macrophages).

LYVE1+MØ2	Similar to LYVE1+MØ1, except not necessarily cardiac monocyte-derived. Enriched in clathrin and cathepsin genes. Related to recently described tissue-resident macrophages associated with cardiovascular remodelling, although they are negative for TIMD4.
LYVE1+MØ3	Similar to LYVE1+MØ1 andLYVE1+MØ2, except LYVE1+MØ3 are Enriched for HLA-DOA, HLA-DQA1/2 and HLA-DQB1. Also related to recently described tissue-resident macrophages associated with cardiovascular remodelling, although negative for TIMD4.
Vascular populations	
PC1_vent (ventricle-enriched pericytes)	Enriched in ventricles. Enriched for adhesion molecules (NCAM2 and CD38), and CSPG4, which is involved in microvascular morphogenesis and EC cross-talk
PC3_str (stromal pericytes)	Co-express pericyte markers and very low levels of pan-EC transcripts. RNA velocity analyses suggest a directionality that indicates PC3_str cells as a transitional state between pericytes and ECs (Extended Data Fig. 4h, i). These observations may relate to bidirectional pericyte or endothelial cell (trans)differentiation, which remains controversial
PC2_atria (atria-enriched pericytes)	Enriched in the atria and express a similar profile of adhesion molecules as PC1_vent.
SMC1_basic	Vascular SMCs that express MYH11, express transcripts that indicate immaturity, including the stem-cell marker LGR6 (Barker and Clevers, 2010), and proliferation-associated RGS5 (Daniel et al., 2016). SMC1_basic may be venous-derived (Vanlandewijck et al., 2018).

Supplementary table 3: Most prominent ECM1 expressing cell population metadata (not including expression level) (1).

	Cell type	**ECM1 negative**	**ECM1 positive**	**total # cells**	**% ECM1+**	**cell type as a % of all cells**	**ECM1+ cells as % of all cells**
Fibroblasts	FB1_VT-canonical	24075	2557	26632	9.601231601	5.48	0.53
	FB2_AT-canonical	12517	1262	13779	9.158864939	2.83	0.26
	FB4_ECM-producing	5079	1067	6146	17.360885 13	1.26	0.22
	FB3_MP-interacting	6854	890	7744	11.4927686	1.59	0.18
	FB5_ECM-organising	1935	583	2518	23.15329627	0.52	0.12
	FB6_Stromal	1383	227	1610	14.09937888	0.33	0.05
	FB7_CM-like	756	156	912	17.10526316	0.19	0.03
	Combined Fibroblasts		6742	59341	11.3614533	12.21	1.39
	Cell type	**ECM1 negative**	**ECM1 positive**	**total # cells**	**% ECM1+**	**cell type as a % of all cells**	**ECM1+ cells as % of all cells**
Vascular Cells	PC1_vent	46535	3560	50095	7.106497654	10.30	0.73
	PC3_str	12385	1846	14231	12.97168154	2.93	0.38
	PC2_atria	10609	714	11323	6.30574936	2.33	0.15

	SMC1_basic	12623	491	13114	3.744090285	2.70	0.10
	EC3_cap	16528	369	16897	2.183819613	3.48	0.08
	EC1_cap	27134	283	27417	1.032206295	5.64	0.06
	EC2_cap	13171	274	13445	2.037932317	2.77	0.06
	EC5_art	20122	195	20317	0.95978737	4.18	0.04
	EC6_ven	8316	170	8486	2.003299552	1.75	0.03
	EC7_atria	4327	158	4485	3.522853958	0.92	0.03
	PC4_CMC-like	2114	93	2207	4.213864975	0.45	0.02
	EC4_immune	5560	77	5637	1.365974809	1.16	0.02
	SMC2_art	3060	68	3128	2.173913043	0.64	0.01
	EC10_CMC-like	2547	61	2608	2.338957055	0.54	0.01
	EC9_FB-like	491	42	533	7.879924953	0.11	0.01
	Meso	712	6	718	0.835654596	0.15	0.00
	EC8_ln	751	3	754	0.397877984	0.16	0.00
	Combined Vascular Cells		8410	195395	4.304101947	40.19	1.73
	Cell type	**ECM1 negative**	**ECM1 positive**	**total # cells**	**% ECM1+**	**cell type as a % of all cells**	**ECM1+ cells as % of all cells**
Leukocytes	LYVE1+MØ	2762	256	3018	8.482438701	0.62	0.05
	MØ_mod	1141	172	1313	13.099777152	0.27	0.04
	MØ_AgP	1135	143	1278	11.189355837	0.26	0.03
	LYVE1+MØ3	1871	86	1957	4.394481349	0.40	0.02
	LYVE1+MØ2	2029	59	2088	2.825670498	0.43	0.01
	DOCK4+MØ1	3188	51	3239	1.574560049	0.67	0.01
	DC	769	45	814	5.528255528	0.17	0.01
	DOCK4+MØ2	1586	40	1626	2.460024 6	0.33	0.01
	CD16+Mo	3247	31	3278	0.945698597	0.67	0.01
	CD8+T_tem	2977	24	3001	0.799733422	0.62	0.00
	Mo_classic	1867	16	1883	0.849707913	0.39	0.00

	CD8+T_cytox	2941	15	2956	0.50744249	0.61	0.00
	CD4+T_cytox	3099	14	3113	0.449726951	0.64	0.00
	Mo_pi	1640	12	1652	0.726392252	0.34	0.00
	NK	3617	11	3628	0.303197354	0.75	0.00
	doublets	614	9	623	1.444622793	0.13	0.00
	CD4+T_tem	1041	6	1047	0.573065903	0.22	0.00
	Mast	1538	5	1543	0.32404407	0.32	0.00
	NKT	1459	4	1463	0.2734108	0.30	0.00
	B_cells	1191	4	1195	0.334728033	0.25	0.00
	IL17RA+Mo	31	1	32	3.125	0.01	0.00
	NØ	121	0	121	0	0.02	0.00
	Combined Leukocytes		1004	40868	2.456689831	8.41	0.21

Supplementary table 4: Most prominent ECM1 expressing cell population, specific expression levels (1); * = all expression values were multiplied by a factor of 10 to produce larger/more visually interpretable numbers.

Cell type	**average ECM1 expression***
FB5_ECM-organising	2.156545642
FB4_ECM-producing	1.495260315
FB1_VT-canonical	0.985049919
PC3_str	0.9548165
FB3_MP-interacting	0.94968919
FB7_CM-like	0.869133827
FB2_AT-canonical	0.809450903
FB6_Stromal	0.717818108
PC1_vent	0.708297307
MØ_mod	0.696993674
LYVE1+MØ2	0.540295116
EC9_FB-like	0.513880249
PC2_atria	0.511881155
LYVE1+MØ1	0.484529609
MØ_AgP	0.462991062
DC	0.400493194
LYVE1+MØ3	0.380614456
EC7_atria	0.328767895
SMC1_basic	0.259398339
DOCK4+MØ1	0.258763987

DOCK4+MØ2	0.245173465
PC4_CMC-like	0.241680387
EC2_cap	0.155614417
CD8+T_tem	0.120402501
EC3_cap	0.120011558
EC6_ven	0.118434211
SMC2_art	0.103660082
EC1_cap	0.101689835
EC4_immune	0.099793675
EC10_CMC-like	0.097193263
Meso	0.089125168
Mo_pi	0.088484013
IL17RA+Mo	0.086873008
CD4+T_cytox	0.086744052
EC5_art	0.063658103
CD8+T_cytox	0.05822222
Mast	0.055934149
Mo_classic	0.050510158
NKT	0.042248601
CD4+T_tem	0.034450231
CD16+Mo	0.032345739
NK	0.031131977
EC8_ln	0.024524133
B_cells	0.023164137
NØ	0

Supplementary table 5: Characteristics of most prominent ECM1 expressing mouse cardiac cell sub-populations. Cell characteristics are as described (3) with the exception of MAC8 cells which we defined here for the first time.

Fibroblast populations	
Fibroblast-Sca1-high (F-SH)	Resident, unactivated fibroblast population, most prominent in sham hearts. Expresses canonical fibroblast markers such as Pdgfra, Pdgfra-GFP, Ddr2 and Col1a1. Contains the highest frequency of Pdgfra and Ly6a(Sca1)-expressing cells, and enriched in S+P+ (SCA1+PDGFRα+) fibroblasts and clonal colony-forming units. Enriched in cardiac colony-forming mesenchymal stromal cell (MSC)-like cells (cCFU-F), which show multi-lineage differentiation and self-renewal in vitro. Characterized by over-representation of genes involved in the biological process (BP) cell adhesion, which included cell surface receptor genes Ackr3(Cxcr-7), Thy1(Cd90), Axl and Cd34.
Fibroblast-Sca1-low (F-SL)	Resident, unactivated fibroblast population, most prominent in sham hearts. Expresses canonical fibroblast markers such as Pdgfra, Pdgfra-GFP, Ddr2 and Col1a1. Characterized by GO BP terms signaling and signal transduction. Within the signal transduction category, majority secreted proteins including APOE, BMP4 and ADM. Thus, F-SL, a major sub-division of fibroblasts, has a unique secretory phenotype distinct from that in F-SH, which is enriched in MSC-like colony forming cells.

Activated fibroblasts (F-Act)	Activated fibroblast population. Express Postn at high levels in ~80% of cells. Express Acta2 in 28% (MI-day 3) and 35% (MI-day 7), much lower levels compared to MYO; suggests a contractile phenotype in some F-Act cells. Most closely related to F-SH & F-SL and is more distant from MYO. F-Act over-represent GOBP terms collagen fibril organization and regulation of wound healing. F-Act top upregulated gene is Cilp, encoding a matricellular protein and inhibitor of TGF-β1 signaling, consistent with F-Act being a pre-MYO population in which fibrosis is constrained. F-Act acts as an intermediary population for MYO, as it expands by proliferation up to MI-day 3 and differentiates to MYO during the transition from MI-day 3 to MI-day 7.
Myofibroblasts (Myo)	Activated fibroblasts. Represent 11.49% of total interstitial cells at MI-day 7; 2nd most populous cell type to M2MΦ at day-7. Express fibrogenic (e.g. Periostin; POSTN) and/or contractile (e.g. αSmooth Muscle Actin; αSMA) proteins. Show strong upregulation of numerous collagen genes (e.g. Col1a1, Col3a1, Col5a2), Postn (99.5%) and Acta2 (61%). Upregulated genes involved in wound healing and cell migration including Fn(Fibronectin) and Cthrc1(Collagen Triple Helix Repeat Containing I). Have decreased expression of Pdgfra, Pdgfra-GFP, Ly6a(Sca1), Thy1(Cd90) and Cd34, indicating loss of stem/progenitor cell markers. GOBP terms are collagen fibril organization and cell adhesion, containing collagen genes Col3a1, Col5a1, Col11a1 and Col14a1, and others involved in cell:cell and cell:matrix adhesion including Thbs1 (encoding Thrombospondin 1) and Fbn1. Other terms included angiogenesis and heart development as well as negative regulation of canonical Wnt signaling pathway.
(F-WntX)	Characterised by an anti-WNT, anti-CTGF and anti-TGF-β extracellular and intracellular signaling milieu. Expressed Postn(Periostin), Acta2(αSMA), Tagln(Transgelin) and Scx(Scleraxis), in both sham and MI conditions, suggesting an activated state even in the absence of injury. Top upregulated gene was Wif1, encoding a secreted canonical WNT pathway inhibitor essential for cardiac repair after MI (Meyer et al., 2017). WIF1 can also antagonize Connective Tissue Growth Factor (CTGF) signaling (Surmann-Schmitt et al., 2012), which plays a supportive role in cardiac fibrosis (Travers et al., 2016). Wif1 was almost uniquely expressed in F-WntX in all conditions. Multiple other WNT pathway-related genes were upregulated encoding WNT ligands (WNT5a, WNT16), soluble WNT antagonists (DKK3, SFRP2), membrane-bound WNT receptor (FRZB) and AXIN2, a component of the β-catenin destruction complex. F-WntX also showed upregulated Fmod, which inhibits fibrillogenesis and sequesters pro-fibrotic factor TGF-β within ECM. Overall, this signature suggests an anti-WNT, anti-CTGF and anti-TGF-β extracellular and intracellular signaling milieu for F-WntX cells.
Leukocyte populations	
Cardiac tissue resident macrophages (MAC-TR)	Cardiac tissue-resident MΦ. Have a cell signature of Cx3cr1high Adgre1(F4/80)high H2-Aa(MHC-II)+ Itgam(CD11b)low Ly6c2low Ccr2-. Upregulated pro-regenerative genes Igf1 and Pdgfb/c.
M1 macrophages (M1MØ)	Classical inflammatory monocyte-derived M1 macrophages (M1MΦ). One of the most abundant cell types at MI day 3. Express a cell signature of Ccr2high Adgre1(F4/80)+ Ly6c2+ H2-Aa(MHC-II)+. Also express additional MΦ markers including Mertk and C1q. Hierarchical clustering shows M1MΦ are most closely related to M1 monocytes. Differentially expressed genes show over-representation in GO terms for leukocyte migration and responses to interleukin-1.

M2 macrophages (M2MØ)	Non-classical M2 MΦ involved in inflammation resolution and repair, and the most prominent population at MI-day 7; M2MΦ population increases late during injury repair from <2% of TIP in sham and MI-day 3 hearts, to 16% at MI-day 7. Closely related to tissue-resident macrophages (MAC-TR). Express a cell signature of Ccr2high Adgre1(F4/80)+ H2-Aa(MHC-II)high Ly6c2-. Also express Cx3cr1, and have upregulated pro-regenerative genes Igf1 and Pdgfb/c. The majority of M2MΦ were Ccr2high (important for migration); however, a minor sub-populaion was Ccr2low and these expressed the highest levels of Igf1 and lower levels of MHC-II. Differentially expressed genes show over-representation of show GO term antigen presentation via MHC class II.
M1 monocytes (M1Mo)	Classical blood-derived M1 monocytes (M1Mo). Characterised by the expression signature Adgre1(F4/80)+ Itgam(CD11b)+ Fcgr1(CD64)+ Ly6c2high Ccr2high H2-Aa(MHC-II)low. Also characterised by having lower size and granularity than MΦ, and lower levels of MΦ markers Adgre(F4/80), Itgam(CD11b) and H2-Aa(MHC-II). At MI-day 3 M1Mo are also low or negative for the MΦ markers Siglec1, Mrc1, Maf, Trem2 and Mertk (involved in phagocytosis), and C1 complement genes C1qa, b and c which are involved in recruitment of new inflammatory cells and protection against autoimmunity (in addition to complement fixation). Differentially expressed genes show over-representation of GO terms for cell migration, inflammation and T cell activation.
(MAC8)	Differentially expressed genes show over-representation in GO terms for inflammatory response and regulation of response to external stimulus. When MAC8 marker genes greater than 1.25-fold upregulated against all other cells were subject to GOnet enrichment, there is an over-representation of GOBP response to stimulus, inflammatory response and myeloid leukocyte/neutrophil/granulocyte/neutrophil cell migration or chemotaxis/locomotion; the top GOMF term was signaling receptor binding. Suggesting a responsive, cell phenotype most notably associated with paracrine signaling and migratory/chemotactic or locomotive effects.
interferon-responsive gene expressing macrophages (MAC-IFNIC)	Macrophages that express interferon-responsive genes (MAC-IFNIC). Showed strong upregulation of interferon (IFN)-induced genes including Ifit3, Ifit1 and Cxcl10. GO term analysis implicate responses to IFN α, β, and γ. Appear to arise from Ccr2+ MΦ as opposed to monocytes, and likely correspond to the recently described inflammatory MΦ subtype that has negative effects on heart repair after MI through promotion of inflammatory cell types, and cytokine and chemokine expression (King et al., 2017).
Vascular populations	
EC1	The majority EC1 population (encompass the largest number of ECs at all time-points) express Ly6a (encodes SCA1) as well as the vascular transcription factor (TF) Sox17, and likely represents microvascular ECs.
EC2	EC2 expressed canonical arterial endothelial markers such as Bmx, Sema3g and Efnb2, as well as TF genes Sox17 and Hey1, the latter acting downstream of NOTCH which is required for arterial EC fate.
EC3	EC3 almost uniquely expressed venous EC marker Nr2f2 (encoding COUPTFII) and Von Willebrand factor (Vwf), and a minority (~3%) expressed Prox1 and Lyve1, consistent with a lymphatic identity.
Mural (contains pericytes)	Mural cells which also encompass pericytes. Characterised as Cspg4+ Pdgfrb+, and a new lineage marker, Vtn, encoding Vitronectin, was specifically expressed in these mural cells

Supplementary table 6: All ECM1 specific cell expression metadata of interstitial cell populations. Data is separated by time-point post-MI and ranked by percentage of ECM1+ cells within each sub-population (3).

Rank	Cluster	Condition	log 2_mean ECM1 expression	ECM1+ Cell #	Total Cell #	% total cells at time	% cells ECM1+	ECM1+ cells as % of total cells at time
1	MYO	Sham	2.238492869	22	22	0.384413769	100.00	0.38
2	MAC8	Sham	2.970180601	13	13	0.227153591	100.00	0.23
3	F-SH	Sham	2.740617996	576	657	11.47999301	87.67	10.06
4	F-Act	Sham	2.619081393	478	553	9.662764284	86.44	8.35
5	F-WntX	Sham	2.157346068	75	96	1.677441901	78.13	1.31
6	M1MΦ	Sham	1.447595789	2	3	0.052420059	66.67	0.03
7	MAC-IFNIC	Sham	0.945456906	2	3	0.052420059	66.67	0.03
8	F-SL	Sham	1.882444173	879	1348	23.55408003	65.21	15.36
9	M2MΦ	Sham	1.060972123	15	26	0.454307182	57.69	0.26
10	Mural	Sham	1.543882794	79	184	3.215096977	42.93	1.38
11	M1Mo	Sham	0.869212862	15	40	0.698934125	37.50	0.26
12	EC3	Sham	1.275397257	69	229	4.001397868	30.13	1.21
13	DC	Sham	0.812502646	7	24	0.419360475	29.17	0.12
14	MAC-TR	Sham	0.746081847	38	159	2.778263149	23.90	0.66
15	EC2	Sham	0.934249764	54	241	4.211078106	22.41	0.94
16	Cyc	Sham	0.67185558	8	37	0.646514066	21.62	0.14
17	Glial	Sham	0.32697169	3	18	0.314520356	16.67	0.05
18	EC1	Sham	0.682852002	188	1215	21.23012406	15.47	3.28
19	MAC6	Sham	0.558419284	5	33	0.576620654	15.15	0.09
20	TC1-Cd8	Sham	0.416955127	23	152	2.655949677	15.1315789	0.40
21	MAC7	Sham	0.401643118	5	44	0.768827538	11.36	0.09
22	NKC	Sham	0.461713702	4	48	0.838720951	8.33	0.07
23	TC2-Cd4	Sham	0.263376191	10	132	2.306482614	7.58	0.17
24	BC	Sham	0.267815358	23	446	7.793115499	5.16	0.40

			Cell Group	total ECM1+ Cell #	Total Cell #	Cell number as % of cells at time	ECM1+ cells as % of cells at time	% of "cell group" ECM1+ at this time
				2593	5723			
			Total Fibroblast	2030	2676	46.75869299	35.47090687	75.85949178
			Total Mo/MΦ	95	321	5.608946357	1.659968548	29.59501558
			Total EC	311	1685	29.44260003	5.434212825	18.45697329
Rank	**Cluster**	**Condition**	**log 2_mean ECM1 expression**	**ECM1+ Cell #**	**Total Cell #**	**% total cells at time**	**% cells ECM1+**	**ECM1+ cells as % of total cells at time**
1	MAC8	MI-day 3	2.689493822	86	106	2.735483871	81.13	2.22
2	MYO	MI-day 3	2.15445348	3	4	0.103225806	75.00	0.08
3	F-SH	MI-day 3	2.266864366	17	25	0.64516129	68.00	0.44
4	F-SL	MI-day 3	1.914871777	27	40	1.032258065	67.5	0.70
5	M1MΦ	MI-day 3	2.201067361	1288	1964	50.68387097	65.58	33.24
6	M2MΦ	MI-day 3	1.582394982	32	49	1.264516129	65.31	0.83
7	F-WntX	MI-day 3	1.687374326	5	8	0.206451613	62.50	0.13
8	MAC-IFNIC	MI-day 3	1.910845894	78	125	3.225806452	62.40	2.01
9	F-Act	MI-day 3	1.829451056	110	185	4.774193548	59.46	2.84
10	Cyc	MI-day 3	0.951493762	27	71	1.832258065	38.03	0.70
11	M1Mo	MI-day 3	1.064162232	151	493	12.72258065	30.63	3.90
12	MAC6	MI-day 3	1.002295762	30	110	2.838709677	27.27	0.77
13	Mural	MI-day 3	0.593866181	2	10	0.258064516	20.00	0.05
14	EC2	MI-day 3	0.935295169	7	37	0.95483871	18.92	0.18
15	MAC-TR	MI-day 3	0.414031548	4	23	0.593548387	17.39	0.10
16	EC3	MI-day 3	0.638135472	13	75	1.935483871	17.33	0.34
17	EC1	MI-day 3	0.731938301	23	162	4.180645161	14.20	0.59
18	MAC7	MI-day 3	0.520784251	6	43	1.109677419	13.95	0.15
19	TC2-Cd4	MI-day 3	0.732044163	2	16	0.412903226	12.50	0.05

20	TC1-Cd8	MI-day 3	0.638773591	3	28	0.722580645	10.71	0.08
21	DC	MI-day 3	0.282727823	23	271	6.993548387	8.49	0.59
22	BC	MI-day 3	0.677956428	2	27	0.696774194	7.41	0.05
23	NKC	MI-day 3	0	0	2	0.051612903	0.00	0.00
24	Glial	MI-day 3	0	0	1	0.025806452	0.00	0.00
			Cell Group	**total ECM1+ Cell #**	**Total Cell #**	**Cell number as % of cells at time**	**ECM1+ cells as % of cells at time**	**% of cell group ECM1+ at this time**
			Cell Group Total Fibroblast	1939	3875			
				162	262	6.761290323	4.180645161	61.83206107
			Total Mo/MΦ	1675	2913	75.17419355	43.22580645	57.50085822
			Total EC	43	274	7.070967742	1.109677419	15.69343066
Rank	**Cluster**	Condition	**log 2_mean ECM1 expression**	**ECM1+ Cell #**	**Total Cell #**	**% total cells at time**	**% cells ECM1+**	**ECM1+ cells as % of total cells at time**
1	MAC8	MI-day 7	2.342406125	18	18	0.482185909	100.00	0.48
2	F-WntX	MI-day 7	2.338816027	13	15	0.401821591	86.67	0.35
3	MYO	MI-day 7	1.745038295	371	429	11.49209751	86.48	9.94
4	F-SH	MI-day 7	2.541490561	142	172	4.607554246	82.56	3.80
5	F-Act	MI-day 7	2.169905672	301	368	9.858023038	81.79	8.06
6	F-SL	MI-day 7	1.901947427	189	265	7.098848111	71.32	5.06
7	M1MΦ	MI-day 7	1.616884584	80	134	3.589606215	59.70	2.14
8	Mural	MI-day 7	1.442130356	21	39	1.044736137	53.85	0.56
9	MAC-IFNIC	MI-day 7	1.120639943	14	27	0.723278864	51.85	0.38
10	M2MΦ	MI-day 7	1.018857222	304	600	16.07286365	50.67	8.14
11	EC3	MI-day 7	0.976321608	30	102	2.73238682	29.41	0.80
12	Cyc	MI-day 7	0.390051435	27	108	2.893115457	25.00	0.72
13	EC2	MI-day 7	0.834251502	22	95	2.544870078	23.16	0.59

14	M1Mo	MI-day 7	0.562480038	17	79	2.11626038	21.52	0.46
15	MAC-TR	MI-day 7	0.73852293	9	55	1.473345834	16.36	0.24
16	EC1	MI-day 7	0.426224253	64	503	13.47441736	12.72	1.71
17	MAC6	MI-day 7	0.328037071	3	26	0.696490758	11.54	0.08
18	DC	MI-day 7	0.15698716	9	96	2.571658184	9.38	0.24
19	NKC	MI-day 7	0.170104439	2	26	0.696490758	7.69	0.05
20	TC2-Cd4	MI-day 7	0.278963287	6	95	2.544870078	6.32	0.16
21	TC1-Cd8	MI-day 7	0.144018553	7	144	3.857487276	4.8611111	0.19
22	BC	MI-day 7	0.051697266	6	278	7.44709349	2.16	0.16
23	MAC7	MI-day 7	0.047210039	1	54	1.446557728	1.85	0.03
24	Glial	MI-day 7	0	0	5	0.13394053	0.00	0.00
			Cell Group	**total ECM1+ Cell #**	**Total Cell #**	**Cell number as % of cells at time**	**ECM1+ cells as % of cells at time**	**% of cell group ECM1+ at this time**
			Cell Group Total Fibroblast	1656	3733			
			Cell Group Total Fibroblast	1016	1249	33.4583445	27.21671578	81.345076066
			Total Mo/MΦ	446	993	26.60058934	11.94749531	44.914400841
			Total EC	116	700	18.75167426	3.107420305	16.571428557

Supplementary table 7: Per-cell Spearman correlation analysis of ECM1 expression against all genes in the mouse scRNAseq dataset(3).

Rank	Gene name	Spearman_rho	p-value
n/a	Ecm1	1.000	0.00E+00
1	Lgals1	0.441	0.00E+00
2	Lrp1	0.435	0.00E+00
3	Rnase4	0.421	0.00E+00
4	S100a6	0.402	0.00E+00
5	Ctsl	0.397	0.00E+00
6	Pcolce2	0.392	0.00E+00
7	Dpt	0.389	0.00E+00
8	Timp2	0.388	0.00E+00
9	Cfh	0.386	0.00E+00

10	Fbln1	0.381	0.00E+00
11	Fxyd1	0.378	0.00E+00
12	Serping1	0.377	0.00E+00
13	Ccdc80	0.377	0.00E+00
14	Entpd2	0.372	0.00E+00
15	Ptgis	0.371	0.00E+00
16	Islr	0.371	0.00E+00
17	Col1a1	0.365	0.00E+00
18	Cd63	0.365	0.00E+00
19	Mfap5	0.364	0.00E+00
20	Col6a1	0.362	0.00E+00
21	Serpinf1	0.361	0.00E+00
22	Meg3	0.360	0.00E+00
23	H2B-EGFP	0.358	0.00E+00
24	Col1a2	0.357	0.00E+00
25	Fstl1	0.356	0.00E+00
26	Loxl1	0.356	0.00E+00
27	Sod3	0.355	0.00E+00
28	Sdc2	0.355	0.00E+00
29	Igfbp6	0.355	0.00E+00
30	Sfrp1	0.354	0.00E+00
31	Medag	0.352	0.00E+00
32	Pmp22	0.352	0.00E+00
33	Lum	0.351	0.00E+00
34	Cygb	0.351	0.00E+00
35	Col6a2	0.350	0.00E+00
36	Ogn	0.349	0.00E+00
37	Mmp2	0.349	0.00E+00
38	Tnxb	0.348	0.00E+00
39	Clec3b	0.348	0.00E+00
40	Ahnak2	0.346	0.00E+00
41	Mxra8	0.346	0.00E+00
42	Serpine2	0.346	0.00E+00
43	Htra3	0.345	0.00E+00
44	Axl	0.345	0.00E+00
45	Lhfp	0.344	0.00E+00
46	Gas1	0.344	0.00E+00
47	Prelp	0.343	0.00E+00
48	Adamts2	0.343	0.00E+00
49	Gpx3	0.342	0.00E+00
50	Cpq	0.338	0.00E+00
51	Emp1	0.338	0.00E+00
52	Olfml3	0.338	0.00E+00
53	Rcn3	0.337	0.00E+00

54	Lpar1	0.335	0.00E+00
55	Anxa1	0.335	0.00E+00
56	Pcolce	0.335	0.00E+00
57	Rbp1	0.334	0.00E+00
58	Nbl1	0.333	0.00E+00
59	Igfbp4	0.333	0.00E+00
60	Bgn	0.333	0.00E+00
61	Rarres2	0.333	0.00E+00
62	Fhl1	0.332	0.00E+00
63	Gpm6b	0.331	0.00E+00
64	Col3a1	0.330	0.00E+00
65	Vcan	0.329	0.00E+00
66	Mmp23	0.327	0.00E+00
67	Camk2n1	0.325	0.00E+00
68	Nupr1	0.324	3.95252516672997E-323
69	Pdlim2	0.323	7.39122206178505e-321
70	Fbn1	0.322	2.07746699025911e-318
71	Oaf	0.320	6.26768887831438e-315
72	Nfix	0.320	1.07432147047222e-314
73	Ugp2	0.320	1.78772680089985e-314
74	Pam	0.317	0.00E+00
75	Qpct	0.317	3.96E-308
76	Pcsk6	0.317	6.49E-308
77	Gsn	0.316	3.38E-307
78	Gfpt2	0.316	5.60E-307
79	Aspn	0.315	1.37E-305
80	Bicc1	0.315	4.27E-304
81	Fbln2	0.314	3.02E-303
82	Cryab	0.313	2.23E-301
83	Aebp1	0.312	2.36E-298
84	Selenbp1	0.311	3.79E-296
85	Cp	0.311	7.29E-296
86	Itgb5	0.311	8.03E-296
87	Crispld2	0.310	1.43E-295
88	Smoc2	0.309	2.66E-293
89	Abca8a	0.309	5.44E-293
90	Lama2	0.309	1.17E-292
91	Tcf21	0.308	1.77E-291
92	Matn2	0.308	2.81E-290
93	Dpep1	0.308	4.57E-290
94	Adamts5	0.305	1.40E-284
95	Pi16	0.304	1.37E-282
96	Mt1	0.304	4.06E-282
97	Cd248	0.302	4.44E-279

98	Cd302	0.302	1.00E-278
99	Pdgfra	0.301	8.41E-278
100	Lamc1	0.301	1.62E-277
101	Snhg18	0.301	1.28E-276
102	Emp3	0.300	2.00E-274

Supplementary table 8: GOnet/DICE GOBP enrichment of the top ECM1 Spearman correlated genes (r ≥ 0.3) from the mouse scRNAseq dataset (3).

	GO_term_ID	GO_term_def	P	P_FDR_adj	NofGenes
1	GO:0030198	extracellular matrix organization	5.23E-18	0.00E+00	18
2	GO:0043062	extracellular structure organization	5.28E-17	0.00E+00	18
3	GO:0048513	animal organ development	1.00E-09	3.08E-06	37
4	GO:0030199	collagen fibril organization	1.20E-09	3.08E-06	7
5	GO:0048731	system development	1.40E-09	3.08E-06	44
6	GO:0032502	developmental process	2.50E-09	4.14E-06	51
7	GO:0007275	multicellular organism development	3.10E-09	4.14E-06	47
8	GO:0048856	anatomical structure development	3.40E-09	4.14E-06	49
9	GO:0032963	collagen metabolic process	3.50E-09	4.14E-06	7
10	GO:0009888	tissue development	3.80E-09	4.14E-06	26
11	GO:0007155	cell adhesion	2.32E-08	2.30E-05	17
12	GO:0022610	biological adhesion	2.84E-08	2.58E-05	17
13	GO:0009611	response to wounding	5.48E-08	4.59E-05	12
14	GO:0032060	bleb assembly	8.59E-08	6.69E-05	4
15	GO:0030334	regulation of cell migration	1.26E-07	8.79E-05	17
16	GO:0030155	regulation of cell adhesion	1.34E-07	8.79E-05	15
17	GO:0001501	skeletal system development	1.37E-07	8.79E-05	13
18	GO:0051270	regulation of cellular component movement	1.81E-07	1.10E-04	18
19	GO:0042060	wound healing	1.95E-07	1.12E-04	10
20	GO:2000145	regulation of cell motility	2.60E-07	1.42E-04	17
21	GO:0009966	regulation of signal transduction	4.47E-07	2.32E-04	30
22	GO:0040012	regulation of locomotion	8.00E-07	3.97E-04	17
23	GO:0070208	protein heterotrimerization	9.84E-07	4.66E-04	4
24	GO:0016043	cellular component organization	1.19E-06	5.25E-04	43
25	GO:0048583	regulation of response to stimulus	1.20E-06	5.25E-04	36
26	GO:0051241	negative regulation of multicellular organismal process	1.97E-06	8.25E-04	19
27	GO:0010646	regulation of cell communication	2.22E-06	8.98E-04	32
28	GO:2000146	negative regulation of cell motility	2.41E-06	9.22E-04	9
29	GO:0023051	regulation of signaling	2.45E-06	9.22E-04	32
30	GO:0010810	regulation of cell-substrate adhesion	2.60E-06	9.43E-04	8
31	GO:0022008	neurogenesis	2.70E-06	9.43E-04	22
32	GO:0097435	supramolecular fiber organization	2.77E-06	9.43E-04	11

33	GO:0071840	cellular component organization or biogenesis	3.22E-06	1.06E-03	43
34	GO:0051239	regulation of multicellular organismal process	3.74E-06	1.20E-03	31
35	GO:0042221	response to chemical	3.94E-06	1.23E-03	34
36	GO:0040007	growth	4.34E-06	1.31E-03	11
37	GO:0048585	negative regulation of response to stimulus	5.49E-06	1.58E-03	20
38	GO:0060346	bone trabecula formation	5.52E-06	1.58E-03	3
39	GO:0031589	cell-substrate adhesion	5.85E-06	1.59E-03	7
40	GO:0040011	locomotion	5.86E-06	1.59E-03	17
41	GO:0051271	negative regulation of cellular component movement	6.25E-06	1.59E-03	9
42	GO:2000026	regulation of multicellular organismal development	6.25E-06	1.59E-03	24
43	GO:0030162	regulation of proteolysis	6.27E-06	1.59E-03	13
44	GO:0050817	coagulation	6.89E-06	1.67E-03	6
45	GO:0007596	blood coagulation	6.89E-06	1.67E-03	6
46	GO:0048523	negative regulation of cellular process	7.18E-06	1.70E-03	38
47	GO:0007599	hemostasis	7.63E-06	1.77E-03	6
48	GO:0048869	cellular developmental process	8.51E-06	1.93E-03	34
49	GO:0040013	negative regulation of locomotion	9.28E-06	2.07E-03	9
50	GO:0050793	regulation of developmental process	9.63E-06	2.10E-03	27
51	GO:0030154	cell differentiation	1.09E-05	2.33E-03	33
52	GO:0009653	anatomical structure morphogenesis	1.13E-05	2.34E-03	24
53	GO:0048608	reproductive structure development	1.15E-05	2.34E-03	10
54	GO:0032501	multicellular organismal process	1.16E-05	2.34E-03	52
55	GO:0048705	skeletal system morphogenesis	1.20E-05	2.34E-03	8
56	GO:0045861	negative regulation of proteolysis	1.20E-05	2.34E-03	9
57	GO:0061458	reproductive system development	1.25E-05	2.39E-03	10
58	GO:0030336	negative regulation of cell migration	1.49E-05	2.81E-03	8
59	GO:0090287	regulation of cellular response to growth factor stimulus	1.62E-05	2.99E-03	8
60	GO:0061430	bone trabecula morphogenesis	1.86E-05	3.37E-03	3
61	GO:0048519	negative regulation of biological process	2.08E-05	3.71E-03	40
62	GO:0060325	face morphogenesis	2.17E-05	3.82E-03	4
63	GO:0000904	cell morphogenesis involved in differentiation	2.68E-05	4.58E-03	11
64	GO:0045595	regulation of cell differentiation	2.70E-05	4.58E-03	21
65	GO:0032101	regulation of response to external stimulus	2.73E-05	4.58E-03	14
66	GO:0035295	tube development	3.14E-05	5.19E-03	14
67	GO:0003414	chondrocyte morphogenesis involved in endochondral bone morphogenesis	3.60E-05	5.69E-03	3
68	GO:0003429	growth plate cartilage chondrocyte morphogenesis	3.60E-05	5.69E-03	3
69	GO:0090171	chondrocyte morphogenesis	3.60E-05	5.69E-03	3
70	GO:0060323	head morphogenesis	3.81E-05	5.93E-03	4

71	GO:0016477	cell migration	4.05E-05	6.22E-03	13
72	GO:0003422	growth plate cartilage morphogenesis	4.36E-05	6.52E-03	3
73	GO:0042063	gliogenesis	4.37E-05	6.52E-03	7
74	GO:0051336	regulation of hydrolase activity	4.51E-05	6.64E-03	14
75	GO:0048699	generation of neurons	4.74E-05	6.75E-03	19
76	GO:0060351	cartilage development involved in endochondral bone morphogenesis	4.90E-05	6.75E-03	4
77	GO:0052547	regulation of peptidase activity	4.96E-05	6.75E-03	9
78	GO:0072275	metanephric glomerulus morphogenesis	4.98E-05	6.75E-03	2
79	GO:0072276	metanephric glomerulus vasculature morphogenesis	4.98E-05	6.75E-03	2
80	GO:0072277	metanephric glomerular capillary formation	4.98E-05	6.75E-03	2
81	GO:0030510	regulation of BMP signaling pathway	5.01E-05	6.75E-03	5
82	GO:0032989	cellular component morphogenesis	5.15E-05	6.84E-03	13
83	GO:0032268	regulation of cellular protein metabolic process	5.63E-05	7.33E-03	24
84	GO:0051128	regulation of cellular component organization	5.70E-05	7.33E-03	24
85	GO:0006950	response to stress	5.76E-05	7.33E-03	28
86	GO:0032879	regulation of localization	5.78E-05	7.33E-03	26
87	GO:0085029	extracellular matrix assembly	6.18E-05	7.60E-03	3
88	GO:0000302	response to reactive oxygen species	6.18E-05	7.60E-03	6
89	GO:0000902	cell morphogenesis	6.21E-05	7.60E-03	12
90	GO:0010466	negative regulation of peptidase activity	6.36E-05	7.71E-03	7
91	GO:0030514	negative regulation of BMP signaling pathway	6.68E-05	7.92E-03	4
92	GO:0010517	regulation of phospholipase activity	6.68E-05	7.92E-03	4
93	GO:0006979	response to oxidative stress	7.42E-05	8.69E-03	8
94	GO:0071230	cellular response to amino acid stimulus	7.78E-05	9.02E-03	6
95	GO:0009887	animal organ morphogenesis	8.62E-05	9.89E-03	14
96	GO:0010171	body morphogenesis	8.90E-05	1.01E-02	4
97	GO:0010951	negative regulation of endopeptidase activity	9.40E-05	1.06E-02	6
98	GO:1903034	regulation of response to wounding	9.69E-05	1.06E-02	6
99	GO:0003418	growth plate cartilage chondrocyte differentiation	9.73E-05	1.06E-02	3
100	GO:0003433	chondrocyte development involved in endochondral bone morphogenesis	9.73E-05	1.06E-02	3
101	GO:0097350	neutrophil clearance	9.93E-05	1.06E-02	2
102	GO:0035582	sequestering of BMP in extracellular matrix	9.93E-05	1.06E-02	2
103	GO:0090101	negative regulation of transmembrane receptor protein serine/threonine kinase signaling pathway	1.04E-04	1.10E-02	5
104	GO:0060324	face development	1.09E-04	1.14E-02	4
105	GO:0008285	negative regulation of cell population proliferation	1.11E-04	1.15E-02	11

106	GO:0034614	cellular response to reactive oxygen species	1.13E-04	1.16E-02	5
107	GO:0010812	negative regulation of cell-substrate adhesion	1.16E-04	1.17E-02	4
108	GO:0043200	response to amino acid	1.16E-04	1.17E-02	6
109	GO:0120036	plasma membrane bounded cell projection organization	1.18E-04	1.18E-02	14
110	GO:0048589	developmental growth	1.21E-04	1.20E-02	9
111	GO:0070206	protein trimerization	1.24E-04	1.22E-02	4
112	GO:0007399	nervous system development	1.33E-04	1.30E-02	22
113	GO:0048565	digestive tract development	1.38E-04	1.33E-02	5
114	GO:0070613	regulation of protein processing	1.40E-04	1.33E-02	4
115	GO:0070887	cellular response to chemical stimulus	1.41E-04	1.33E-02	24
116	GO:0060343	trabecula formation	1.44E-04	1.34E-02	3
117	GO:0046688	response to copper ion	1.44E-04	1.34E-02	3
118	GO:0060284	regulation of cell development	1.50E-04	1.37E-02	14
119	GO:1901701	cellular response to oxygen-containing compound	1.50E-04	1.37E-02	14
120	GO:0030308	negative regulation of cell growth	1.51E-04	1.37E-02	6
121	GO:1903317	regulation of protein maturation	1.58E-04	1.41E-02	4
122	GO:0051674	localization of cell	1.59E-04	1.41E-02	13
123	GO:0048870	cell motility	1.59E-04	1.41E-02	13
124	GO:0006928	movement of cell or subcellular component	1.63E-04	1.43E-02	16
125	GO:0036072	direct ossification	1.65E-04	1.43E-02	2
126	GO:0001957	intramembranous ossification	1.65E-04	1.43E-02	2
127	GO:0007162	negative regulation of cell adhesion	1.72E-04	1.48E-02	7
128	GO:0051246	regulation of protein metabolic process	1.79E-04	1.53E-02	24
129	GO:0060536	cartilage morphogenesis	1.82E-04	1.54E-02	3
130	GO:0050866	negative regulation of cell activation	1.93E-04	1.61E-02	6
131	GO:0010721	negative regulation of cell development	1.96E-04	1.62E-02	8
132	GO:0043933	protein-containing complex subunit organization	1.96E-04	1.62E-02	17
133	GO:0030030	cell projection organization	1.98E-04	1.62E-02	14
134	GO:0019222	regulation of metabolic process	2.00E-04	1.63E-02	41
135	GO:0061061	muscle structure development	2.12E-04	1.71E-02	9
136	GO:0055123	digestive system development	2.23E-04	1.78E-02	5
137	GO:0003413	chondrocyte differentiation involved in endochondral bone morphogenesis	2.26E-04	1.80E-02	3
138	GO:0060191	regulation of lipase activity	2.33E-04	1.84E-02	4
139	GO:0051346	negative regulation of hydrolase activity	2.37E-04	1.86E-02	8
140	GO:0009605	response to external stimulus	2.43E-04	1.88E-02	22
141	GO:0072103	glomerulus vasculature morphogenesis	2.47E-04	1.88E-02	2
142	GO:0072239	metanephric glomerulus vasculature development	2.47E-04	1.88E-02	2
143	GO:0072104	glomerular capillary formation	2.47E-04	1.88E-02	2

144	GO:0031323	regulation of cellular metabolic process	2.51E-04	1.90E-02	38
145	GO:0080090	regulation of primary metabolic process	2.58E-04	1.93E-02	37
146	GO:0060350	endochondral bone morphogenesis	2.59E-04	1.93E-02	4
147	GO:0030324	lung development	2.62E-04	1.95E-02	6
148	GO:0030323	respiratory tube development	2.83E-04	2.08E-02	6
149	GO:0061041	regulation of wound healing	2.92E-04	2.13E-02	5
150	GO:0001503	ossification	2.97E-04	2.16E-02	6
151	GO:0045785	positive regulation of cell adhesion	2.98E-04	2.16E-02	8
152	GO:0050680	negative regulation of epithelial cell proliferation	3.01E-04	2.16E-02	5
153	GO:0030574	collagen catabolic process	3.04E-04	2.17E-02	3
154	GO:0090288	negative regulation of cellular response to growth factor stimulus	3.11E-04	2.20E-02	5
155	GO:0051171	regulation of nitrogen compound metabolic process	3.18E-04	2.23E-02	36
156	GO:0009968	negative regulation of signal transduction	3.22E-04	2.25E-02	14
157	GO:0071310	cellular response to organic substance	3.33E-04	2.29E-02	20
158	GO:0048566	embryonic digestive tract development	3.34E-04	2.29E-02	3
159	GO:0003417	growth plate cartilage development	3.34E-04	2.29E-02	3
160	GO:0071694	maintenance of protein location in extracellular region	3.45E-04	2.32E-02	2
161	GO:0061439	kidney vasculature morphogenesis	3.45E-04	2.32E-02	2
162	GO:0061438	renal system vasculature morphogenesis	3.45E-04	2.32E-02	2
163	GO:0009636	response to toxic substance	3.48E-04	2.33E-02	7
164	GO:0060255	regulation of macromolecule metabolic process	3.55E-04	2.36E-02	38
165	GO:0050790	regulation of catalytic activity	3.59E-04	2.37E-02	18
166	GO:0030335	positive regulation of cell migration	3.78E-04	2.48E-02	9
167	GO:0065009	regulation of molecular function	3.90E-04	2.54E-02	22
168	GO:0001558	regulation of cell growth	4.03E-04	2.61E-02	8
169	GO:0001655	urogenital system development	4.11E-04	2.64E-02	7
170	GO:0090092	regulation of transmembrane receptor protein serine/threonine kinase signaling pathway	4.12E-04	2.64E-02	6
171	GO:0071417	cellular response to organonitrogen compound	4.15E-04	2.65E-02	9
172	GO:0072224	metanephric glomerulus development	4.59E-04	2.91E-02	2
173	GO:0048518	positive regulation of biological process	4.72E-04	2.97E-02	41
174	GO:0043086	negative regulation of catalytic activity	4.73E-04	2.97E-02	10
175	GO:0052548	regulation of endopeptidase activity	4.83E-04	3.01E-02	7
176	GO:0031214	biomineral tissue development	4.98E-04	3.06E-02	4
177	GO:0110148	biomineralization	4.98E-04	3.06E-02	4
178	GO:2000147	positive regulation of cell motility	5.04E-04	3.09E-02	9
179	GO:0051094	positive regulation of developmental process	5.22E-04	3.18E-02	16

180	GO:0060541	respiratory system development	5.48E-04	3.32E-02	6
181	GO:0031175	neuron projection development	5.86E-04	3.48E-02	10
182	GO:0035581	sequestering of extracellular ligand from receptor	5.88E-04	3.48E-02	2
183	GO:0032964	collagen biosynthetic process	5.88E-04	3.48E-02	2
184	GO:0032429	regulation of phospholipase A2 activity	5.88E-04	3.48E-02	2
185	GO:0003416	endochondral bone growth	5.92E-04	3.48E-02	3
186	GO:0006508	proteolysis	5.93E-04	3.48E-02	13
187	GO:0042542	response to hydrogen peroxide	6.12E-04	3.57E-02	4
188	GO:0010035	response to inorganic substance	6.18E-04	3.58E-02	8
189	GO:0002063	chondrocyte development	6.37E-04	3.67E-02	3
190	GO:0051272	positive regulation of cellular component movement	6.40E-04	3.67E-02	9
191	GO:0008347	glial cell migration	6.84E-04	3.90E-02	3
192	GO:0045926	negative regulation of growth	6.88E-04	3.91E-02	6
193	GO:0051259	protein complex oligomerization	7.05E-04	3.98E-02	9
194	GO:0043588	skin development	7.31E-04	4.06E-02	6
195	GO:0098868	bone growth	7.33E-04	4.06E-02	3
196	GO:1900115	extracellular regulation of signal transduction	7.33E-04	4.06E-02	2
197	GO:1900116	extracellular negative regulation of signal transduction	7.33E-04	4.06E-02	2
198	GO:0010243	response to organonitrogen compound	7.37E-04	4.06E-02	11
199	GO:0040017	positive regulation of locomotion	7.49E-04	4.10E-02	9
200	GO:0051216	cartilage development	8.01E-04	4.37E-02	5
201	GO:0010648	negative regulation of cell communication	8.27E-04	4.49E-02	14
202	GO:0030850	prostate gland development	8.38E-04	4.52E-02	3
203	GO:0023057	negative regulation of signaling	8.59E-04	4.61E-02	14
204	GO:0044092	negative regulation of molecular function	8.81E-04	4.71E-02	12
205	GO:0030195	negative regulation of blood coagulation	8.93E-04	4.71E-02	3
206	GO:0072102	glomerulus morphogenesis	8.94E-04	4.71E-02	2
207	GO:0043589	skin morphogenesis	8.94E-04	4.71E-02	2
208	GO:1901699	cellular response to nitrogen compound	9.14E-04	4.79E-02	9
209	GO:0006935	chemotaxis	9.30E-04	4.85E-02	8
210	GO:1900047	negative regulation of hemostasis	9.51E-04	4.91E-02	3
211	GO:0030282	bone mineralization	9.51E-04	4.91E-02	3
212	GO:0048584	positive regulation of response to stimulus	9.55E-04	4.91E-02	20
213	GO:0042330	taxis	9.68E-04	4.95E-02	8
214	GO:0007548	sex differentiation	9.76E-04	4.97E-02	6

Supplementary table 9: GOnet/DICE GOBP enrichment of significantly upregulated genes (DEGs) in ECM1+ F-Act cells, relative to ECM1- F-act cells.

Rank	GO_term_def	P	P_FDR_adj	NofGenes
1	extracellular structure organization	5.00E-10	5.32E-06	9
2	extracellular matrix organization	4.50E-09	2.47E-05	8
3	regulation of complement activation	2.29E-06	8.33E-03	3
4	regulation of response to stimulus	4.26E-06	1.16E-02	19
5	cellular component organization	1.90E-05	4.15E-02	21
6	regulation of humoral immune response	2.86E-05	4.64E-02	3
7	cellular component organization or biogenesis	3.38E-05	4.64E-02	21
8	response to wounding	3.54E-05	4.64E-02	6
9	regulation of nitrogen compound metabolic process	4.38E-05	4.64E-02	20
10	myelination	4.69E-05	4.64E-02	4
11	ensheathment of neurons	5.16E-05	4.64E-02	4
12	axon ensheathment	5.16E-05	4.64E-02	4
13	paranodal junction assembly	5.53E-05	4.64E-02	2
14	negative regulation of blood coagulation	6.00E-05	4.65E-02	3
15	negative regulation of hemostasis	6.40E-05	4.65E-02	3
16	negative regulation of coagulation	6.82E-05	4.65E-02	3
17	collagen fibril organization	7.26E-05	4.66E-02	3

Supplementary table 10: GOnet/DICE GOBP enrichment of significantly upregulated genes (DEGs) in ECM1+ F-SH cells, relative to ECM1- F-SH cells.

Rank	GO_term_def	P	P_FDR_adj	NofGenes
1	extracellular structure organization	6.00E-10	6.86E-06	8
2	extracellular matrix organization	8.80E-09	4.77E-05	7
3	supramolecular fiber organization	7.30E-07	2.65E-03	7
4	membrane raft organization	1.60E-06	4.36E-03	3
5	negative regulation of multicellular organismal process	1.41E-05	2.32E-02	9
6	negative regulation of blood coagulation	2.09E-05	2.32E-02	3
7	negative regulation of hemostasis	2.23E-05	2.32E-02	3
8	response to other organism	2.24E-05	2.32E-02	9
9	response to external biotic stimulus	2.26E-05	2.32E-02	9
10	negative regulation of coagulation	2.38E-05	2.32E-02	3
11	collagen fibril organization	2.53E-05	2.32E-02	3
12	response to biotic stimulus	2.56E-05	2.32E-02	9
13	regulation of body fluid levels	4.44E-05	3.72E-02	5
14	regulation of protein processing	5.65E-05	4.22E-02	3
15	negative regulation of cellular process	5.86E-05	4.22E-02	15
16	regulation of protein maturation	6.20E-05	4.22E-02	3
17	negative regulation of wound healing	7.08E-05	4.28E-02	3
18	membrane raft assembly	7.17E-05	4.28E-02	2
19	multi-organism process	7.46E-05	4.28E-02	11
20	regulation of blood coagulation	9.83E-05	4.77E-02	3
21	regulation of plasminogen activation	1.02E-04	4.77E-02	2
22	regulation of hemostasis	1.02E-04	4.77E-02	3

23	negative regulation of cell population proliferation	1.14E-04	4.77E-02	6
24	regulation of coagulation	1.14E-04	4.77E-02	3
25	positive regulation of biological process	1.15E-04	4.77E-02	17
26	negative regulation of multi-organism process	1.15E-04	4.77E-02	4
27	regulation of protein metabolic process	1.24E-04	4.77E-02	11
28	vesicle organization	1.30E-04	4.77E-02	4
29	fibrinolysis	1.36E-04	4.77E-02	2
30	negative regulation of response to wounding	1.37E-04	4.77E-02	3
31	regulation of proteolysis	1.38E-04	4.77E-02	6
32	regulation of developmental process	1.40E-04	4.77E-02	11

Supplementary table 11: GOnet/DICE GOBP enrichment of significantly upregulated genes (DEGs) in ECM1+ M1MΦ cells, relative to ECM1- M1MΦ cells.

Rank	GO_term_def	P	P_FDR_adj	NofGenes
1	neutrophil chemotaxis	1.30E-09	8.47E-06	5
2	granulocyte chemotaxis	2.10E-09	8.47E-06	5
3	neutrophil migration	2.30E-09	8.47E-06	5
4	granulocyte migration	4.10E-09	1.12E-05	5
5	myeloid leukocyte migration	1.25E-08	2.72E-05	5
6	leukocyte chemotaxis	2.04E-08	3.71E-05	5
7	organonitrogen compound catabolic process	4.62E-08	7.19E-05	8
8	organic substance catabolic process	1.04E-07	1.42E-04	9
9	leukocyte migration	1.74E-07	2.00E-04	5
10	positive regulation of immune system process	1.96E-07	2.00E-04	8
11	cell chemotaxis	2.02E-07	2.00E-04	5
12	catabolic process	5.06E-07	4.60E-04	9
13	chemotaxis	5.82E-07	4.70E-04	6
14	taxis	6.04E-07	4.70E-04	6
15	regulation of leukocyte chemotaxis	8.85E-07	6.43E-04	4
16	cellular catabolic process	2.40E-06	1.55E-03	8
17	positive regulation of leukocyte migration	2.42E-06	1.55E-03	4
18	regulation of apoptotic process	2.86E-06	1.67E-03	8
19	regulation of immune system process	2.91E-06	1.67E-03	8
20	regulation of programmed cell death	3.20E-06	1.67E-03	8
21	regulation of epithelial cell proliferation	3.22E-06	1.67E-03	5
22	regulation of mononuclear cell migration	5.09E-06	2.48E-03	3
23	regulation of cell population proliferation	5.23E-06	2.48E-03	8
24	negative regulation of neuron apoptotic process	5.99E-06	2.65E-03	4
25	immune system process	6.32E-06	2.65E-03	9
26	regulation of cell death	6.33E-06	2.65E-03	8
27	regulation of leukocyte migration	9.06E-06	3.66E-03	4
28	inflammatory response	9.89E-06	3.85E-03	5
29	positive regulation of response to external stimulus	1.06E-05	3.96E-03	5

30	regulation of chemotaxis	1.16E-05	4.22E-03	4
31	regulation of cell communication	1.49E-05	5.24E-03	10
32	regulation of signaling	1.55E-05	5.28E-03	10
33	negative regulation of neuron death	2.04E-05	6.73E-03	4
34	negative regulation of apoptotic process	2.27E-05	7.19E-03	6
35	positive regulation of cell migration	2.34E-05	7.19E-03	5
36	regulation of response to external stimulus	2.37E-05	7.19E-03	6
37	negative regulation of programmed cell death	2.52E-05	7.43E-03	6
38	positive regulation of leukocyte chemotaxis	2.71E-05	7.61E-03	3
39	regulation of neuron apoptotic process	2.76E-05	7.61E-03	4
40	positive regulation of cell motility	2.83E-05	7.61E-03	5
41	regulation of signal transduction	2.86E-05	7.61E-03	9
42	response to oxygen-containing compound	3.03E-05	7.86E-03	7
43	positive regulation of cellular component movement	3.32E-05	8.23E-03	5
44	regulation of localization	3.32E-05	8.23E-03	9
45	complement receptor mediated signaling pathway	3.41E-05	8.27E-03	2
46	positive regulation of locomotion	3.69E-05	8.56E-03	5
47	negative regulation of cellular process	3.69E-05	8.56E-03	11
48	regulation of cellular component movement	4.10E-05	9.31E-03	6
49	negative regulation of response to stimulus	4.52E-05	1.01E-02	7
50	negative regulation of cell death	4.69E-05	1.02E-02	6
51	regulation of angiogenesis	4.77E-05	1.02E-02	4
52	protein catabolic process	4.85E-05	1.02E-02	5
53	regulation of response to stimulus	6.54E-05	1.35E-02	10
54	regulation of cytokine production	7.13E-05	1.42E-02	5
55	regulation of vasculature development	7.17E-05	1.42E-02	4
56	regulation of biological quality	8.61E-05	1.63E-02	10
57	positive regulation of cellular metabolic process	8.66E-05	1.63E-02	9
58	negative regulation of signal transduction	8.81E-05	1.63E-02	6
59	locomotion	8.85E-05	1.63E-02	6
60	regulation of endothelial cell proliferation	8.98E-05	1.63E-02	3
61	positive regulation of macrophage chemotaxis	9.16E-05	1.64E-02	2
62	response to molecule of bacterial origin	9.62E-05	1.69E-02	4
63	regulation of multicellular organismal process	9.92E-05	1.69E-02	9
64	regulation of neuron death	9.93E-05	1.69E-02	4
65	negative regulation of cytokine production involved in immune response	1.10E-04	1.85E-02	2
66	positive regulation of chemotaxis	1.12E-04	1.85E-02	3
67	negative regulation of biological process	1.21E-04	1.96E-02	11
68	positive regulation of vascular endothelial growth factor production	1.31E-04	2.06E-02	2
69	positive regulation of neutrophil chemotaxis	1.31E-04	2.06E-02	2
70	positive regulation of macrophage migration	1.41E-04	2.20E-02	2
71	negative regulation of cell communication	1.49E-04	2.28E-02	6
72	negative regulation of signaling	1.52E-04	2.28E-02	6

73	positive regulation of granulocyte chemotaxis	1.53E-04	2.28E-02	2
74	defense response	1.71E-04	2.52E-02	6
75	positive regulation of metabolic process	1.74E-04	2.52E-02	9
76	negative regulation of multicellular organismal process	1.80E-04	2.58E-02	6
77	macromolecule catabolic process	1.90E-04	2.69E-02	5
78	cell migration	1.93E-04	2.70E-02	5
79	regulation of macrophage chemotaxis	2.02E-04	2.72E-02	2
80	regulation of vascular endothelial growth factor production	2.02E-04	2.72E-02	2
81	regulation of neutrophil chemotaxis	2.02E-04	2.72E-02	2
82	epithelial tube branching involved in lung morphogenesis	2.29E-04	3.05E-02	2
83	positive regulation of neutrophil migration	2.43E-04	3.20E-02	2
84	negative regulation of immune system process	2.52E-04	3.20E-02	4
85	regulation of cell migration	2.53E-04	3.20E-02	5
86	positive regulation of angiogenesis	2.55E-04	3.20E-02	3
87	negative regulation of production of molecular mediator of immune response	2.58E-04	3.20E-02	2
88	defense response to protozoan	2.58E-04	3.20E-02	2
89	positive regulation of epithelial cell proliferation	3.16E-04	3.84E-02	3
90	response to protozoan	3.21E-04	3.84E-02	2
91	regulation of cell motility	3.21E-04	3.84E-02	5
92	response to chemical	3.27E-04	3.87E-02	9
93	positive regulation of vasculature development	3.39E-04	3.98E-02	3
94	regulation of macrophage migration	3.55E-04	4.11E-02	2
95	cell motility	3.64E-04	4.13E-02	5
96	localization of cell	3.64E-04	4.13E-02	5
97	regulation of neutrophil migration	3.72E-04	4.18E-02	2
98	positive regulation of cell population proliferation	3.78E-04	4.21E-02	5
99	cellular response to lipid	3.83E-04	4.22E-02	4
100	positive regulation of nitrogen compound metabolic process	4.27E-04	4.65E-02	8
101	proteolysis involved in cellular protein catabolic process	4.59E-04	4.96E-02	4
102	regulation of locomotion	4.66E-04	4.98E-02	5

Supplementary table 12: Full phosphoproteomics mass spectrometry output of ECM1 treated HuCFb cells, only significantly different phosphoproteins proteins shown, relative to controls treated with media alone.

Gene names	Student's T-test p-value C_ECM	Student's T-test q-value C_ECM	Student's T-test Difference C_ECM	Student's T-test Test statistic C_ECM	fold-change relative to control	Amino acid	Charge	Multiplicity	Position	Proteins	Positions within proteins
MAP1B	8.97E-08	0	-4.7712303	-10.57971834	27.30759396	S	3	___2	1256	P46821	1256
ARHGEF11	0.000459376	0.0155	-3.366064231	-4.434164424	10.31065608	S	3	___2	255	O15085	255
ANAPC4	0.000877879	0.033176471	-1.961994211	-3.773570706	3.896001441	S	3	___2	779	Q9UJX5	779
ANAPC4	0.000132604	0.014857143	-1.826141437	-4.514573506	3.545874405	S	3	___2	777	Q9UJX5	777
MYO9B	0.001906845	0.048117647	-1.465417862	-3.248461957	2.761434412	S	3	___1	1972	Q13459	1972
CETN2	0.000234864	0.028	-1.435140729	-4.016619868	2.704085426	S	3	___1	20	P41208	20
SURF2	0.000665651	0.03752381	-1.383230329	-3.59405929	2.608517891	T	3	___1	195	Q15527	195
MAP1B	0.001150431	0.045384615	-1.369524479	-3.384729774	2.583853867	S	3	___3	1254	P46821	1254
PTPN12	0.000178712	0.029333333	-1.208638668	-3.908257684	2.311194488	T	3	___1	509	Q05209	509
KIFAP3	0.001233123	0.049333333	-1.203920841	-3.24962641	2.303648883	S	2	___1	60	Q92845	60
MAP7D1	0.001382455	0.047666667	1.238786896	3.234603326	-2.36000006	S	3	___1	410	Q3KQU3	410
BICC1	0.001433061	0.051466667	1.319898764	3.274372861	-2.49648591	S	2	___2	637	Q9H694	637
KRI1	0.000751492	0.037833333	1.339380105	3.520007074	-2.530425685	S	2	___1	136	Q8N9T8	136
SSH3	0.000868397	0.03888	1.358298063	3.480351593	-2.563825484	S	2	___1	649	Q8TE77	649
PSMF1	0.000618388	0.038	1.36594673	3.609092566	-2.577454089	S	2	___1	153	Q92530	153
TNKS1BP1	0.001552672	0.052965517	1.375632366	3.278059626	-2.594816226	S	2	___1	1533	Q9C0C2	1533
BAG6	0.000376195	0.032533333	1.396229585	3.812620405	-2.632127884	S	2	___1	1117	P46379	1117
CNOT2	0.00035516	0.031714286	1.404216448	3.839747385	-2.646739942	S	2	___1	165	Q9NZN8	165
THRAP3	0.001997747	0.050625	1.505913258	3.249983132	-2.840043954	S	2	___1	248	Q9Y2W1	248
GBF1	0.000860681	0.036363636	1.535160542	3.589664068	-2.8982068	S	2	___1	1780	Q92538	1780

SLC38A1	0.000827163	0.041333333	1.569841345	3.623812515	-2.96872065	S	2	___1	49	Q9H2H9	49
LIG3	0.00096835	0.035826087	1.602434595	3.578791051	-3.036553095	S	2	___1	242	P49916	242
RBM8A	0.001698068	0.045037037	1.60259827	3.357168859	-3.036897613	S	2	___1	42	Q9Y5S9	42
TBX3	0.000328471	0.030666667	1.635954301	4.025616439	-3.107930625	S	2	___1	438	O15119	438
SRRM2	0.001877444	0.045571429	1.652579904	3.338344645	-3.143953552	T	2	___3	903	Q9UQ35	903
VIM;GFAP	0.000719681	0.03375	1.78734831	3.786098847	-3.451798646	S	2	___1	339	P08670;P14136	339;305
PRPF38B	0.002575276	0.050451613	1.823613246	3.271126174	-3.539666027	S	3	___1	529	Q5VTL8	529
ARHGEF12	0.000577838	0.028	2.018076261	3.975523649	-4.05043333	S	3	___1	309	Q9NZN5	309
SRRM1	0.000761342	0.032615385	2.054057717	3.868579735	-4.152723215	S	2	___1	414	Q8IYB3	414
HECTD1	0.003517391	0.049028571	2.195672035	3.235367072	-4.581030078	S	2	___1	357	Q9ULT8	357
RNPS1	0.003564491	0.046378378	2.212842464	3.23315445	-4.635877564	S	2	___2	139	Q15287	139
RNPS1	0.003564491	0.045157895	2.212842464	3.23315445	-4.635877564	S	2	___2	141	Q15287	141
LEMD2	9.86E-06	0.002	2.574077249	6.197602049	-5.954899865	S	3	___2	134	Q8NC56	134
DNAJC17	0.001915034	0.04	2.703021765	3.61338929	-6.511643716	S	2	___1	112	Q9NVM6	112
TRA2B;TRA2A;SRRM1	0.000332722	0.012	3.230564634	4.575530162	-9.386352454	S	2	___3	308	P62995;Q13595;Q8IYB3	282;276;308
TRA2B;TRA2A;SRRM1	0.000147457	0.010666667	3.451596777	5.051771502	-10.94042423	S	2	___3	310	P62995;Q13595;Q8IYB3	284;278;310
SRSF1	0.000153994	0.008	3.474500934	5.033116997	-11.11549995	S	2	___3	225	Q07955	225
SRSF1	0.000170493	0.0064	3.479526083	4.979083187	-11.15428461	S	2	___3	227	Q07955	227

Supplementary table 13: Fisher's exact test (Perseus software) of GO terms significantly enriched in ECM1 treated HuCFb samples (from phosphoproteomics data) ranked by p-value.

GO Category	GOBP term	Enrichment factor	P value	Benj. Hoch. FDR
GOBP name	regulation of calcium-dependent cell-cell adhesion	234.38	0.0042667	0.99573
GOBP name	positive regulation of calcium-dependent cell-cell adhesion	234.38	0.0042667	0.99573
GOBP name	monocyte chemotaxis	234.38	0.0042667	0.99573
GOBP name	macrophage chemotaxis	234.38	0.0042667	0.99573
GOBP name	centriole replication	117.19	0.0085015	0.99573
GOBP name	mitochondrion transport along microtubule	78.125	0.012705	0.99573
GOBP name	lamellipodium morphogenesis	78.125	0.012705	0.99573
GOBP name	establishment or maintenance of monopolar cell polarity	78.125	0.012705	0.99573
GOBP name	establishment of monopolar cell polarity	78.125	0.012705	0.99573
GOBP name	establishment of mitochondrion localization, microtubule-mediated	78.125	0.012705	0.99573
GOBP name	plus-end-directed vesicle transport along microtubule	58.594	0.016876	0.99573
GOBP name	plus-end-directed organelle transport along microtubule	58.594	0.016876	0.99573
GOBP name	establishment of mitochondrion localization	58.594	0.016876	0.99573
GOBP name	establishment of cell polarity	39.062	4.00E-05	0.23881
GOBP name	organelle transport along microtubule	39.062	0.0010186	0.99573
GOBP name	Rho protein signal transduction	23.438	0.0028574	0.99573
GOBP name	microtubule-based transport	20.38	0.0037681	0.99573
GOBP name	establishment or maintenance of cell polarity	19.003	0.00036192	0.99573
GOBP name	cytoskeleton-dependent intracellular transport	18.75	0.0044391	0.99573
GOBP name	microtubule-based movement	14.205	0.0076121	0.99573
GOBP name	Ras protein signal transduction	9.9734	0.014886	0.99573
GOBP name	regulation of cell growth	9.0144	0.017962	0.99573
GOBP name	nuclear division	8.8443	0.018605	0.99573
GOBP name	mitosis	8.8443	0.018605	0.99573
GOBP name	microtubule-based process	7.9003	0.0045818	0.99573
GOBP name	cellular component movement	6.0484	0.002252	0.99573
GOBP name	cellular component organization at cellular level	2.1769	0.019938	0.99573
GO Category	**GOCC term**	**Enrichment factor**	**P value**	**Benj. Hoch. FDR**

GOCC name	photoreceptor connecting cilium	156.25	4.77E-05	0.039271
GOCC name	nonmotile primary cilium	66.964	0.00032935	0.13569
GOCC name	cell projection	5.5804	0.00066742	0.18332
GOCC name	cytosol	3.0159	0.00095965	0.19769
GOCC name	primary cilium	33.482	0.0013954	0.22078
GOCC name	cytoskeletal part	4.6137	0.0016076	0.22078
GOCC name	cilium	21.307	0.0034516	0.39064
GOCC name	intraflagellar transport particle	234.38	0.0042667	0.39064
GOCC name	filopodium tip	234.38	0.0042667	0.39064
GOCC name	microtubule associated complex	15.121	0.0067477	0.52726
GOCC name	intracellular	13.787	0.0080615	0.52726
GOCC name	kinesin II complex	117.19	0.0085015	0.52726
GOCC name	cell projection part	6.2223	0.0088278	0.52726
GOCC name	protein complex	2.5476	0.0089583	0.52726
GOCC name	XPC complex	78.125	0.012705	0.58159
GOCC name	nucleotide-excision repair complex	78.125	0.012705	0.58159
GOCC name	nuclear ubiquitin ligase complex	78.125	0.012705	0.58159
GOCC name	anaphase-promoting complex	78.125	0.012705	0.58159
GOCC name	axoneme part	58.594	0.016876	0.69529
GOCC name	axoneme	58.594	0.016876	0.69529
GO Category	**GOMF term**	**Enrichment factor**	**P value**	**Benj. Hoch. FDR**
GOMF name	non-membrane spanning protein tyrosine phosphatase activity	234.38	0.0042667	0.99573
GOMF name	microfilament motor activity	78.125	0.012705	0.99573
GOMF name	actin-dependent ATPase activity	58.594	0.016876	0.99573

Supplementary table 14: Proteins significantly enriched in ECM1 coated pull-down beads relative to control beads (no protein pre-bound). Both 1x detergent buffer and 1/4x detergent buffer lists are shown ranked by p-value. Proteins common to both conditions are highlighted in green.

1x detergent			
Rank	**Gene names**	**p-value**	**fold enriched vs Control**
1	ECM1	6.90E-06	144.7585
2	PYGB	0.0003	4.9739
3	PDIA3	0.0004	1.7735

4	CCT4	0.0014	3.1153
5	**CTNND1**	0.0022	1.2584
6	ACO2	0.0047	1.3705
7	**DHX9**	0.0067	4.9925
8	ALDH1L2	0.0096	1.2362
9	SCFD1	0.0097	1.3799
10	SLC25A11	0.0109	2.4087
11	COL4A1	0.0114	3.9163
12	DDX3X;DDX3Y	0.0143	2.0017
13	COL6A2	0.0149	2.6839
14	GOLGA2	0.0190	1.1222
15	TRIM28	0.0211	1.3973
16	RPN2	0.0215	1.2742
17	ACTR3	0.0229	4.6466
18	RTCB	0.0229	1.4070
19	HNRNPA3	0.0236	2.8054
20	**DYNC1I2**	0.0245	1.2434
21	CLPTM1	0.0250	2.3811
22	LEPREL2	0.0264	1.8544
23	ACSL1	0.0295	2.2224
24	GOT2	0.0321	2.2796
25	COG4	0.0324	1.5295
26	GLUD1;GLUD2	0.0329	4.9317
27	MTHFD1L	0.0390	1.3823
28	GFM1	0.0395	2.3159
29	ACADVL	0.0420	1.2893
30	PDIA6	0.0443	1.5933
31	**HK1**	0.0443	1.2590
32	UBA52;RPS27A;UBB;UBC	0.0462	5.3013
33	LARS2	0.0477	1.3948
34	GALNT2	0.0486	1.1839
35	SERPINH1	0.0493	1.3098
1/4x detergent			
Rank	**Gene names**	**p-value**	**fold enriched vs Control**
1	ECM1	5.22E-05	197.2461
2	ACSL3	0.0004	4.0783
3	PKM	0.0010	1.2029
4	SFXN1	0.0015	2.2405
5	UBR5	0.0016	1.2256
6	PLOD2	0.0018	1.3724
7	LAMB1	0.0040	1.3397
8	PTPN1	0.0044	1.2871

9	UQCRC1	0.0061	1.9840
10	SF3B3	0.0080	1.6916
11	HSPA9	0.0094	1.5586
12	MYH10	0.0110	1.1019
13	HNRNPK	0.0112	1.8484
14	PDHA1	0.0120	1.8828
15	**CTNND1**	0.0121	1.3325
16	HNRNPH1	0.0137	1.4941
17	RPS9	0.0144	5.4532
18	SEC31A	0.0155	1.2766
19	LAMC1	0.0158	1.1964
20	RPS18	0.0170	6.2656
21	IDH2	0.0186	1.1340
22	**DYNC1I2**	0.0188	1.4935
23	H6PD	0.0193	1.2323
24	EPB41L2	0.0194	1.1858
25	ERLEC1	0.0199	1.8035
26	FAT4	0.0209	1.2084
27	LRP1	0.0216	1.2710
28	**DHX9**	0.0217	1.4647
29	GLG1	0.0232	1.3764
30	SAFB	0.0241	2.7103
31	**HK1**	0.0244	1.2813
32	NID2	0.0249	1.7587
33	GNB2L1	0.0280	1.2504
34	ESYT1	0.0287	1.2303
35	RPL23	0.0290	1.3240
36	GOLGB1	0.0292	1.6317
37	FN1	0.0311	1.1258
38	EFTUD2	0.0313	1.8142
39	PSMD12	0.0315	2.5457
40	PML	0.0366	1.2059
41	PSMC6	0.0373	1.2704
42	SF3B2	0.0382	1.2115
43	HNRNPA0	0.0386	1.2336
44	IGF2R	0.0388	1.3452
45	LTBP2	0.0399	1.4444
46	DDX5	0.0402	1.8944
47	NUP205	0.0404	1.1138
48	HLA-B;HLA-C;HLA-H;HLA-E;HLA-A	0.0428	1.2818
49	GYS1	0.0433	1.7215
50	CCAR2	0.0445	1.1356
51	VCAN	0.0457	1.2882

52	FAM134C	0.0461	1.1796
53	PCBP1;PCBP3	0.0470	1.8588
54	STOM	0.0471	1.1866
55	SRRM2	0.0475	1.4305
56	GCN1L1	0.0476	1.0971
57	RAB7A	0.0484	1.7180
58	PLXDC2	0.0493	1.2453
Averaged across both conditions			
Rank	**Gene names**	**Average p-value**	**Average Fold-Change**
1	CTNND1	0.0071	1.2955
2	DHX9	0.0142	3.2286
3	DYNC1I2	0.0217	1.3684
4	HK1	0.0344	1.2702